

A NUMERICAL STUDY OF LAMINAR FLOW  
HEAT TRANSFER IN CURVED TUBES

---

A Thesis

Presented to

the Faculty of the Department of Chemical Engineering

The University of Missouri

Columbia, Missouri

---

In Partial Fulfillment of

the Requirements for the Degree

Master of Science in Chemical Engineering

---

by

William Terry Sappenfield

August, 1968

The undersigned, appointed by the Dean of the Graduate Faculty,  
have examined a thesis entitled

A NUMERICAL STUDY OF LAMINAR FLOW  
HEAT TRANSFER IN CURVED TUBES

presented by William Terry Sappenfield

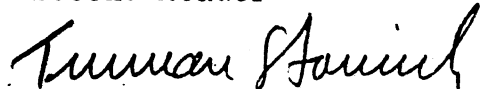
a candidate for the degree of Master of Science

and hereby certify that in their opinion it is worthy of acceptance.

Dr. Bert Wilkins, Jr.  
Research Advisor

A handwritten signature in cursive script that reads "Bert Wilkins, Jr." with a stylized flourish at the end.

Dr. Truman S. Storvick  
Second Reader

A handwritten signature in cursive script that reads "Truman Storvick" with a stylized flourish at the end.

## ACKNOWLEDGMENTS

The author wishes to express his thanks to Dr. Bert Wilkins, Jr., his faculty advisor, for the direction and helpful suggestions offered during the compilation of this work.

The large amount of computer time needed to complete this work was made available through the University of Missouri's Engineering Computer Center under the direction of Mr. Dick Lewis.

The author's wife, Mrs. Nancy Jean Sappenfield, spent many long hours typing both rough draft and final copies of this study. Her encouragement and devotion added to the completion of this work in no small measure.

## TABLE OF CONTENTS

CHAPTER	PAGE
I. INTRODUCTION . . . . .	1
II. LITERATURE REVIEW . . . . .	6
III. MATHEMATICAL DESCRIPTION OF THE PROBLEM . . . . .	13
IV. NUMERICAL RESULTS . . . . .	25
V. CONCLUSIONS AND RECOMMENDATIONS . . . . .	45
NOMENCLATURE . . . . .	47
BIBLIOGRAPHY . . . . .	52
APPENDICES . . . . .	56
A. THE NAVIER-STOKES, CONTINUITY, AND ENERGY EQUATIONS FOR CURVED PIPE FLOW . . . . .	57
B. COMMENTS ON S. N. BARUA'S WORK . . . . .	66
C. DEVELOPMENT OF CALCULATION SCHEME . . . . .	79
D. COMPUTER APPLICATION OF CALCULATION SCHEME . . . . .	99
VITA . . . . .	120

LIST OF TABLES

TABLE

PAGE

I. Summary of Cases and Parameters Studied . . . . . 26

## LIST OF FIGURES

FIGURE	PAGE
1. Secondary Flow in Curved Pipes . . . . .	2
2. Diagram of Problem . . . . .	14
3. Helical Geometry and Coordinate System . . . . .	16
4. Initial Portion of the Finite Difference Grid . . . . .	21
5. Comparison of Numerical Scheme with Classical Graetz Solution . . . . .	28
6. Numerical and Experimental Comparison of Arithmetic Mean Nusselt Numbers . . . . .	30
7. Numerical and Experimental Comparison of Local Nusselt Numbers . . . . .	31
8. Arithmetic Mean Nusselt Numbers at Dean Numbers of 385, 485, and 1154 . . . . .	33
9. Arithmetic Mean Nusselt Numbers at Dean Numbers of 1455, 1633, and 2433 . . . . .	34
10. Illustration of Prandtl Number Effect . . . . .	35
11. Local Nusselt Numbers at Inner and Outer Walls . . . . .	36
12. Local Nusselt Numbers at Inner and Outer Tube Walls for Dean Numbers of 385 and 1633 . . . . .	37
13. Mean Temperature Development as a Function of Distance down the Pipe . . . . .	38
14. Mean Temperature Development as a Function of the Graetz Number . . . . .	39
15. Angular Temperature Profiles for a Graetz Number of 2312 . . . . .	40

FIGURE	PAGE
16. Angular Temperature Profiles for a Graetz Number of 167 .	41
17. Radial Temperature Profiles in the Plane of Symmetry . . . .	42
18. Axial Temperature Profiles . . . . .	43
19. Vector Diagram . . . . .	57
20. Axial Velocity Profile in the Plane of Symmetry, $N_{De} = 273$ .	68
21. Axial Velocity Profile in the Plane of Symmetry, $N_{De} = 228$ .	69
22. Axial Velocity Profile in the Plane of Symmetry, $N_{De} = 205$ .	70

## CHAPTER I

### INTRODUCTION

Compared to the relatively simple case of steady flow in a straight tube, flow in a curved tube is extremely complex. When a fluid flows through a curved tube, a pressure gradient is set up across the tube to balance the centrifugal force arising from the curvature, the pressure near the outer wall being greater than that at the inner wall. Thus, secondary flow patterns, as shown in figure 1, emerge within the cross section. This secondary circulation is superimposed on the main stream in such a way that the resultant flow in the upper and lower halves of the tube is helical in nature. Further, the secondary flow effect tends to distort the axial velocity profile, shifting the region of maximum axial velocity from the center towards the outer wall of the pipe. The total frictional loss of energy near the wall increases and the flow experiences more resistance in passing through the tube. Also, the viscous shear at the outer wall increases, causing the volumetric rate of flow to be less for a curved system than for that of a straight pipe at an equal axial pressure gradient.

Various experimentalists have collected heat transfer data for curved systems and noted that higher heat transfer coefficients were obtained for curved systems than for corresponding straight pipe configurations.



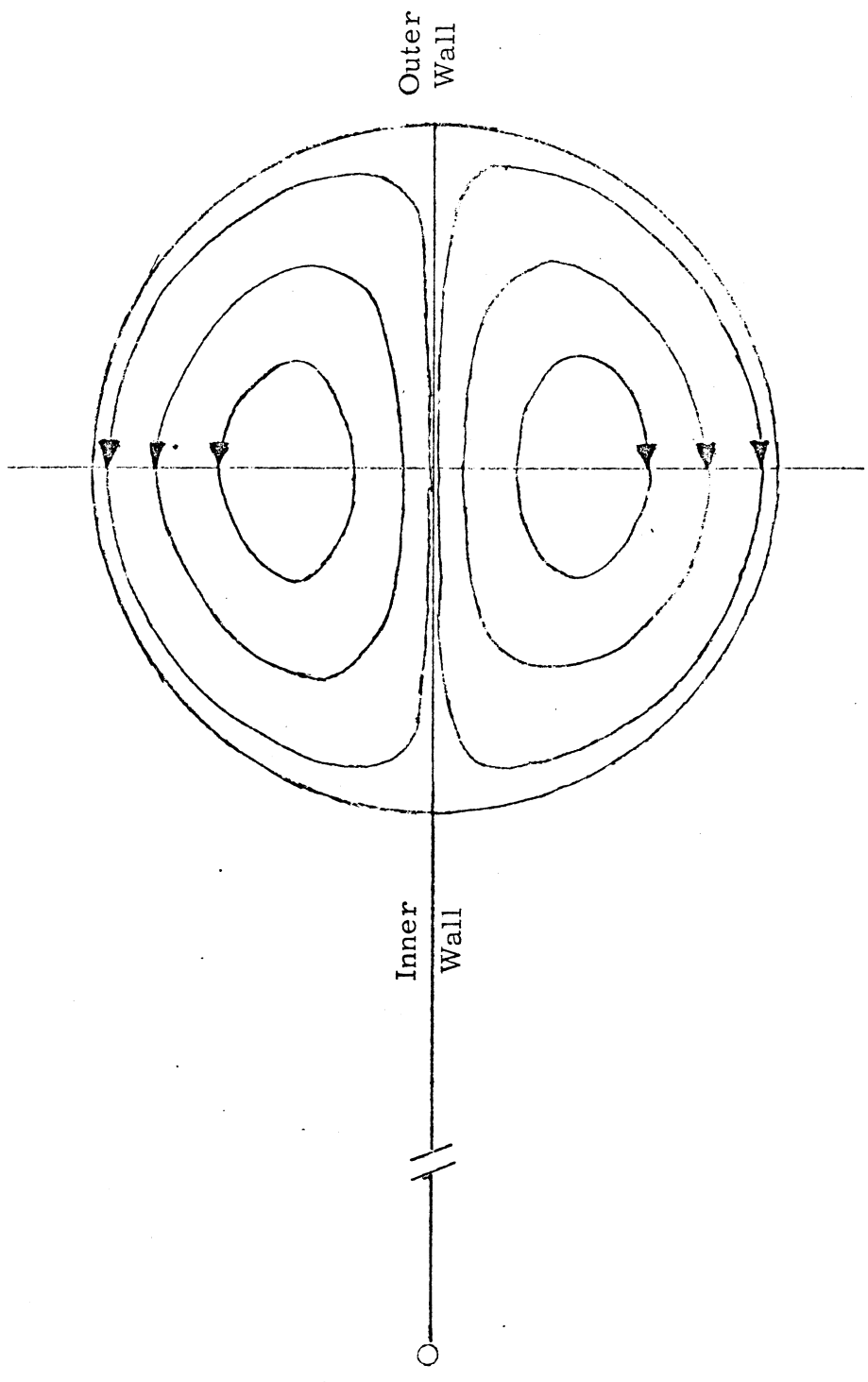


Figure 1. Secondary Flow in Curved Pipes

Chemical engineers have a special interest in fluid flow and heat transfer in curved channels. Three examples of applications are: 1.) coiled tube heat exchanger design, 2.) homogeneous chemical reactor design, and 3.) bioengineering investigations.

Heat transfer characteristics of coiled tube heat exchangers are known to be superior to those of the conventional straight tube variety.

Truesdell (22) gives a rigorous discussion of the advantages of coiled tube chemical reactors over the more frequently encountered straight tube models.

An example of a bioengineering application deals with the investigation seeking the causes of atherosclerosis, a disease of the arterial portion of the circulatory system, characterized by the presence of discrete plaques, or fatty deposits on the inner walls of curved or bent portions of the arteries. An understanding of the transport phenomena encountered in curved tube flow is important in understanding this behavior (20).

An analytical solution to the system of equations describing fluid flow and heat transfer in a curved system would be desirable, but the mathematical difficulties encountered are overwhelming. Thus, the numerical method of attack is the best and possibly the only way to examine the properties of such a system theoretically.

Numerical techniques are in general quite pliable and would in theory appear to have few limitations, though in practice many problems

arise preventing their unlimited application. Excessive computer time, the intolerable growth of error inherent in the numerical approximation, and non-convergence of the numerical equations to the actual equations in the mathematical sense of the limit can singly or together invalidate the results obtained through numerical calculation. With respect to these problems, a preliminary analysis of numerical schemes designed to solve non-linear partial differential equations of three independent variables is impossible, at present, for all but the very simplest of cases. For this reason, a tolerance for "experimental" mathematical techniques must be developed. This is not intended to imply a neglect of sound mathematical principles, but is meant to point out that often a suitably chosen trial run can decisively rule out an invalid approach to a solution which might be impossible to analyze theoretically. Thus, it becomes increasingly apparent that the numerical approach places a high value on a thorough understanding of the physical principles associated with the problem under consideration. The work described in this study is of this nature.

This study presents a numerical solution to a simplified form of the equation of energy describing the steady laminar flow heat transfer of an incompressible, constant property, Newtonian fluid in motion at high Dean numbers in a curved pipe of radius  $a^*$ , coiled in a circle of radius  $R^*$  with constant wall temperature. Numerical results are compared with experimental findings contained in the literature, and the effect of

the distorted axial velocity profile on curved tube heat transfer characteristics is demonstrated.

## CHAPTER II

### LITERATURE REVIEW

#### EXPERIMENTAL BACKGROUND

Secondary flow patterns generated by the motion of a fluid through a curved system were first described by Thompson (21) in 1876. In 1927, Dean (6) described this secondary motion as an "independent circulation," with the fluid on either side of the plane of symmetry (the horizontal plane dividing the tube into two equal sections) not mixing during laminar flow.

In 1910, Eustice (8) made the observation that if the velocity of flow through a curved system was increased, the curvature of the streamlines was also increased.

Eustice (9) continued his experimental work by injecting a stream of colored dye into a fluid flowing through a glass tube in order to examine and trace the streamlines. Eustice noted that a filament in the tube's plane of symmetry approaching the outer wall broke into two parts at impact with the wall. These two parts of the color filament then flowed in opposite directions around the semi-circular cross section to the inner wall of the tube and then back into the plane of symmetry. After returning to the inner wall, the filaments were observed to remain in their own particular half of the cross section, never crossing the plane of symmetry during laminar flow.

Eustice additionally tried to determine the critical Reynolds number (the Reynolds number at which transition from laminar to turbulent flow occurs) for such curved systems, hoping to compare the results with known values for straight pipe flow, but realized little success in this endeavor.

In 1929, Taylor (19) hypothesized that Eustice's inability to detect an increase in the critical Reynolds number for curved systems was due to the fact that Eustice had injected his colored filament into the stream at the pipe entrance. Thus, the filament had broken up before the curvature of the pipe had an opportunity to stabilize the flow. Taylor's final conclusion was that the critical Reynolds number as well as the stability of the flow was increased by curvature.

Other experimental work concerning flow in curved channels has been recorded by Bailey (2) and White (24).

Although little heat transfer data has been collected for curved systems, Kubair and Kuloor (12) have recorded data on pressure drop and heat transfer to aqueous solutions of glycerol flowing in different types of coiled tubes for laminar flow in the range of Reynolds numbers from 80-6000. Heat transfer data was taken under the condition of constant wall temperature and the results presented as plots relating the arithmetic mean Nusselt number as a function of the Graetz number.

Berg and Bonilla (4) have collected heat transfer data for the

laminar flow of water, air, and oil through several curved tube configurations. Data were taken under the condition of constant wall temperature and the results presented in a manner similar to that used by Kubair and Kuloor (12).

Seban and McLaughlin (16) present heat transfer data for the laminar flow of oil in coiled tubes under the condition of constant heat flux. Local values of the Nusselt number as a function of the Graetz number are given.

Although the majority of available experimental findings show heat transfer results for curved systems to be above corresponding straight pipe values, when taken together, the data appear to be scattered, varying over a fairly large range.

## THEORETICAL BACKGROUND

Little successful theoretical work has been reported on fluid flow in curved systems, and much of what does exist has grown out of experimental studies.

Dean's (7) analytical work consisted of an approximation of the Navier-Stokes and continuity equations obtained by expanding velocities and pressures in a power series of the ratio of the pipe radius to the radius of curvature,  $(a^*/R^*)$ . Dean confined his study to a section of the curved system free from entrance or exit effects and assumed the

fluid to be incompressible and in streamline flow. Restricting his analysis to small ( $a^*/R^*$ ) or curvature ratios, Dean showed that axial pressure gradients are a function of the dimensionless quantity  $N_{Re}(a^*/R^*)^{1/2}$ , now commonly referred to as the Dean number. Unfortunately, Dean's solution applied for only very small values of the curvature ratio, and thus is restricted to Dean numbers below approximately 50. Dean's results are, though, in good qualitative agreement with the experimental observations of Eustice. Dean notes that a complete analytical solution, free from restricting assumptions, would be extremely difficult, if not impossible to obtain.

Adler (1) applied boundary layer theory to systems of slight curvature, treating cases of high Reynolds numbers near the transition zone between laminar and turbulent flow. Various assumptions were made by Adler concerning the shape of the axial velocity profiles and of the secondary flow patterns encountered in the cross section. Adler's solution provides estimates of the variation of velocities with pressure gradient and curvature ratio in this transition zone. Although Adler's results are reliable at higher Dean numbers than the analytical solution provided by Dean, questionable results are obtained for Dean numbers in excess of 200.

Truesdell (22) in 1963, adapted the Navier-Stokes and continuity equations to describe fully developed laminar flow through helical



conduits of circular and elliptical cross section. A relaxation technique was used to solve a numerical approximation of these equations. Numerical solutions in the form of an axial velocity profile and a stream function describing velocities in the cross sectional plane were obtained on a digital computer. Truesdell presented ten numerical solutions, covering cases with Dean numbers up to 200. For Dean numbers above 200, the numerical method employed was found to be unstable.

Rogers (14) solved the Navier-Stokes and continuity equations numerically on a digital computer for the case of steady flow of an incompressible Newtonian fluid through a helically coiled conduit of rectangular cross section. A Gauss-Seidel iterative technique was employed to provide the solution to nineteen different fluid mechanical situations. Computer solutions were in the form of axial velocity profiles, a stream function, and cross sectional velocity values. The highest Dean number achieved by Rogers was approximately 66. At higher Dean numbers, convergence and stability difficulties were encountered.

Barua (3) considered the case of an incompressible, Newtonian fluid in laminar flow through a curved tube at high Dean numbers. He assumed that the flow in the cross section of a curved system consisted of a non-turbulent core moving slowly outwards, surrounded by an inward moving boundary layer. Barua further assumed that when the Dean number is large, viscous forces are important only in the thin boundary

layer near the wall, and that no cross flow exists outside the boundary layer. Barua applied a Pohlhausen type solution to the Navier-Stokes and continuity equations, obtaining a solution which described analytically the velocity components  $u^*$ ,  $v^*$ , and  $w^*$  both inside and outside the boundary layer. Barua's results show good agreement with the experimental findings of Squire (18), Hawes (10), and White (24) and also with the axial velocity profiles, experimentally determined at Dean numbers above 200, presented by Adler (1).

In summary, Dean's (7) analytical work is restricted to Dean numbers below 50, and the solutions provided by Adler (1) and Truesdell (22) are of questionable accuracy for Dean numbers in excess of 200. Thus, of all the theoretical and numerical work done on flow in curved tubes, Barua's (3) solution is the most universally applicable in terms of both the range and the magnitude of Dean numbers that can be considered, being quite accurate for Dean numbers substantially greater than 200.

Weissman and Mockros (23) provide a numerical solution to the mass transfer problem describing the transport of oxygen into and carbon dioxide out of blood flowing in coiled circular tubes at Dean numbers below 50. Some of the solutions provided by Weissman and Mockros also apply to heat transfer problems, since heat transfer requires only the substitution of the Prandtl number for the Schmidt number  $N_{Sc} = \mu/\rho D$ , where  $D$  is the diffusivity.

No strictly theoretical or numerical work has been done in the area of laminar flow heat transfer in curved systems at high Dean numbers.

## CHAPTER III

### MATHEMATICAL DESCRIPTION OF THE PROBLEM

A physical description of the problem with which this work deals is given in detail in the following discussion. A mathematical model in terms of a system of partial differential equations is proposed and a numerical calculation scheme for the solution of the system based on a combination of Barua's (3) work and finite difference approximations is outlined.

#### Description of the Problem

Consider the steady laminar flow of a constant property, Newtonian fluid in a curved tube of radius  $a^*$ , coiled in a circle of radius  $R^*$  under the following conditions: (1) the temperature at the tube wall is maintained at a constant value; (2) the fluid enters the tube with a uniform temperature and a fully developed velocity profile; (3) the direction of flow is "helically horizontal"; (4) the flow is axially symmetric with respect to a horizontal plane passing through the center of the tube and dividing the cross section into two equal halves; and (5) heat generation due to viscous dissipation is negligible.

The above description is represented schematically in figure 2. A compilation of terms and symbols used in this work is presented in the Nomenclature.

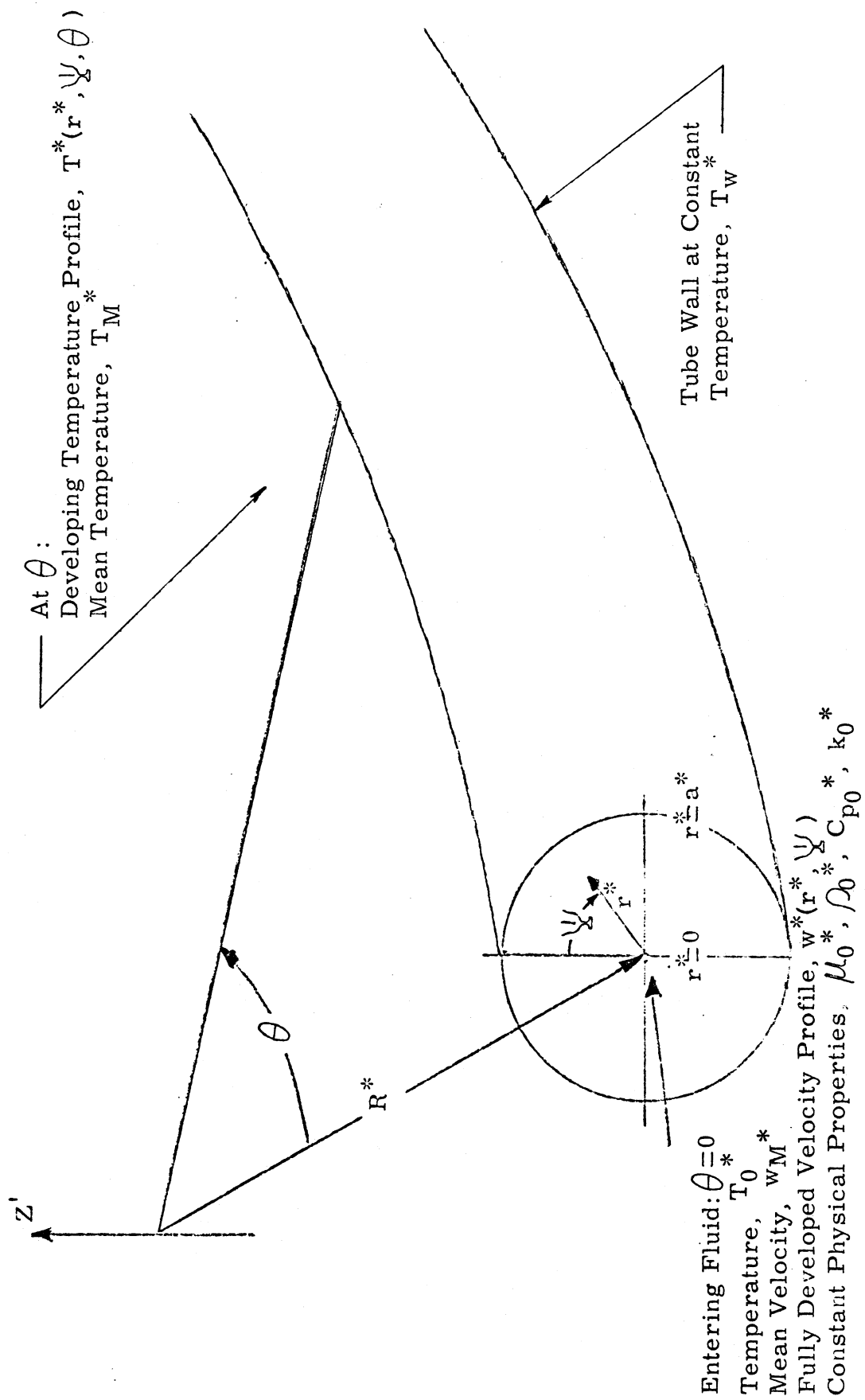


Figure 2. Diagram of Problem

Mathematical Model

The general equations of continuity, motion, and energy in the rectangular, cylindrical, and spherical coordinate systems for laminar flow are given by Bird (5). In order to apply these equations to the problem under consideration, the equations of continuity, motion, and energy in the cylindrical coordinate system were transformed to the helical coordinate system presented by Dean (6), shown in figure 3. A detailed account of this transformation procedure is given in Appendix A. Thus, the equations applying to the present case are

(Continuity)

$$\frac{\partial u^*}{\partial r^*} + \frac{u^*}{r^*} + \frac{u^* \sin \Psi}{R^* + r^* \sin \Psi} + \frac{1}{r^*} \frac{\partial v^*}{\partial \Psi} + \frac{v^* \cos \Psi}{R^* + r^* \sin \Psi} = 0 \quad (1)$$

(Motion)

$$u^* \frac{\partial u^*}{\partial r^*} + \frac{v^*}{r^*} \frac{\partial u^*}{\partial \Psi} - \frac{v^{*2}}{r^*} - \frac{w^{*2} \sin \Psi}{R^* + r^* \sin \Psi} = - \frac{\partial}{\partial r^*} \left[ \frac{P^*}{\rho^*} \right] - v^* \left[ \frac{1}{r^*} \frac{\partial}{\partial \Psi} + \frac{\cos \Psi}{R^* + r^* \sin \Psi} \right] \left[ \frac{\partial v^*}{\partial r^*} + \frac{v^*}{r^*} - \frac{1}{r^*} \frac{\partial u^*}{\partial \Psi} \right] \quad (2)$$

$$u^* \frac{\partial v^*}{\partial r^*} + \frac{v^*}{r^*} \frac{\partial v^*}{\partial \Psi} + \frac{u^* v^*}{r^*} - \frac{w^{*2} \cos \Psi}{R^* + r^* \sin \Psi} = - \frac{1}{r^*} \frac{\partial}{\partial \Psi} \left[ \frac{P^*}{\rho^*} \right] + v^* \left[ \frac{\partial}{\partial r^*} + \frac{\sin \Psi}{R^* + r^* \sin \Psi} \right] \left[ \frac{\partial v^*}{\partial r^*} + \frac{v^*}{r^*} - \frac{1}{r^*} \frac{\partial u^*}{\partial \Psi} \right] \quad (3)$$

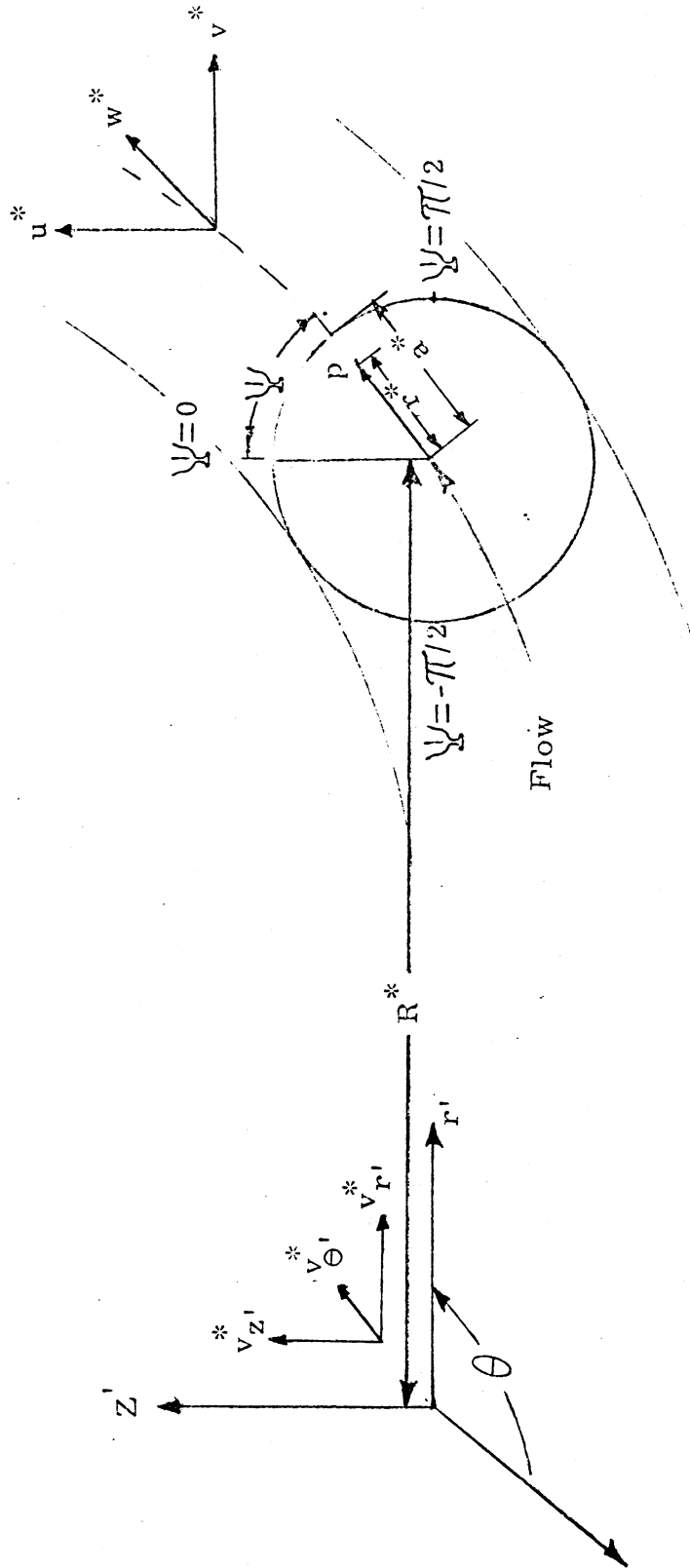


Figure 3. Helical Geometry and Coordinate System

Coordinates  $(r^*, \psi, \theta)$

Velocities  $(u^*, v^*, w^*)$

$$\begin{aligned}
u^* & \frac{\partial w^*}{\partial r^*} + \frac{v^*}{r^*} \frac{\partial w^*}{\partial \Psi} + \frac{u^* w^* \sin \Psi}{R^* + r^* \sin \Psi} + \frac{v^* w^* \cos \Psi}{R^* + r^* \sin \Psi} \\
& = - \frac{1}{R^* + r^* \sin \Psi} \frac{\partial}{\partial \theta} \left[ \frac{P^*}{\rho^*} \right] + \nu^* \left[ \left( \frac{\partial}{\partial r^*} + \frac{1}{r^*} \right) \left( \frac{\partial w^*}{\partial r^*} \right. \right. \\
& \quad \left. \left. + \frac{w^* \sin \Psi}{R^* + r^* \sin \Psi} \right) + \frac{1}{r^*} \frac{\partial}{\partial \Psi} \left( \frac{1}{r^*} \frac{\partial w^*}{\partial \Psi} + \frac{w^* \cos \Psi}{R^* + r^* \sin \Psi} \right) \right] \quad (4)
\end{aligned}$$

(Energy, neglecting viscous dissipation terms)

$$\begin{aligned}
u^* & \frac{\partial T^*}{\partial r^*} + \frac{w^*}{R^* + r^* \sin \Psi} \frac{\partial T^*}{\partial \theta} + \frac{v^*}{r^*} \frac{\partial T^*}{\partial \Psi} = \frac{\nu^*}{N_{Pr}} \left[ \frac{\partial^2 T^*}{\partial r^{*2}} \right. \\
& \quad + \frac{1}{r^*} \frac{\partial T^*}{\partial r^*} + \frac{1}{r^{*2}} \frac{\partial^2 T^*}{\partial \Psi^2} + \frac{\sin \Psi}{R^* + r^* \sin \Psi} \frac{\partial T^*}{\partial r^*} \\
& \quad \left. + \frac{\cos \Psi}{r^* (R^* + r^* \sin \Psi)} \frac{\partial T^*}{\partial \Psi} + \frac{1}{(R^* + r^* \sin \Psi)^2} \frac{\partial^2 T^*}{\partial \theta^2} \right] \quad (5)
\end{aligned}$$

A boundary layer order of magnitude analysis, detailed in Appendix A, was used to simplify equations (1), (2), (3), (4), and (5). These simplified equations are listed below in terms of dimensionless variables.

$$\frac{\partial u}{\partial r} + \frac{1}{r} \frac{\partial v}{\partial \Psi} + \frac{v \cos \Psi}{R + r \sin \Psi} = 0 \quad (\text{Continuity}) \quad (6)$$

$$\frac{-v^2}{r} - \frac{w^2 \sin \Psi}{R + r \sin \Psi} = - \frac{\partial P}{\partial r} \quad (\text{Motion}) \quad (7)$$



$$u \frac{\partial v}{\partial r} + \frac{v}{r} \frac{\partial v}{\partial \Psi} - \frac{w^2 \cos \Psi}{R + r \sin \Psi} = -\frac{1}{r} \frac{\partial P}{\partial \Psi} + \frac{1}{N_{Re}} \frac{\partial^2 v}{\partial r^2} \quad (8)$$

$$u \frac{\partial w}{\partial r} + \frac{v}{r} \frac{\partial w}{\partial \Psi} + \frac{vw \cos \Psi}{R + r \sin \Psi} = -\frac{1}{R + r \sin \Psi} \frac{\partial P}{\partial \theta} + \frac{1}{N_{Re}} \frac{\partial^2 w}{\partial r^2} \quad (9)$$

(Energy)

$$u \frac{\partial T}{\partial r} + \frac{w}{R + r \sin \Psi} \frac{\partial T}{\partial \theta} + \frac{v}{r} \frac{\partial T}{\partial \Psi} = \frac{1}{N_{Pe}} \left[ \frac{\partial^2 T}{\partial r^2} + \frac{1}{r} \frac{\partial T}{\partial r} + \frac{\sin \Psi}{R + r \sin \Psi} \frac{\partial T}{\partial r} + \frac{\cos \Psi}{r(R + r \sin \Psi)} \frac{\partial T}{\partial \Psi} \right] \quad (10)$$

Equations (6), (7), (8), (9), and (10) serve as a basis for the calculations found in the following pages. For the problem of interest, the associated boundary conditions in terms of dimensionless variables are

I.  $\theta = 0 \dots \dots \dots T = 0 (0 \leq r \leq 1/2, -\pi/2 \leq \Psi \leq \pi/2)$

II.  $\theta \geq 0 \dots \dots \dots \mu = \rho = C_p = k = 1 (0 \leq r \leq 1/2, -\pi/2 \leq \Psi \leq \pi/2)$

Fully developed axial velocity profile,  
 $w = w(r, \Psi)$

$$\text{III. } r = 1/2 \dots \dots \dots u = v = w = 0 \quad (\theta \geq 0, -\pi/2 \leq \psi \leq \pi/2)$$

$$T = 1 \quad (\theta > 0, -\pi/2 \leq \psi \leq \pi/2)$$

The dimensionless variables are defined as:

$$Z = \frac{L^*}{D^*} = \frac{R^* \theta}{D^*}, \quad r = \frac{r^*}{D^*}, \quad R = \frac{R^*}{D^*}, \quad u = \frac{u^*}{w_M^*}, \quad v = \frac{v^*}{w_M^*}$$

$$w = \frac{w^*}{w_M^*}, \quad T = \frac{T^* - T_0^*}{T_w^* - T_0^*}, \quad P = \frac{P^*}{\rho^* w_M^{*2}}, \quad \mu = \frac{\mu^*}{\mu_0^*}$$

$$\rho = \frac{\rho^*}{\rho_0^*}, \quad k = \frac{k^*}{k_0^*}, \quad C_P = \frac{C_P^*}{C_{P_0}^*}, \quad N_{Re} = \frac{w_M^* \rho^* D^*}{\mu^*}$$

$$N_{Pr} = \frac{C_P^* \mu^*}{k^*}, \quad N_{Pe} = N_{Re} N_{Pr}$$

The star indicates a dimensional quantity, the subscript 0 indicates entrance conditions, the subscript w indicates wall conditions, and  $w_M^*$  represents the mean fluid velocity.

### Outline of Numerical Solution

Barua (3) provides an approximate solution to equations (6), (7), (8), and (9) which yields analytical expressions for the velocity components  $u^*$ ,  $v^*$ , and  $w^*$ . Barua found that the axial velocity profile was

greatly distorted from the classical parabolic form commonly encountered in straight pipe laminar flow. His analysis also showed that the  $w^*$  component of velocity was generally 10 to 100 times greater than the  $u^*$  or  $v^*$  component. A discussion of Barua's work is given in Appendix B.

Using dimensionless forms of the velocity profiles given by Barua (3), the equation of energy was solved numerically by replacing partial derivatives with corresponding finite difference approximations. The accuracy of the axial velocity profiles generated using Barua's (3) work was tested using equation (81), as presented in Appendix C.

Although a number of attempts were made to solve equation (10) numerically, while including the radial and angular velocity components,  $u$  and  $v$ , all attempts proved to be numerically unstable. This is unfortunate, but local Nusselt numbers calculated at the inner and outer tube walls in the plane of symmetry would remain unaffected, as at these points,  $u = v = 0$ . Also, as previously mentioned, the axial component of velocity is substantially greater than either the radial or angular component. Thus, the deletion of the  $u$  and  $v$  velocity components from equation (10) should not result in a significant error.

In order to devise a numerical method by which equation (10) may be solved numerically, consider a semi-infinite series of cross sectional grids superimposed on half of the flow field, as shown in figure 4. The grid is used to locate point functions defined in terms of functional

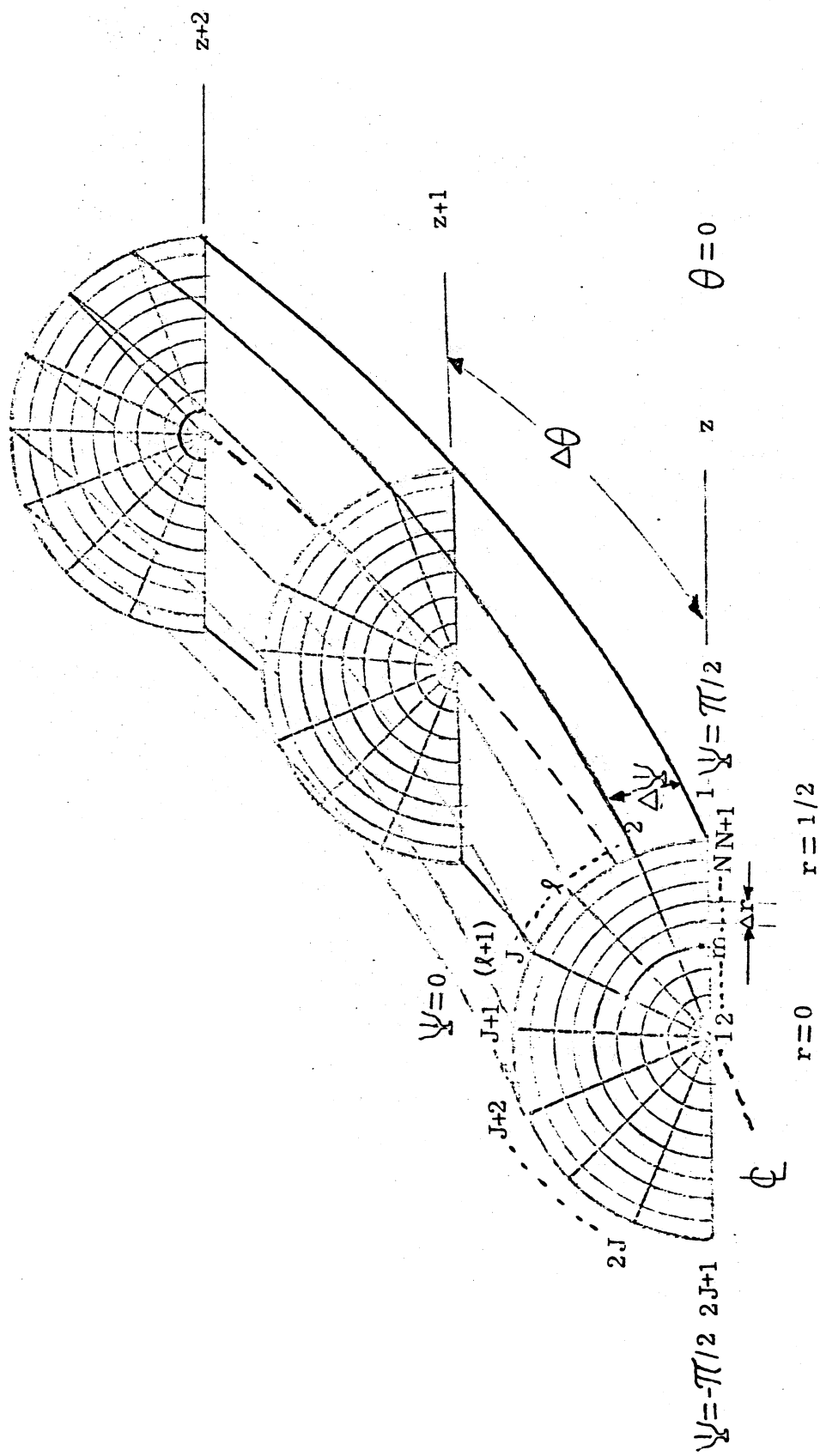


Figure 4. Initial Portion of the Finite Difference Grid

notation as

$$f_{m, \ell, z} = f \left[ (m-1) \Delta r, \pi/2 - (\ell - 1)\Delta\psi, (z-1)\Delta\theta \right]$$

The variables in equation (10) are considered point functions on this grid and the derivatives are replaced by finite difference approximations. These approximations lead to systems of linear algebraic equations. The resulting algebraic equations are summarized below in matrix-vector notation.

In matrix-vector notation, the finite difference equations of energy at  $\psi = \pi/2$  can be written as

$$\underline{A}_1 \vec{t}_1 = \vec{b}_1 \quad (11)$$

This equation applies at step  $z + 1$  and all components of  $\underline{A}_1$  and  $\vec{b}_1$  are either constants or are values determined at steps up to and including  $z + 1$ . The matrix  $\underline{A}_1$  is tridiagonal in form. Thus, equation (11) must be solved for  $\vec{t}_1$ , which represents point values of the temperature, for  $0 \leq r \leq 1/2 - \Delta r$  and  $\psi = \pi/2$ .

With  $\vec{t}_1$  known, the finite difference equations of energy at  $\psi = \pi/2 - \Delta\psi$ , i. e., at angular grid step  $\ell = 2$ , can be written in matrix-vector notation as

$$\underline{A}_2 \vec{t}_2 = \vec{b}_2 \quad (12)$$

Again, this equation applies at step  $z + 1$  and all components of  $\underline{A}_2$  and  $\vec{b}_2$  are either constants or values previously calculated, such as  $\vec{t}_1$ . The matrix  $\underline{A}_2$  is also tridiagonal in form. Equation (12) is solved for  $\vec{t}_2$ , giving point values of the temperature for  $0 + \Delta r \leq r \leq 1/2 - \Delta r$ ,

$$\Psi = \pi/2 - \Delta\Psi.$$

In like manner, the angular marching progression is continued around the semi-circular cross section. In matrix-vector notation, the remaining equations may be represented by

$$\underline{A}_\ell \vec{t}_\ell = \vec{b}_\ell, \quad \text{for } \ell = 3, 4, \dots, 2J + 1 \quad (13)$$

As in equations (11) and (12), the above equation applies at axial step  $z + 1$  and all components of  $\underline{A}_\ell$  and  $\vec{b}_\ell$  are constants or values previously calculated. As before, matrix  $\underline{A}_\ell$  is tridiagonal in form and when equation (13) is solved for  $\vec{t}_\ell$ , point values of the temperature are obtained for  $\Delta r \leq r \leq 1/2 - \Delta r$  and  $\Psi = \pi/2 - (\ell - 1)\Delta\Psi$ .

After all point values of the temperature have been calculated at axial step  $z + 1$ ,  $\theta$  is increased by  $\Delta\theta$  and the above described calculation scheme is repeated at axial step  $z + 2$ .

This numerical procedure calls for the use of a simple, but highly accurate computational scheme, which provides the solution vector for a matrix-vector equation, the coefficient matrix of which is tridiagonal in form. This scheme is applicable to tridiagonal matrices of a high

order and is very efficient with respect to computer time.

With the temperature field known for a given cross section, arithmetic mean and local Nusselt numbers can be calculated as a function of the Graetz number.

A more detailed description of the elements of the matrices and vectors in the above equations and an expanded description of the numerical calculation scheme are given in Appendix C.

The computer program used to implement the numerical procedure is included in Appendix D.

## CHAPTER IV

### NUMERICAL RESULTS

The overall goal of this work was to develop a calculation procedure for equation (10) for the case of constant property laminar flow heat transfer in a curved tube with constant wall temperature. Only the axial velocity component was included in this analysis. The results obtained using the numerical scheme developed are given in this chapter. The axial velocity profile was generated using Barua's (3) method, details of which are found in Appendix B. The general calculation scheme has been previously summarized in Chapter III, and details are given in Appendix C.

#### Cases Considered

Parameters varied included  $N_{Re}$ ,  $N_{Pr}$ , and  $a^*/R^*$ , dimensionless groups arising from and found in the non-dimensional equations of continuity, motion, and energy. A total of ten different fluid mechanical and heat transfer situations were investigated. Each numerical solution required approximately one hour of computer time. A summary of the cases considered for analysis is given in table 1.

#### Comparison with Straight Pipe Graetz Solution

The Classical Graetz problem for constant property laminar flow heat transfer in a straight tube with constant wall temperature has been



TABLE I. SUMMARY OF CASES AND PARAMETERS STUDIED

Run No.	$N_{Re}$	$N_{Pr}$	$N_{Pe}$	$N_{De}$	$a^*/R^*$	$\mathcal{L}_w$	
						Calculated	% deviation*
1	6000	1	6000	1154	1/27	0.9916	0.84
2	6000	20	120,000	1154	1/27	0.9916	0.84
3	6000	50	300,000	1154	1/27	0.9916	0.84
4	2000	50	100,000	385	1/27	1.0010	0.10
5	6000	50	300,000	1455	1/17	0.9891	1.09
6	2000	50	100,000	485	1/17	0.9968	0.32
7	6000	50	300,000	1446	1/17.21	0.9891	1.09
8	6000	50	300,000	1633	1/13.5	0.9876	1.24
9	6000	50	300,000	2433	1/6.08	0.9829	1.71
10	6000	50	300,000	190	1/1000	0.9999	0.01

\* Deviation from value predicted by Equation (81)

solved analytically (11). To test the convergence of the numerical scheme to the limiting case of straight pipe flow, a curvature ratio of 1/1000 and a parabolic velocity profile was incorporated into the numerical model. (For straight tubes,  $a^*/R^* \rightarrow 1/\infty$ ). Calculated values, shown in figure 5, were consistently within 1 to 2% of the analytically derived values given by  $N_{Nu_{a.m.}} = 1.75 (N_{Gz})^{1/3}$ , for  $N_{Gz} > 10$  (12).

### Comparison with Experiment

As previously mentioned in Chapter II, Kubair and Kuloor (12) as well as Berg and Bonilla (4) have recorded experimental laminar flow heat transfer data for a variety of curved systems with constant wall temperature, while Seban and McLaughlin (16) took data under constant heat flux conditions. All of the above experimentalists achieved variation of the Graetz number by changing the mass flow rate and thus, the Reynolds number. Consequently, data taken at a specified curvature ratio and Prandtl number are recorded at a variety of Dean numbers.

Kubair and Kuloor (12) determined the laminar or turbulent state of flow by employing the friction factor vs.  $N_{Re}$  method, using data taken isothermally. This would appear to be a poor criteria for the judgement of whether the flow is laminar during heat transfer, as heat transfer data is taken with an initial temperature difference between the tube wall and entering fluid of approximately 75°C. Due to the large temperature difference employed, the effects of secondary motion could well be

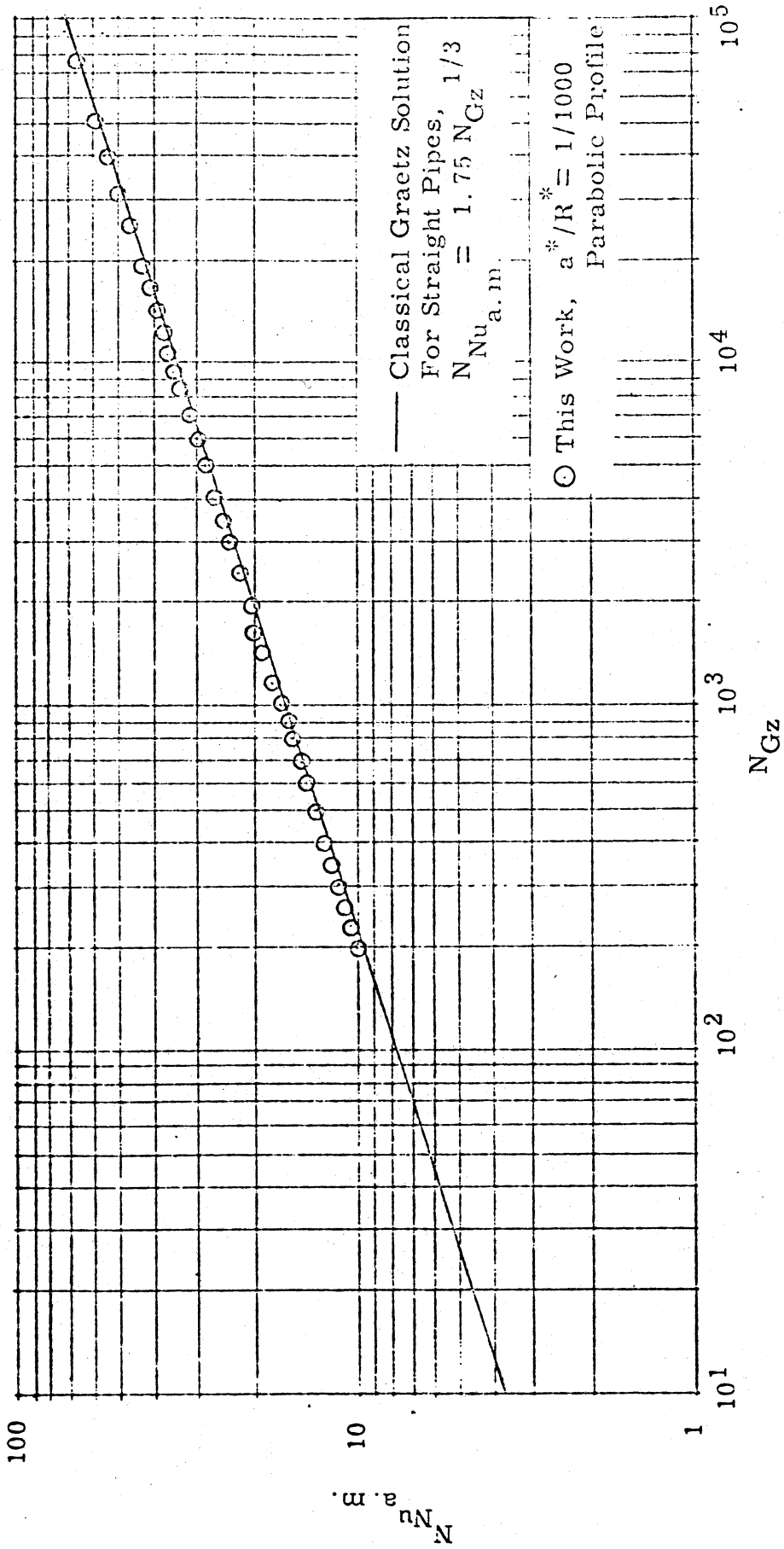


Figure 5. Comparison of Numerical Scheme with Classical Graetz Solution

enhanced to cause turbulence at lower  $N_{Re}$  than would be expected.

Kubair and Kuloor's (12) data is generally higher than that of Berg and Bonilla (4), who actually record some values of  $N_{Nu_{a.m.}}$  that are lower than corresponding straight pipe values.

Although the boundary conditions employed differ from those of this work, the data gathered by Seban and McLaughlin (16) are presented for comparison with local Nusselt numbers generated using the numerical scheme developed in this work. Judging by analogous straight pipe situations (11), it would follow that the local values recorded under constant heat flux conditions are higher than corresponding constant wall temperature values.

Comparison between calculated and experimental values having comparable curvature ratios is given in figures 6 and 7. In general, the experimental data is scattered and no final conclusion can be drawn as to numerical and experimental agreement. It is felt, however, that the effect of fluid property variation with temperature, which would be enhanced by the secondary motion of the fluid, could definitely increase heat transfer coefficients. The effect of variable properties on heat transfer in straight tubes has been amply demonstrated by Wilkins (25).

### Numerical Solutions

All cases considered showed curved pipe heat transfer characteristics to be greater than corresponding straight pipe values. Figures

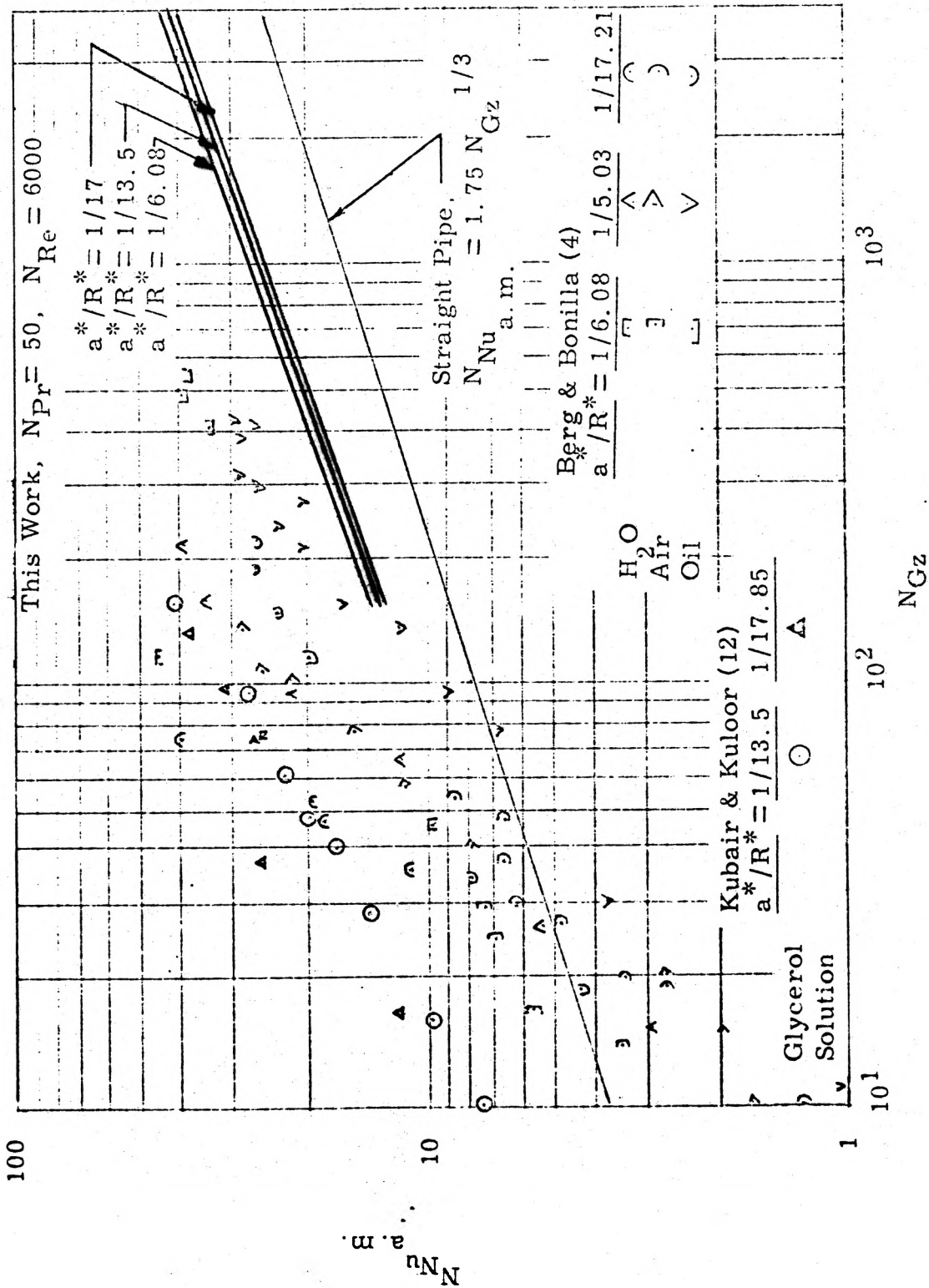


Figure 6. Numerical and Experimental Comparison of Arithmetic Mean Nusselt Numbers

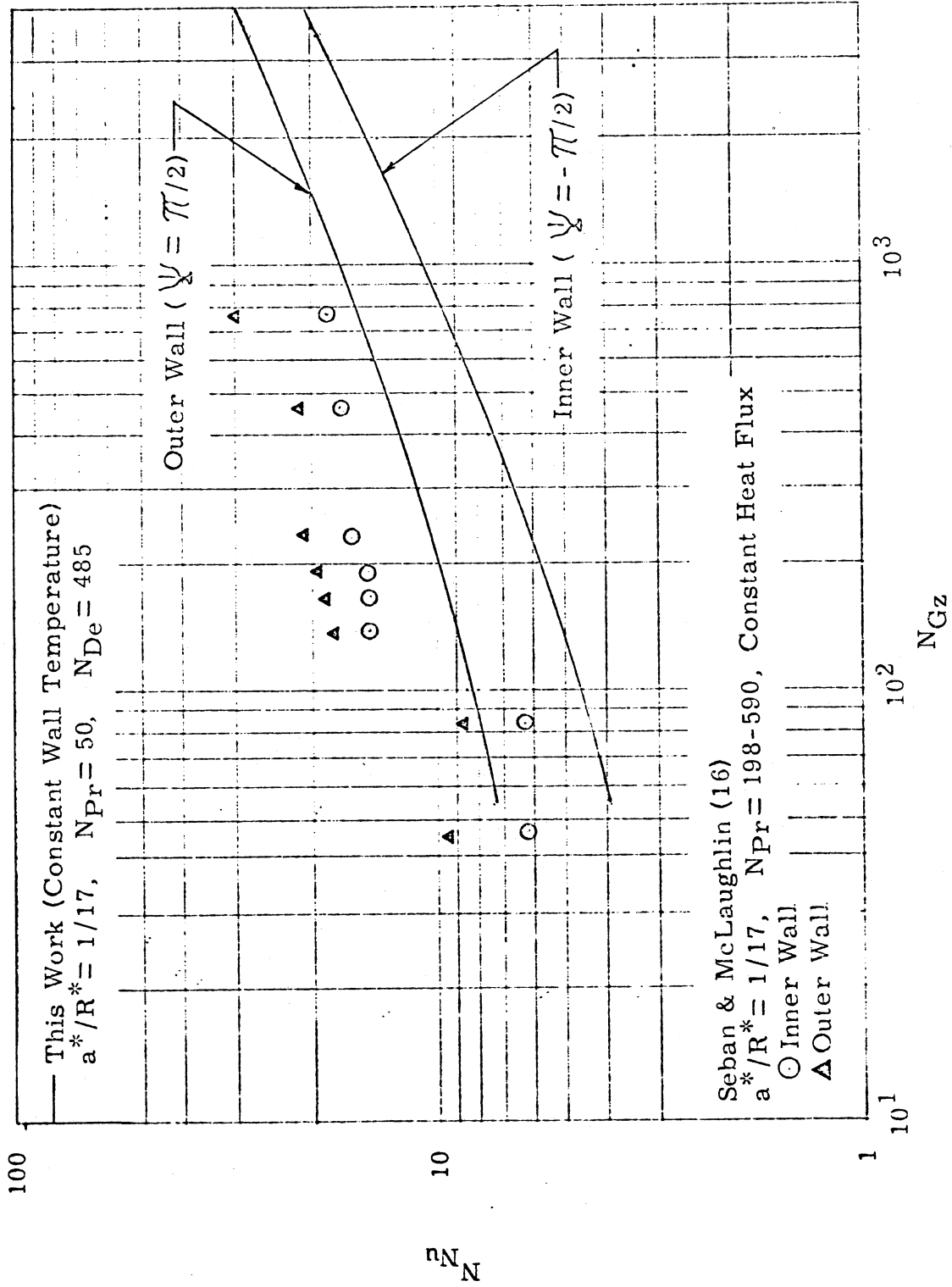


Figure 7. Numerical and Experimental Comparison of Local Nusselt Numbers

8 and 9 show that as the Dean number increases, so also does the arithmetic mean Nusselt number. Depending on the  $N_{De}$ , increases in  $N_{Nu_{a.m.}}$  from 20 to 60 per cent were realized over straight pipe values.

Figure 10 reveals a small, but insignificant Prandtl number effect. A more noticeable Prandtl effect might be realized if the  $\Psi$ -component of velocity had been included in the analysis.

Figures 11 and 12 show that the local Nusselt number is 60 to 90 per cent greater at the outer as opposed to the inner wall of the tube. This is to be expected, as the region of maximum axial velocity is shifted near the outer wall. Also, the "Dean number effect" is again observed.

As expected, the temperature profile and thus the mean temperature was found to develop more rapidly at lower  $N_{Pr}$ . This phenomena is shown graphically in figures 13 and 14.

The angular development of a typical temperature profile is shown in figures 15 and 16. Due to the distortion of the axial velocity profile caused by secondary flow, the temperature profile develops faster near the inner wall. The development of a temperature profile in the plane of symmetry is shown in figure 17. The development of characteristic temperature profiles as a function of  $N_{Gz}$  is shown in figure 18.

#### Calculation Conditions

The original goal of this work was to solve equation (10) numerically, while including all three velocity components. Numerous attempts were

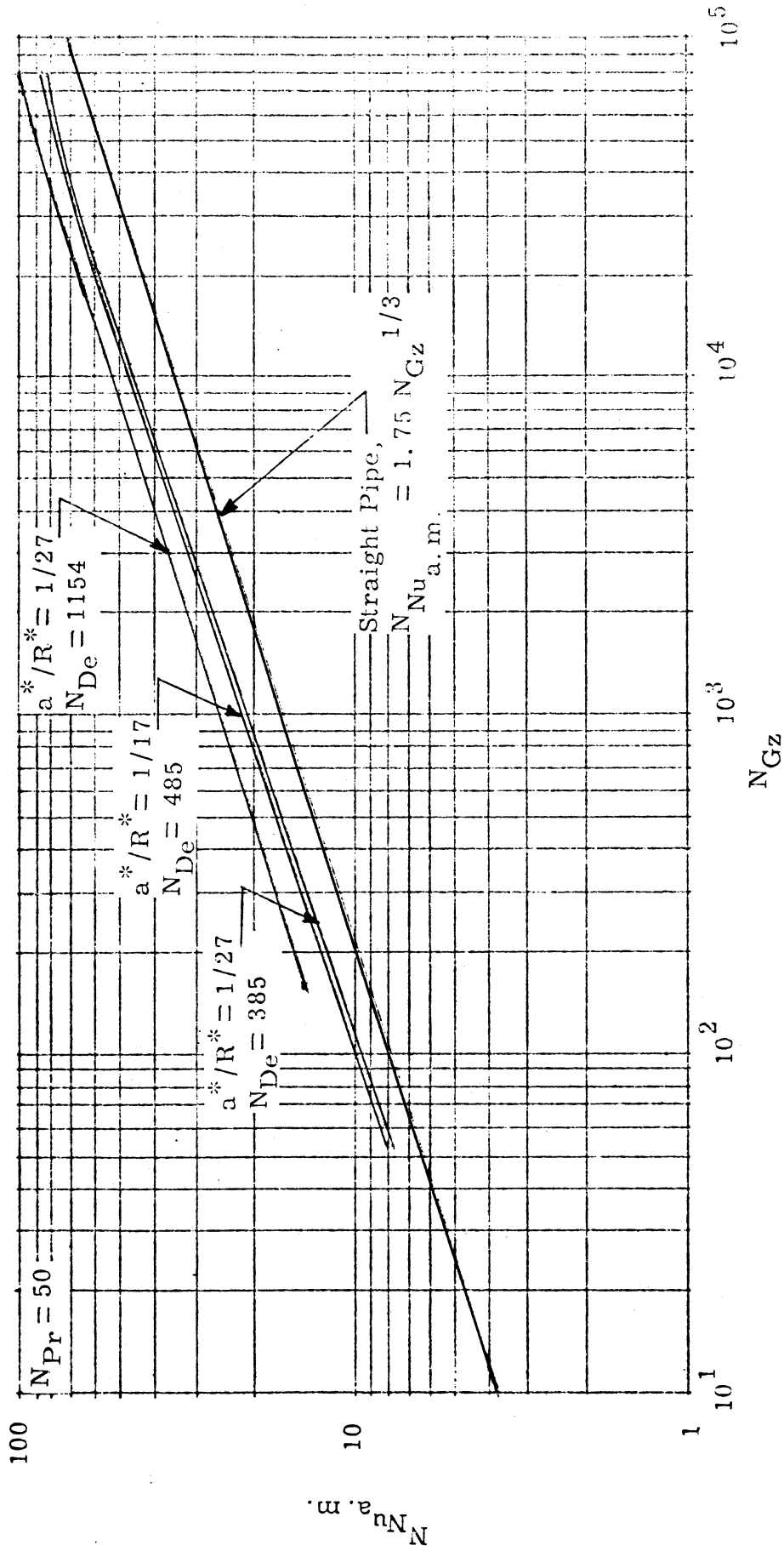


Figure 8. Arithmetic Mean Nusselt Numbers at Dean Numbers of 385, 485, and 1154



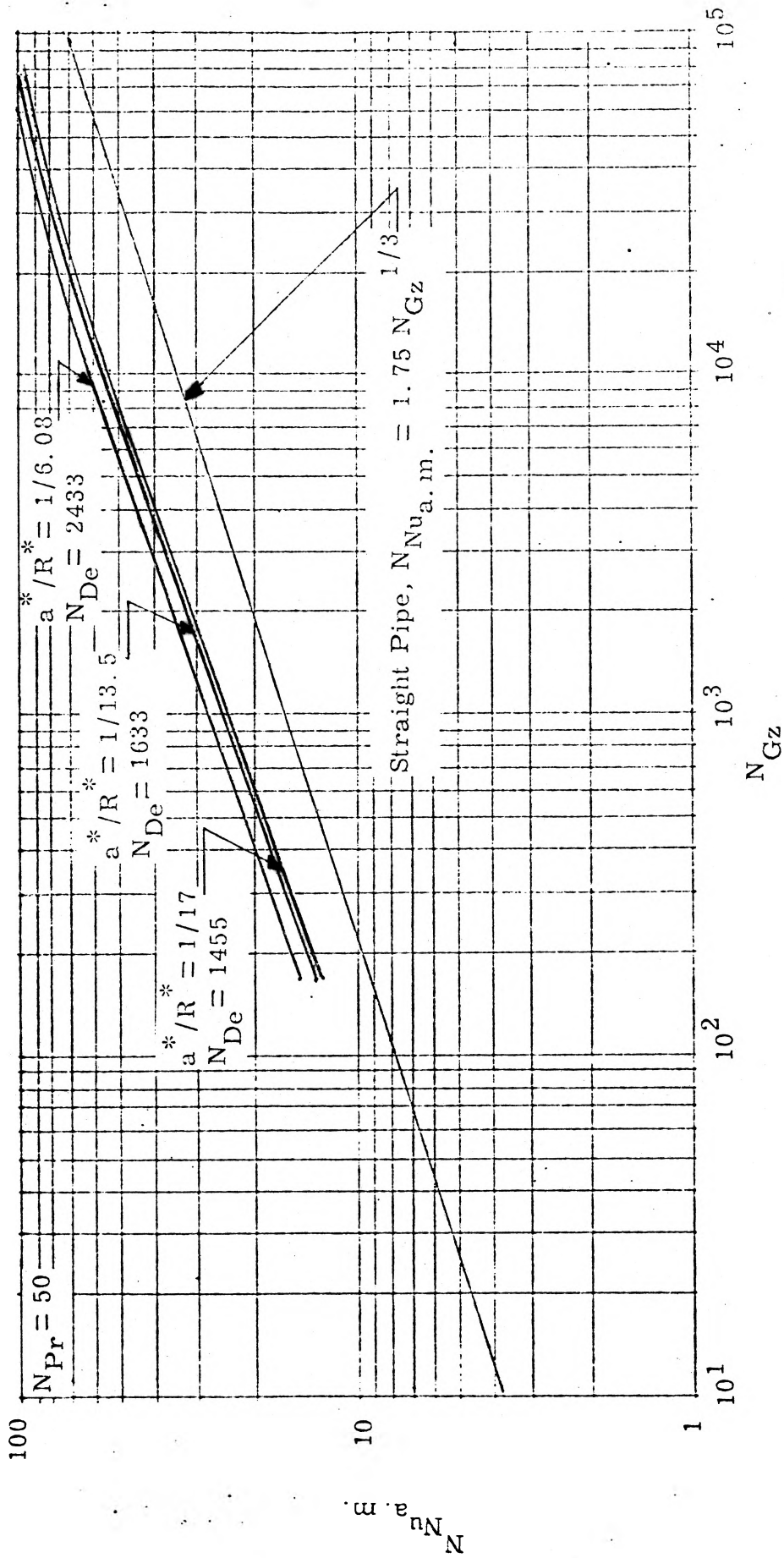


Figure 9. Arithmetic Mean Nusselt Numbers at Dean Numbers of 1455, 1633, and 2433

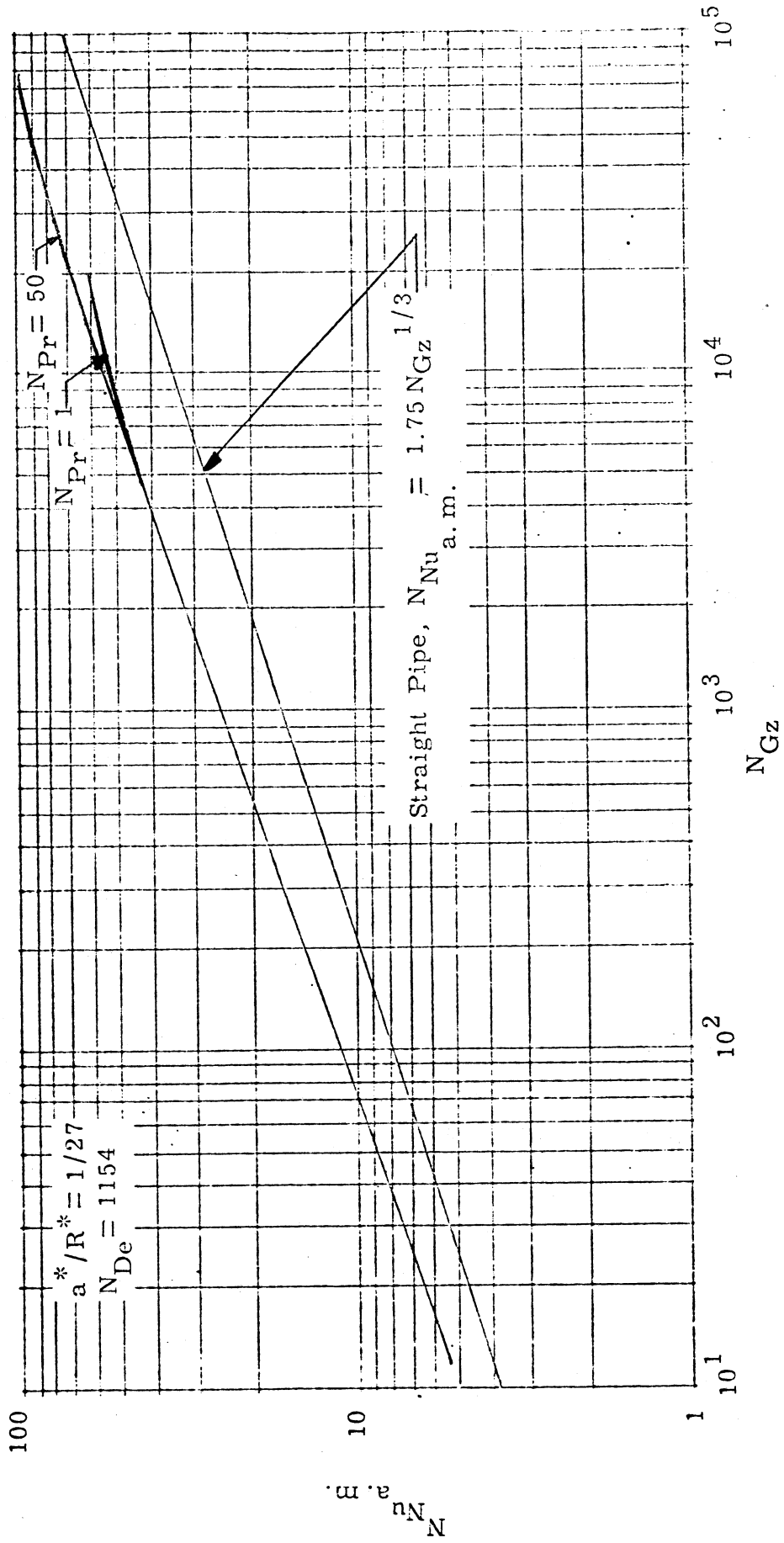


Figure 10. Illustration of Prandtl Number Effect

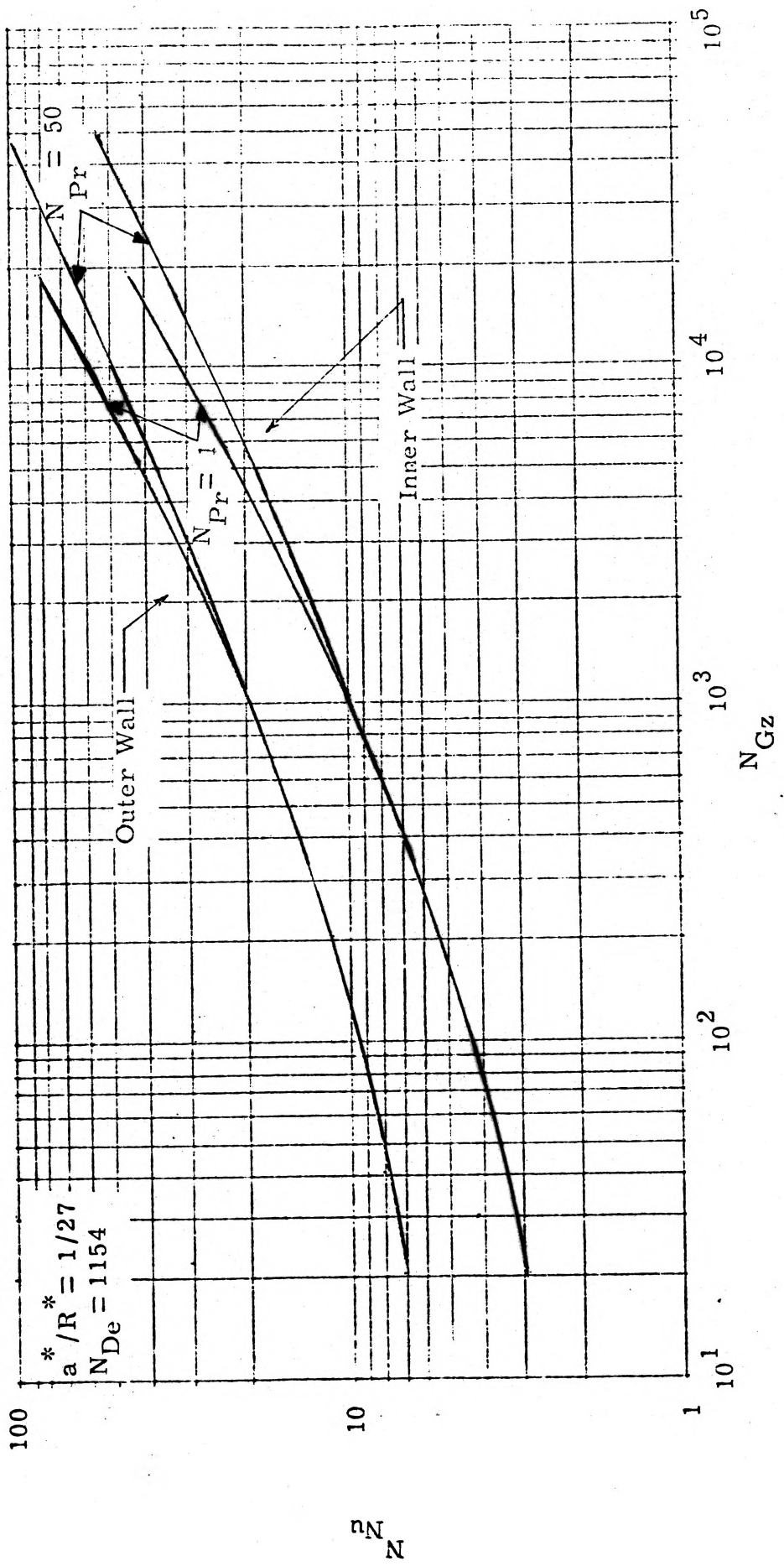


Figure 11. Local Nusselt Numbers at Inner and Outer Walls

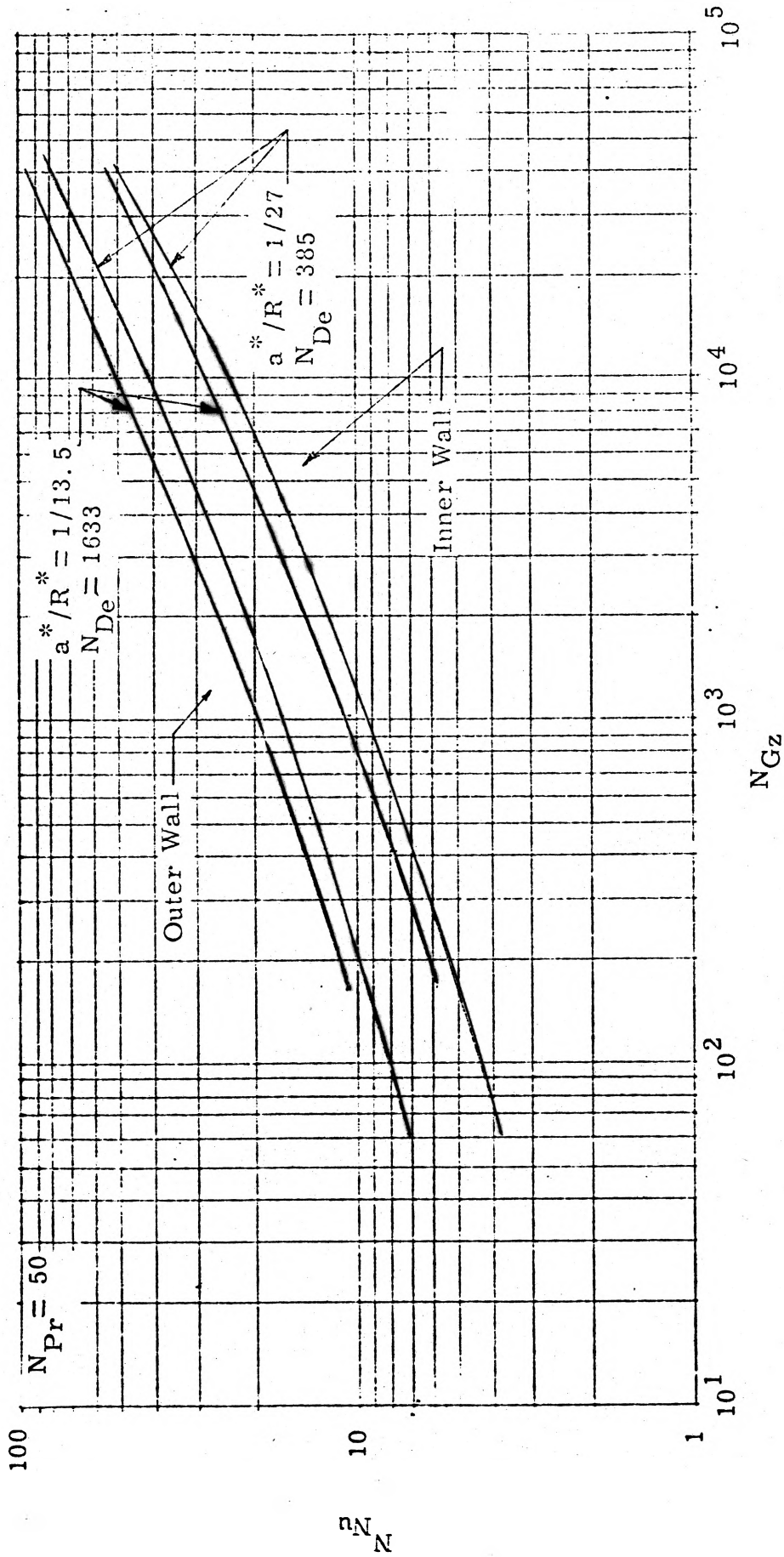


Figure 12. Local Nusselt Numbers at Inner and Outer Tube Walls for Dean Numbers of 385 and 1633

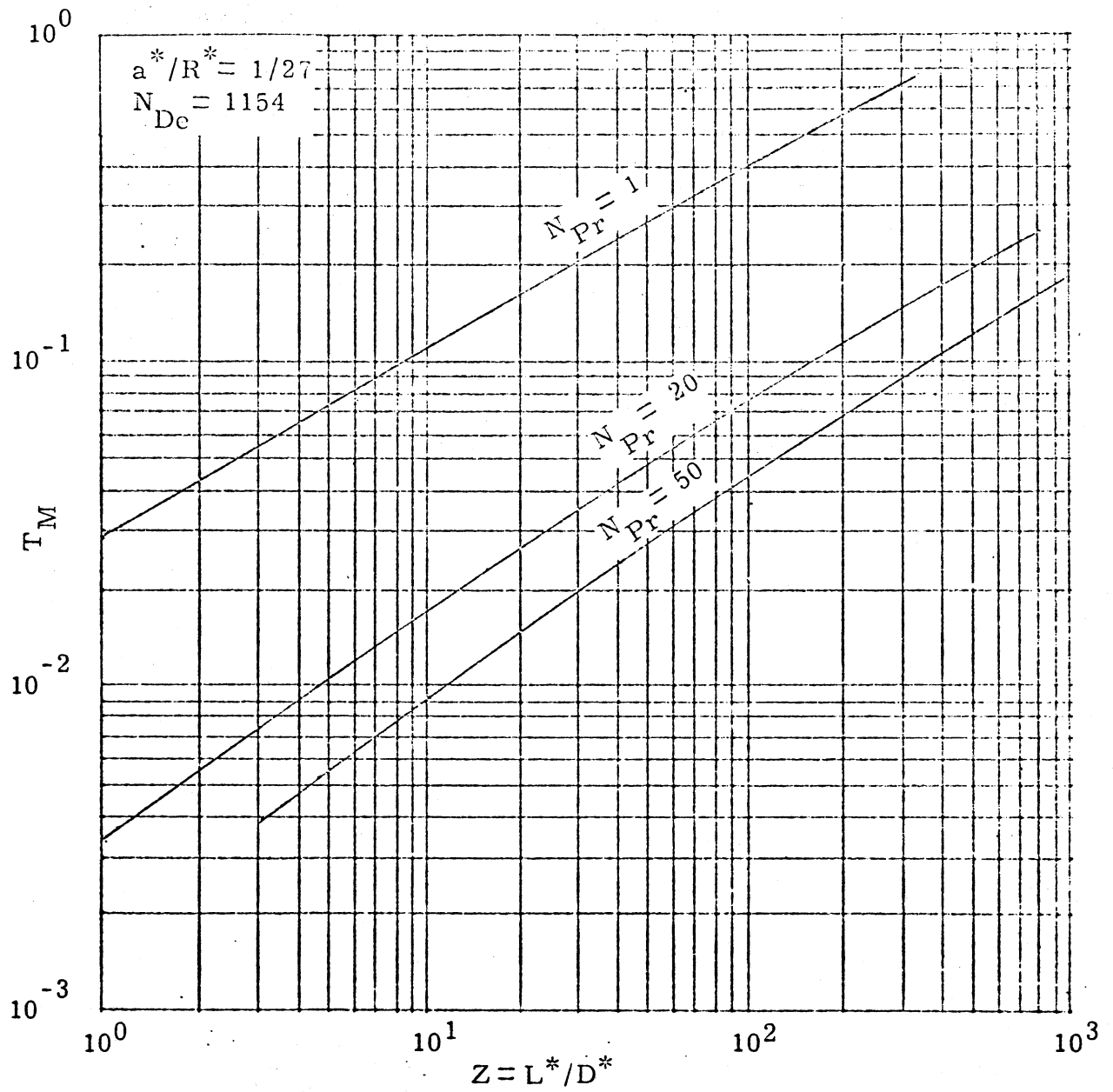


Figure 13. Mean Temperature Development as a Function of Distance Down the Pipe

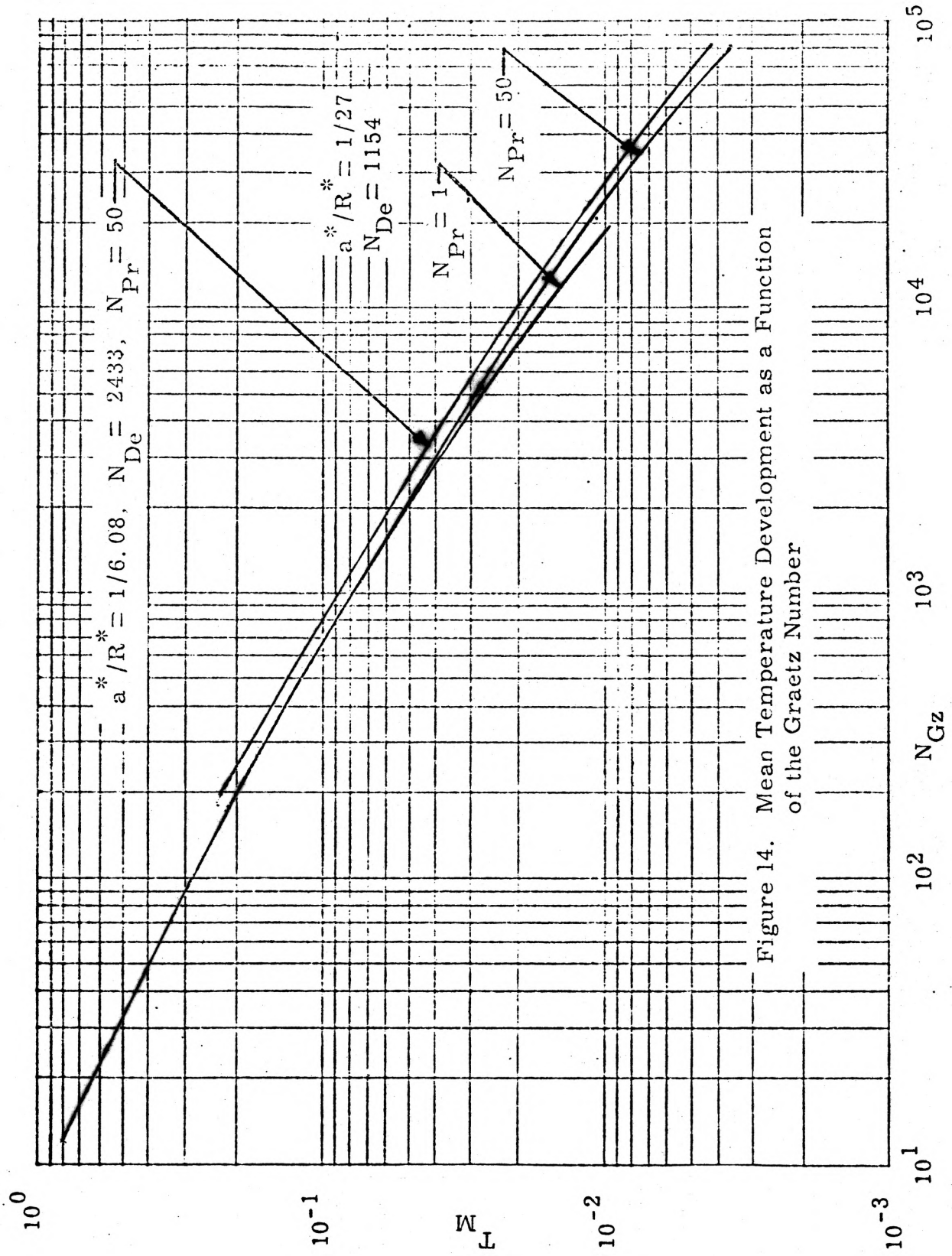


Figure 14. Mean Temperature Development as a Function of the Graetz Number

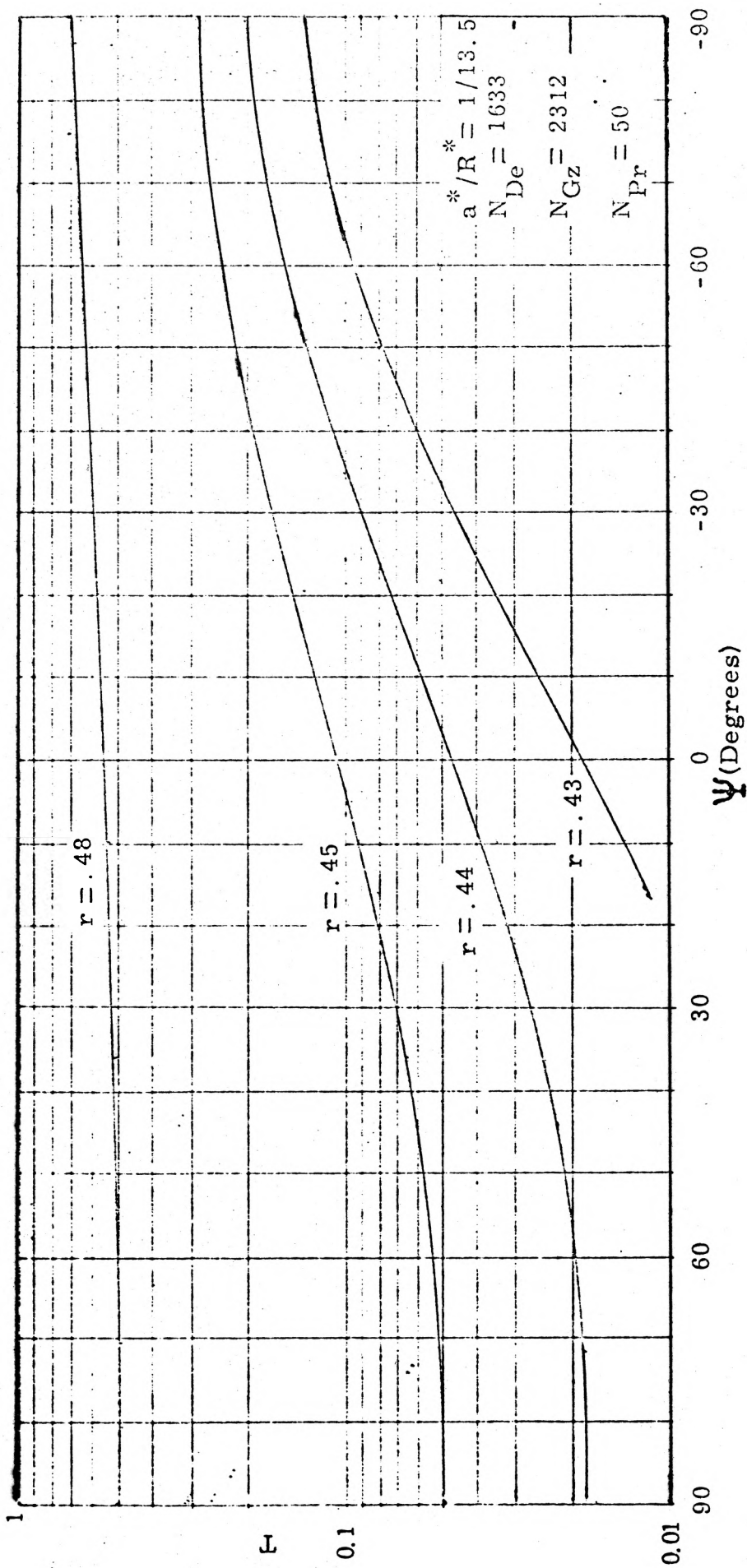


Figure 15. Angular Temperature Profiles for a Graetz Number of 2312

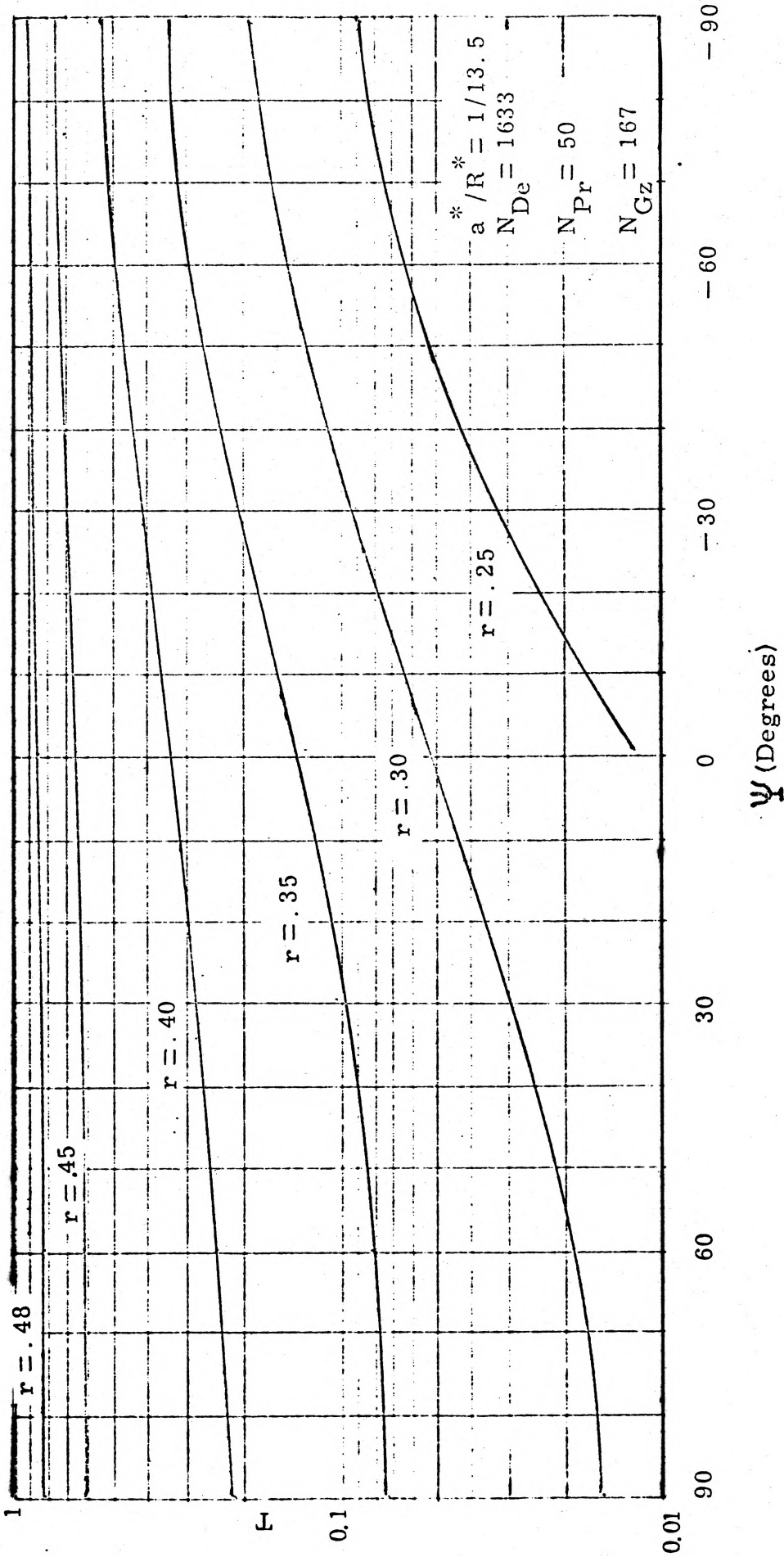


Figure 16. Angular Temperature Profiles for a Graetz Number of 167



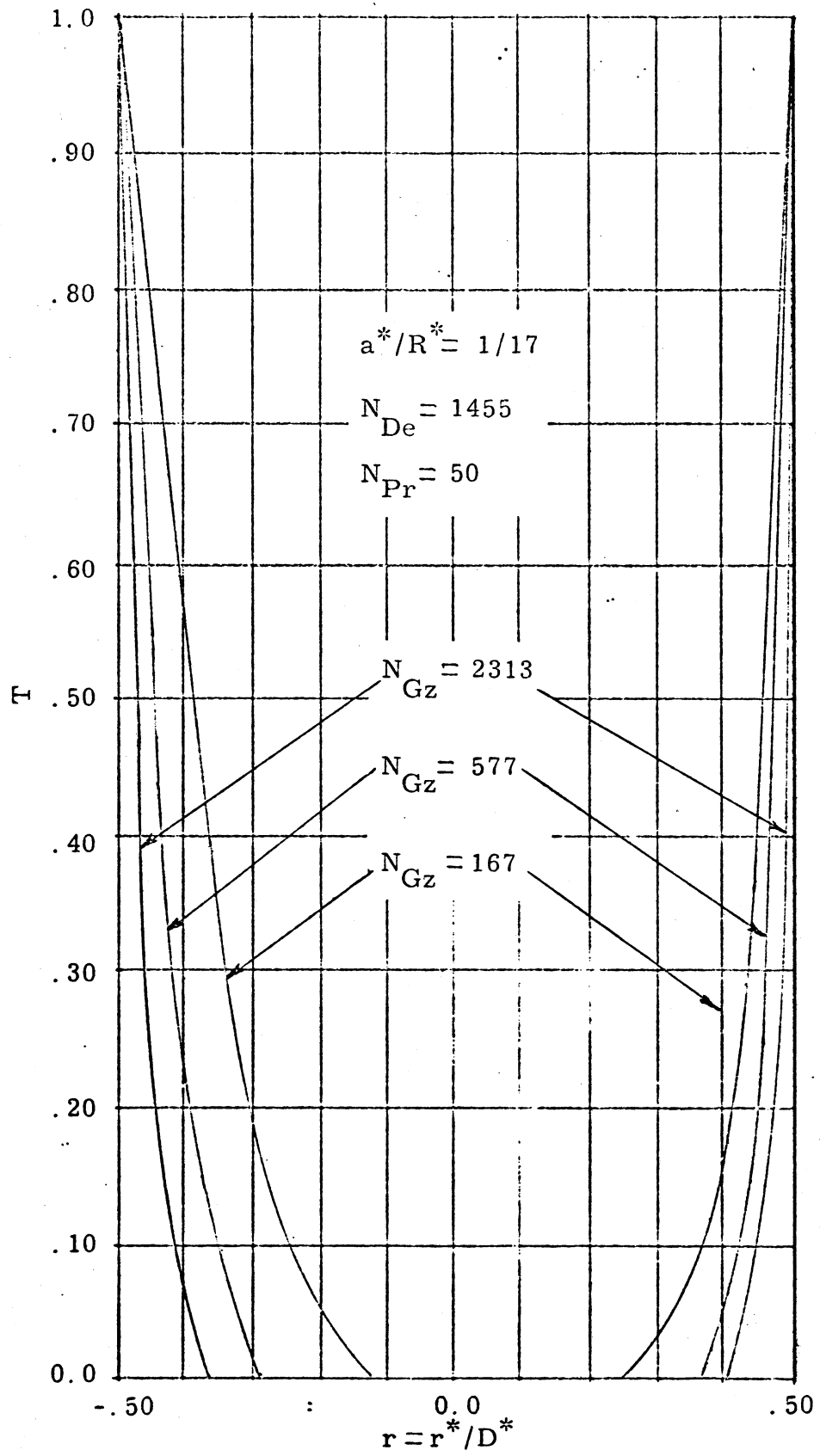


Figure 17. Radial Temperature Profiles in the Plane of Symmetry

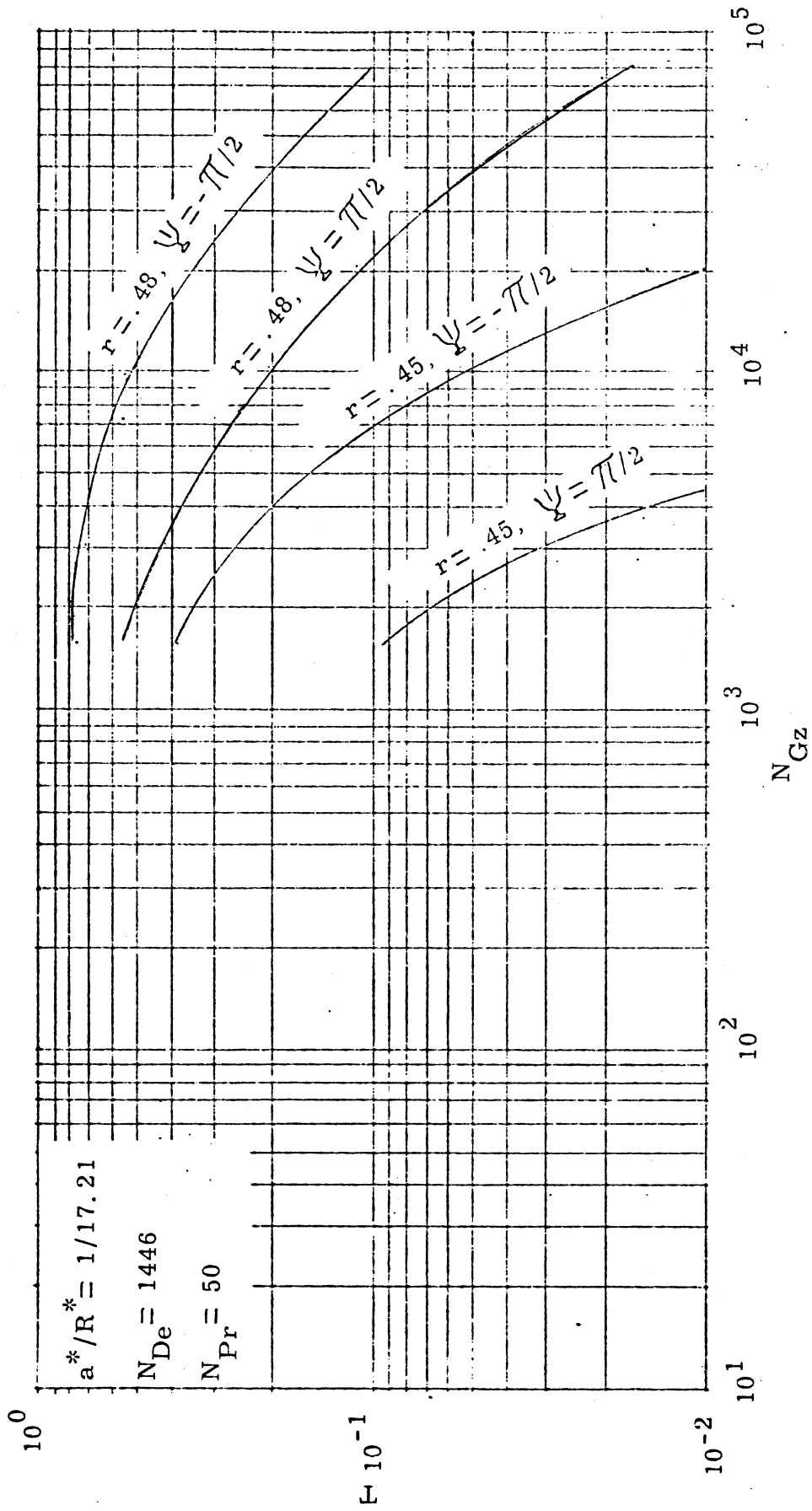


Figure 18. Axial Temperature Profiles

made to achieve this goal, but all numerical schemes including the u and v velocity components proved to be numerically unstable after only a few axial steps.

For the case under consideration, the optimum number of radial grid steps was found to be 50, while only 10 angular steps were determined to be necessary. This, of course, called for the solution of a system of roughly 500 equations at each axial step.

As previously emphasized, the temperature profile was found to develop more quickly for lower  $N_{Pr}$ , as shown in figure 13. Thus, the selection of an optimum axial step size is intimately coupled with this behavior. For cases involving  $N_{Pr}$  of 1 and 20, a  $\Delta Z$  of 0.5 pipe diameters was used for the first 100 axial steps. A step size of 1.5 pipe diameters was employed for the next 100 steps, after which a  $\Delta Z$  of 5 pipe diameters was utilized. For the more slowly developing temperature profile created at  $N_{Pr} = 50$ , axial step sizes used for the first, second, and third 100 step intervals were 1, 3, and 10 pipe diameters respectively.

## CHAPTER V

### CONCLUSIONS AND RECOMMENDATIONS

#### Conclusions

Based on this work, the following conclusions are reached:

- (1) Significant increases in laminar flow heat transfer characteristics at high Dean numbers for curved systems are realized over corresponding straight pipe values, even when only the axial velocity component is included in the analysis.
- (2) Comparison between calculated and experimental values shows that the angular and radial velocity components may add to curved tube heat transfer characteristics.
- (3) A definite "Dean Effect" exists, i. e. , as the  $N_{De}$  is increased, so also are the corresponding heat transfer coefficients.
- (4) Local Nusselt numbers (and thus local heat transfer coefficients) are significantly greater at the outer, rather than at the inner wall of a curved system.
- (5) Temperature profiles develop more rapidly and thus temperatures are greater at the inner wall of a curved tube.
- (6) Barua's (3) method, apparently never before tested in a numerical manner, predicts accurate values for axial velocity profiles at high Dean numbers in curved systems.
- (7) The solutions presented in this study are also applicable to cases

involving low mass transfer rates at high Dean numbers. For mass transfer, one need only substitute the Schmidt number,  $N_{Sc} = \mu/\rho D$ , where  $D$  is the diffusivity, for the Prandtl number.

### Recommendations

Recommendations for additional studies are suggested by this work.

They are:

- (1) The development of another numerical scheme, which would include radial and angular velocity terms, more fully describing curved system flow.
- (2) The extension of this work to the case of variable property solutions.
- (3) The more precise and well planned measurement of additional curved tube heat transfer data over a wide range of parameters.

## NOMENCLATURE

This table contains symbols used frequently throughout this work. Common mathematical symbols or symbols defined and used locally are not included. Dimensional variables are starred to distinguish them from non-dimensional quantities. Vector quantities are denoted by an arrow.

<u>SYMBOL</u>	<u>DEFINITION</u>
$A_1$	matrix defined by equation (93)
$A_f$	matrix defined by equation (107)
$a^*$	radius of pipe, ft.
$\vec{b}_1$	vector defined by equation (100)
$\vec{b}_f$	vector defined by equation (112)
$c_p$	dimensionless heat capacity, $(c_p^*/c_{p0}^*)$
$D^*$	pipe diameter, ft.
$g$	dimensionless transverse velocity (used in Barua's (3) analysis)
$g_L^*$	acceleration of gravity in axial direction, ft/sec <sup>2</sup>
$H$	dimensionless enthalpy, $\frac{H^*}{c_{p0}^*(T_w^* - T_0^*)}$
$H^*$	enthalpy, $c_{p0}^*(T^* - T_0^*)$ , BTU/lb <sub>m</sub>
$h^*$	local heat transfer coefficient, BTU/ft <sup>2</sup> -hr-°F

SYMBOLDEFINITION $h^*_{a. m.}$ arithmetic mean heat transfer coefficient, BTU/ft<sup>2</sup>-hr-°F. $\mathcal{I}_T$ 

integral defined by equation (119)

 $\mathcal{I}_w$ 

integral defined by equation (81)

 $k$ dimensionless thermal conductivity, ( $k^*/k_0^*$ ) $L^*$ axial length, ( $R^*\theta$ ), ft. $N_{De}$ Dean number,  $N_{Re} (a^*/R^*)^{1/2}$  $N_{Gz}$ Graetz number,  $(\pi/4)N_{Pe} (D^*/L^*)$  $N_{Nu}$ local Nusselt number,  $\frac{h^*D^*}{k^*}$  $N_{Nu_{a. m.}}$ arithmetic mean Nusselt number,  $\frac{h^*_{a. m.} D^*}{k^*_{a. m.}}$  $N_{Pe}$ Peclet number, ( $N_{Re} N_{Pr}$ ) $N_{Pr}$ Prandtl number,  $\frac{c_p^* \mu^*}{k^*}$  $N_{Re}$ Reynolds number,  $\frac{w_M^* \rho^* D^*}{\mu^*}$  $P$ dimensionless pressure, ( $P^*/\rho^* w_M^{*2}$ ) $Q^*$ 

heat flow, BTU/hr

 $r^*$ 

dimensional cross sectional radial coordinate, ft. (See figure 3.)

 $\Delta r$ 

radial grid spacing

<u>SYMBOL</u>	<u>DEFINITION</u>
$r$	dimensionless cross sectional radial coordinate ( $r^*/D^*$ )
$R^*$	radius of curvature of the curved system, ft.
$R$	dimensionless radius of curvature, ( $R^*/D^*$ )
$T^*$	local temperature, °F
$T$	dimensionless temperature, $\frac{T^* - T_0^*}{T_w^* - T_0^*}$
$T_M$	dimensionless mean temperature, defined by equation (119)
$\vec{t}_1$	vector defined by equation (99)
$\vec{t}_l$	vector defined by equation (111)
$u^*$	radial velocity component, ft/sec
$u$	dimensionless radial velocity component, ( $u^*/w_M^*$ )
$\vec{V}^*$	net velocity vector, ft/sec
$v^*$	$\Psi$ - component of velocity, ft/sec
$v$	dimensionless $\Psi$ -velocity component, ( $v^*/w_M^*$ )
$v_0$	dimensionless $\Psi$ -velocity component at boundary layer edge (used in Barua's (3) analysis)
$W_f^*$	mass flow rate, $lb_m/sec$
$w^*$	axial velocity component, ft/sec



<u>SYMBOL</u>	<u>DEFINITION</u>
$w$	dimensionless axial velocity component, $(w^*/w_M^*)$
$w_M^*$	mean or bulk velocity, ft/sec
$w_M$	dimensionless mean velocity, defined by equation (81)
$Z$	dimensionless axial length, $(L^*/D^*)$
$\Delta Z$	axial grid spacing, $(R\Delta\theta)$

## GREEK SYMBOLS

<u>SYMBOL</u>	<u>DEFINITION</u>
$\delta$	dimensionless boundary layer thickness, $(\delta^*/D^*)$
$\delta_1$	dimensionless boundary layer variable (used in Barua's (3) analysis)
$\delta_M$	dimensionless mean boundary layer thickness, $\frac{\delta_M^*}{D^*}$
$\theta$	coordinate denoting the section of the curved system under consideration, radians or degrees (see figure 3)
$\mu^*$	viscosity, $\text{lb}_m/\text{ft-sec}$
$\nu^*$	kinematic viscosity, $(\mu^*/\rho^*)$ , $\text{ft}^2/\text{sec}$
$\rho$	dimensionless density $(\rho^*/\rho_0^*)$
$\Psi$	angular cross-sectional coordinate, radians or degrees (see figure 3)

SYMBOL $\Delta\psi$ DEFINITION

angular grid spacing

## SUBSCRIPTS

SYMBOL

a. m.

arithmetic mean, i. e., evaluated at  

$$\frac{T_M^* + T_0^*}{2}$$

M

average or mean value

m

radial grid coordinate

 $\lambda$ 

angular grid coordinate

z

axial grid coordinate

0

entrance conditions or evaluated at  $T_0^*$

## BIBLIOGRAPHY

## BIBLIOGRAPHY

- (1) Adler, M. "Stromung in Gekrummten Rohren," Zeitschrift fur Angewandte Mathematik and Mechanik, 14:257-275, 1934.
- (2) Bailey, R. L. Pressure Drop in Helically Coiled Conduits. Unpublished M. S. thesis, Ames, Iowa, Library, Iowa State University of Science and Technology, 1964.
- (3) Barua, S. N. "On Secondary Flow in Stationary Curved Pipes," Quarterly Journal of Mechanics and Applied Mathematics, Vol. XVI, Pt. I, pp. 61-77, 1963.
- (4) Berg, R. R., and C. F. Bonilla. "Heating of Fluids in Coils," Transactions of the New York Academy of Sciences, 13:12-18, 1950.
- (5) Bird, R. B., W. E. Stewart, and E. N. Lightfoot. Transport Phenomena. John Wiley and Sons, New York, 1960.
- (6) Dean, W. R. "Note on the Motion of Fluid in a Curved Pipe," London, Edinburgh, and Dublin Philosophical Magazine, Series 7, 4:208-223, 1927.
- (7) Dean, W. R. "The Stream-line Motion of Fluid in a Curved Pipe," London, Edinburgh, and Dublin Philosophical Magazine, Series 7, 5:673-695, 1928.
- (8) Eustice, J. "Flow of Water in Curved Pipes," Royal Society of London Proceedings, Series A, 84:107-118, 1910.
- (9) Eustice, J. "Experiments on Stream-line Motion in Curved Pipes," Royal Society of London Proceedings, Series A, 85:119-131, 1911.
- (10) Hawes, W. B. Unpublished, 1930, in S. N. Barua, "On Secondary Flow in Stationary Curved Pipes," Quarterly Journal of Mechanics and Applied Mathematics, Vol. XVI, Pt. I, pp. 61-77, 1963.
- (11) Knudsen, J. G., and D. L. Katz. Fluid Dynamics and Heat Transfer. McGraw-Hill Book Co., New York, 1958.

- (12) Kubair, V., and N. R. Kuloor. "Heat Transfer to Newtonian Fluids in Coiled Pipes in Laminar Flow," International Journal of Heat and Mass Transfer, 9:63-75, 1966.
- (13) Lapidus, L. Digital Computations for Chemical Engineers. McGraw-Hill Book Co., New York, 1962.
- (14) Rogers, D. N. Numerical Analysis of Flow through a Helically Coiled Tube. Unpublished M. S. thesis, Ames, Iowa, Library, Iowa State University of Science and Technology, 1966.
- (15) Schlichting, H. Boundary Layer Theory. Pergamon Press, New York, 1955.
- (16) Seban, R. A., and E. F. McLaughlin. "Heat Transfer in Tube Coils with Laminar and Turbulent Flow," International Journal of Heat and Mass Transfer, 6:387-395, 1963.
- (17) Southward, R. W., and S. L. Deleeuw. Digital Computational and Numerical Methods. McGraw-Hill Book Co., New York, 1965.
- (18) Squire, H. B. Unpublished, 1954, in S. N. Barua, "On Secondary Flow in Stationary Curved Pipes," Quarterly Journal of Mechanics and Applied Mathematics, Vol. XVI, Pt. I, pp. 61-77, 1963.
- (19) Taylor, G. I. "The Criterion for Turbulence in Curved Pipes," Royal Society of London Proceedings, Series A, 124:243-249, 1929.
- (20) Texon, M. "The Role of Vascular Dynamics in the Development of Atherosclerosis," Journal of the American Medical Association, 194(11), 1226, 1965.
- (21) Thompson, J. "On the Origin of Windings of Rivers in Alluvial Plains, with Remarks on the Flow of Water Round Bends in Pipes," Royal Society of London Proceedings, Series A, 25: 5-8, 1876.
- (22) Truesdell, Leonard C., Jr. Numerical Treatment of Laminar Flow through Helical Conduits. Microfilm copy, unpublished Ph. D. thesis, Ann Arbor, Michigan, University Microfilms, Inc., 1963.

- (23) Weissman, Michael H. , and Lyle F. Mockros. "Gas Transfer to Blood Flowing in Coiled Circular Tubes," Journal of the Engineering Mechanics Division, Proceedings of the American Society of Civil Engineers, June, 1968, pp. 857-872.
- (24) White, C. M. "Stream-line Flow through Curved Pipes," Royal Society of London Proceedings, Series A, 123:645-663, 1929.
- (25) Wilkins, Bert, Jr. Nonisothermal Laminar Flow and Heat Transfer with Temperature Dependent Physical Properties. Unpublished Ph. D. thesis, Atlanta, Georgia, Georgia Institute of Technology, 1965.

## APPENDICES

## APPENDIX A

### THE NAVIER-STOKES, CONTINUITY, AND ENERGY EQUATIONS FOR CURVED PIPE FLOW

The Navier-Stokes and continuity equations were transformed from the cylindrical coordinates system  $(r', \theta', z')$  to the helical coordinate system  $(r^*, \Psi, \theta)$ , shown in figure 3.

The vector diagram shown in figure 19 was used to determine the relationship existing between the velocity components  $v_{r'}^*$ ,  $v_{\theta'}^*$ , and  $v_{z'}^*$  in the cylindrical coordinate system and the velocity components  $u^*$ ,  $v^*$ , and  $w^*$  in the helical coordinate system.

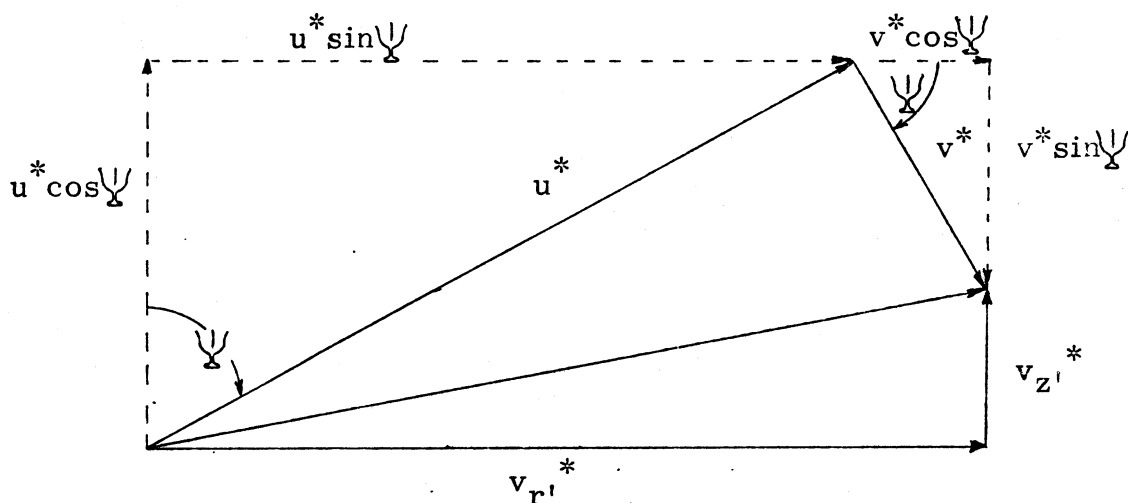


Figure 19. Vector Diagram

Examination of figures 19 and 3 reveals that,

$$r' = R^* + r^* \sin \Psi \quad r^* = (r'^2 - 2r'R^* + R^{*2} + z'^2)^{1/2}$$

$$\theta' = \theta \quad \theta = \theta'$$

$$z' = r^* \cos \Psi \quad \Psi = \tan^{-1} \left[ \frac{r' - R^*}{z'} \right] \quad (14)$$



and,

$$\begin{aligned}
 v_{r'}^* &= u^* \sin \Psi + v^* \cos \Psi \\
 v_{\theta'}^* &= w^* \\
 v_{z'}^* &= u^* \cos \Psi - v^* \sin \Psi
 \end{aligned} \tag{15}$$

Performing the transformation, one obtains,

$$\begin{aligned}
 u^* \frac{\partial u^*}{\partial r^*} + \frac{v^*}{r^*} \frac{\partial u^*}{\partial \Psi} - \frac{v^{*2}}{r^*} - \frac{w^{*2} \sin \Psi}{R^* + r^* \sin \Psi} &= -\frac{\partial}{\partial r^*} \left[ \frac{P^*}{\rho^*} \right] \\
 - \nu^* \left[ \frac{1}{r^*} \frac{\partial}{\partial \Psi} + \frac{\cos \Psi}{R^* + r^* \sin \Psi} \right] \left[ \frac{\partial v^*}{\partial r^*} + \frac{v^*}{r^*} - \frac{1}{r^*} \frac{\partial u^*}{\partial \Psi} \right] &\tag{16}
 \end{aligned}$$

$$\begin{aligned}
 u^* \frac{\partial v^*}{\partial r^*} + \frac{v^*}{r^*} \frac{\partial v^*}{\partial \Psi} + \frac{u^* v^*}{r^*} - \frac{w^{*2} \cos \Psi}{R^* + r^* \sin \Psi} &= -\frac{1}{r^*} \frac{\partial}{\partial \Psi} \left[ \frac{P^*}{\rho^*} \right] \\
 + \nu^* \left[ \frac{\partial}{\partial r^*} + \frac{\sin \Psi}{R^* + r^* \sin \Psi} \right] \left[ \frac{\partial v^*}{\partial r^*} + \frac{v^*}{r^*} - \frac{1}{r^*} \frac{\partial u^*}{\partial \Psi} \right] &\tag{17}
 \end{aligned}$$

$$\begin{aligned}
 u^* \frac{\partial w^*}{\partial r^*} + \frac{v^*}{r^*} \frac{\partial w^*}{\partial \Psi} + \frac{u^* w^* \sin \Psi}{R^* + r^* \sin \Psi} + \frac{v^* w^* \cos \Psi}{R^* + r^* \sin \Psi} \\
 = -\frac{1}{R^* + r^* \sin \Psi} \frac{\partial}{\partial \theta} \left[ \frac{P^*}{\rho^*} \right] + \nu^* \left[ \left( \frac{\partial}{\partial r^*} + \frac{1}{r^*} \right) \right. \\
 \left. \left( \frac{\partial w^*}{\partial r^*} + \frac{w^* \sin \Psi}{R^* + r^* \sin \Psi} \right) + \frac{1}{r^*} \frac{\partial}{\partial \Psi} \left( \frac{1}{r^*} \frac{\partial w^*}{\partial \Psi} + \frac{w^* \cos \Psi}{R^* + r^* \sin \Psi} \right) \right] &\tag{18}
 \end{aligned}$$

$$\frac{\partial u^*}{\partial r^*} + \frac{u^*}{r^*} + \frac{u^* \sin \Psi}{R^* + r^* \sin \Psi} + \frac{1}{r^*} \frac{\partial v^*}{\partial \Psi} + \frac{v^* \cos \Psi}{R^* + r^* \sin \Psi} = 0 \quad (19)$$

In dimensionless form, equations (16) through (19) appear as,

$$\begin{aligned} u \frac{\partial u}{\partial r} + \frac{v}{r} \frac{\partial u}{\partial \Psi} - \frac{v^2}{r} - \frac{w^2 \sin \Psi}{R + r \sin \Psi} &= - \frac{\partial P}{\partial r} - \frac{1}{N_{Re}} \left[ \frac{1}{r} \frac{\partial^2 v}{\partial \Psi \partial r} \right. \\ (\delta) \quad (1) \quad (1) \quad (\delta) \quad (1) \quad (1) \quad (?) \quad (\delta^2) \quad \left. \left( \frac{1}{\delta} \right) \right. \\ + \frac{1}{r^2} \frac{\partial v}{\partial \Psi} - \frac{1}{r^2} \frac{\partial^2 u}{\partial \Psi^2} + \frac{\cos \Psi}{R + r \sin \Psi} \frac{\partial v}{\partial r} + \frac{\cos \Psi}{R + r \sin \Psi} \left. \left[ \frac{v}{r} \right] \right. \\ (1) \quad (\delta) \quad \left( \frac{1}{\delta} \right) \quad (1) \\ - \frac{\cos \Psi}{R + r \sin \Psi} \left. \left( \frac{1}{r} \frac{\partial u}{\partial \Psi} \right) \right] \quad (20) \\ (\delta) \end{aligned}$$

$$\begin{aligned} u \frac{\partial v}{\partial r} + \frac{v}{r} \frac{\partial v}{\partial \Psi} + \frac{uv}{r} - \frac{w^2 \cos \Psi}{R + r \sin \Psi} &= - \frac{1}{r} \frac{\partial P}{\partial \Psi} + \frac{1}{N_{Re}} \left[ \frac{\partial^2 v}{\partial r^2} \right. \\ (\delta) \quad \left( \frac{1}{\delta} \right) \quad (1) \quad (1) \quad (\delta) \quad (1) \quad (?) \quad (\delta^2) \quad \left. \left( \frac{1}{\delta^2} \right) \right. \\ + \frac{1}{r} \frac{\partial v}{\partial r} - \frac{v}{r^2} - \frac{1}{r} \frac{\partial^2 u}{\partial r \partial \Psi} + \frac{1}{r^2} \frac{\partial u}{\partial \Psi} + \frac{\sin \Psi}{R + r \sin \Psi} \frac{\partial v}{\partial r} \\ \left( \frac{1}{\delta} \right) \quad (1) \quad (1) \quad (\delta) \quad \left( \frac{1}{\delta} \right) \\ + \frac{\sin \Psi}{R + r \sin \Psi} \left[ \frac{v}{r} \right] - \frac{\sin \Psi}{R + r \sin \Psi} \left. \left( \frac{1}{r} \frac{\partial u}{\partial \Psi} \right) \right] \quad (21) \\ (1) \quad (\delta) \end{aligned}$$

$$\begin{aligned}
& u \frac{\partial w}{\partial r} + \frac{v}{r} \frac{\partial w}{\partial \Psi} + \frac{u w \sin \Psi}{R + r \sin \Psi} + \frac{v w \cos \Psi}{R + r \sin \Psi} = - \frac{1}{R + r \sin \Psi} \frac{\partial P}{\partial \theta} \\
& (\delta) \left( \frac{1}{\delta} \right) (1) (1) (\delta) (1) (?) \\
& + \frac{1}{N_{Re}} \left[ \frac{\partial^2 w}{\partial r^2} + \frac{\sin \Psi}{R + r \sin \Psi} \frac{\partial w}{\partial r} - \frac{w \sin^2 \Psi}{(R + r \sin \Psi)^2} + \frac{1}{r} \frac{\partial w}{\partial r} \right. \\
& (\delta^2) \left( \frac{1}{\delta^2} \right) \left( \frac{1}{\delta} \right) (1) \left. \left( \frac{1}{\delta} \right) \right] \\
& + \frac{1}{r^2} \frac{\partial^2 w}{\partial \Psi^2} + \frac{\cos \Psi}{R + r \sin \Psi} \left( \frac{1}{r} \frac{\partial w}{\partial \Psi} \right) - \frac{w \cos^2 \Psi}{(R + r \sin \Psi)^2} \quad (22) \\
& (1) (1) (1)
\end{aligned}$$

$$\begin{aligned}
& \frac{\partial u}{\partial r} + \frac{u}{r} + \frac{u \sin \Psi}{R + r \sin \Psi} + \frac{1}{r} \frac{\partial v}{\partial \Psi} + \frac{v \cos \Psi}{R + r \sin \Psi} = 0 \quad (23) \\
& (1) (\delta) (\delta) (1) (1)
\end{aligned}$$

In order to simplify the dimensionless equations of motion and continuity, a qualitative "order of magnitude" analysis is performed. A similar analysis is given in Schlichting (16). This procedure is at best non-rigorous, but is an attempt to simplify the equations as systematically as possible, and is commonly applied in boundary layer type analysis.

It is postulated that the order of magnitude of several quantities will be at most unity, i. e., the values of these variables do not differ considerably from the reference values. The notation  $O(x)$  in this

context means "of the order no greater than  $x$ ." Thus, it is assumed that in the boundary layer,

$$u = 0 \quad (O)$$

$$v = 0 \quad (1)$$

$$w = 0 \quad (1)$$

$$\text{where, } O(O) \ll O(1)$$

$$\text{Thus, for example, } \frac{\partial w}{\partial r} = O\left(\frac{1}{O}\right) \quad \text{and} \quad \frac{\partial^2 w}{\partial r^2} = O\left(\frac{1}{O^2}\right).$$

It has been shown by Schlichting (16) that  $O \sim \sqrt{\nu}$

$$\text{Thus, } N_{Re} = O\left(\frac{1}{O^2}\right).$$

Further, it is assumed that in the boundary layer, differentiation with respect to  $\Psi$  does not change the order of magnitude, i.e.,

$$\frac{\partial u}{\partial \Psi} = O(u).$$

The order of magnitude of each term is shown in equations (20) through (23).

After eliminating terms having small orders of magnitude, the equations become,

$$-\frac{v^2}{r} - \frac{w^2 \sin \Psi}{R + r \sin \Psi} = -\frac{\partial P}{\partial r} \quad (24)$$

$$u \frac{\partial v}{\partial r} + \frac{v}{r} \frac{\partial v}{\partial \Psi} - \frac{w^2 \cos \Psi}{R + r \sin \Psi} = -\frac{1}{r} \frac{\partial P}{\partial \Psi} + \frac{1}{N_{Re}} \frac{\partial^2 v}{\partial r^2} \quad (25)$$

$$u \frac{\partial w}{\partial r} + \frac{v}{r} \frac{\partial w}{\partial \Psi} + \frac{v w \cos \Psi}{R + r \sin \Psi} = -\frac{1}{R + r \sin \Psi} \frac{\partial P}{\partial \theta} + \frac{1}{N_{Re}} \frac{\partial^2 w}{\partial r^2} \quad (26)$$

$$\frac{\partial u}{\partial r} + \frac{1}{r} \frac{\partial v}{\partial \Psi} + \frac{v \cos \Psi}{R + r \sin \Psi} = 0 \quad (27)$$

Now, following Barua (3), it is clear from equation (24) that variations of  $P$  across the boundary layer may be neglected. Also, assuming the pressure gradient in the  $\theta$ -direction to be constant, the first term on the right hand side of equation (26) is negligible with respect to the other terms in the equation. The above assumptions would imply that outside the boundary layer, the cross flow is small compared with the flow along the pipe. Thus, equation (25) shows that outside the boundary layer,

$$-\frac{w^2 \cos \Psi}{R + r \sin \Psi} = -\frac{1}{r} \frac{\partial P}{\partial \Psi}$$

Denoting the velocity along the pipe just outside the boundary layer as  $w_0^*$  and introducing the dimensionless variable  $w_0 = \frac{w_0^*}{w M^*}$ , one finds that

$$-\frac{w_0^2 \cos \Psi}{R + 1/2 \sin \Psi} = -\frac{1}{r} \frac{\partial P}{\partial \Psi}$$

Thus, equations (25) and (26) become

$$u \frac{\partial v}{\partial r} + \frac{v}{r} \frac{\partial v}{\partial \Psi} + \frac{w_0^2 \cos \Psi}{R + 1/2 \sin \Psi} - \frac{w^2 \cos \Psi}{R + r \sin \Psi} = \frac{1}{N_{Re}} \frac{\partial^2 v}{\partial r^2} \quad (28)$$

$$u \frac{\partial w}{\partial r} + \frac{v}{r} \frac{\partial w}{\partial \Psi} + \frac{vw \cos \Psi}{R + r \sin \Psi} = \frac{1}{N_{Re}} \frac{\partial^2 w}{\partial r^2} \quad (29)$$

Equations (27), (28), and (29) are the dimensionless analogs of equations (6), (7), and (8) given in Barua's (3) work.

### THE EQUATION OF ENERGY

When the equation of energy (4) (neglecting viscous dissipation terms) is transformed from the cylindrical to the helical coordinate system, one obtains,

$$\begin{aligned} u^* \frac{\partial T^*}{\partial r^*} + \frac{w^*}{R^* + r^* \sin \Psi} \frac{\partial T^*}{\partial \theta} + \frac{v^*}{r^*} \frac{\partial T^*}{\partial \Psi} \\ = \frac{\nu^*}{N_{Pr}} \left[ \frac{\partial^2 T^*}{\partial r^{*2}} + \frac{1}{r^*} \frac{\partial T^*}{\partial r^*} + \frac{1}{r^{*2}} \frac{\partial^2 T^*}{\partial \Psi^2} + \frac{\sin \Psi}{R^* + r^* \sin \Psi} \frac{\partial T^*}{\partial r^*} \right. \\ \left. + \frac{\cos \Psi}{r^* (R^* + r^* \sin \Psi)} \frac{\partial T^*}{\partial \Psi} + \frac{1}{(R^* + r^* \sin \Psi)^2} \frac{\partial^2 T^*}{\partial \theta^2} \right] \quad (30) \end{aligned}$$

In dimensionless form, the equation becomes,

$$\begin{aligned}
 u \frac{\partial T}{\partial r} + \frac{w}{R+r \sin \Psi} \frac{\partial T}{\partial \theta} + \frac{v}{r} \frac{\partial T}{\partial \Psi} = \frac{1}{N_{Pe}} \left[ \frac{\partial^2 T}{\partial r^2} + \frac{1}{r} \frac{\partial T}{\partial r} \right. \\
 + \frac{1}{r^2} \frac{\partial^2 T}{\partial \Psi^2} + \frac{\sin \Psi}{R+r \sin \Psi} \frac{\partial T}{\partial r} + \frac{\cos \Psi}{r(R+r \sin \Psi)} \frac{\partial T}{\partial \Psi} \\
 \left. + \frac{1}{(R+r \sin \Psi)^2} \frac{\partial^2 T}{\partial \theta^2} \right] \quad (31)
 \end{aligned}$$

As the fluid moves down the pipe, more heat is transferred by convective, rather than conductive means. Thus, it is reasonable to neglect the term containing  $\frac{\partial^2 T}{\partial \theta^2}$ . Also, since secondary flow exists, similar reasoning leads to the deletion of the term containing  $\frac{\partial^2 T}{\partial \Psi^2}$ .

Thus, the equation of energy is reduced to,

$$\begin{aligned}
 u \frac{\partial T}{\partial r} + \frac{w}{R+r \sin \Psi} \frac{\partial T}{\partial \theta} + \frac{v}{r} \frac{\partial T}{\partial \Psi} = \frac{1}{N_{Pe}} \left[ \frac{\partial^2 T}{\partial r^2} + \frac{1}{r} \frac{\partial T}{\partial r} \right. \\
 \left. + \frac{\sin \Psi}{R+r \sin \Psi} \frac{\partial T}{\partial r} + \frac{\cos \Psi}{r(R+r \sin \Psi)} \frac{\partial T}{\partial \Psi} \right] \quad (32)
 \end{aligned}$$

If one further assumes that:

- (1) the fluid properties are constant;
- (2) the laminar velocity profiles are established before heating or cooling of the fluid;
- (3) at  $L^* = 0$ , the temperature of the tube wall changes from  $T_0^*$

to  $T_w^*$  and is uniform at this value for  $L^* > 0$ ,

then, a problem analogous to the straight tube Graetz problem has been imposed on curved tube flow.



## APPENDIX B

### COMMENTS ON S. N. BARUA'S WORK

#### Summary

Barua (3) considered the steady laminar flow of a Newtonian fluid through a curved tube of radius  $a^*$ , coiled in a circle of radius  $R^*$  at high Dean numbers. Barua assumed: (1) that the flow consisted of a non-turbulent core moving slowly outwards, surrounded by an inward moving boundary-layer; (2) that at large  $N_{De}$ , viscous forces are important only in a thin boundary-layer near the wall; (3) that the section of pipe under consideration was free from entrance or exit effects, and that the velocity profiles were fully developed, being identical at each cross section; and (4) that the motion outside of the boundary layer was confined to planes parallel to the plane of symmetry.

#### Method of Solution and Results

Using the Pohlhausen boundary-layer method, Barua obtained an approximate solution to equations (6), (7), (8), and (9) in the form of expressions describing the velocity components  $u^*$ ,  $v^*$ , and  $w^*$  both inside and outside the boundary layer.

In order to utilize Barua's solution over a large range of parameters, the equations given by Barua were put in dimensionless form.

Barua's work shows that the axial velocity profile,  $w = w(r, \Psi)$ , is greatly distorted from the parabolic profile commonly encountered

in laminar flow in straight tubes. The region of maximum axial velocity moves toward the outer wall of the tube, reaching its greatest value at the boundary layer edge. Barua also showed that the radial and angular velocities are of a negligible nature when compared to the larger axial velocities.

#### Accuracy of Solution

The accuracy of Barua's solution, apparently never before examined numerically, was tested in two ways. The axial velocity profiles generated were compared both with the experimental work given by Adler (1) and with the restriction imposed by equation (81). Comparison with experimental findings, shown in figures 20, 21, and 22, shows good agreement. Also, the values of  $\psi_w$  for the cases shown in table 1 were consistently within 1.71 per cent of unity.

#### Solution in Dimensionless Form

As many of the assumptions made by Barua were omitted from the text of his paper, it became necessary to re-derive Barua's work from a non-dimensional point of view. It should also be noted that a number of publication errors were discovered in the text of Barua's paper; hence, the reason for any apparent discrepancy between the form of the equations presented in this work and those given by Barua. Specifically, errors found in Barua's work included:

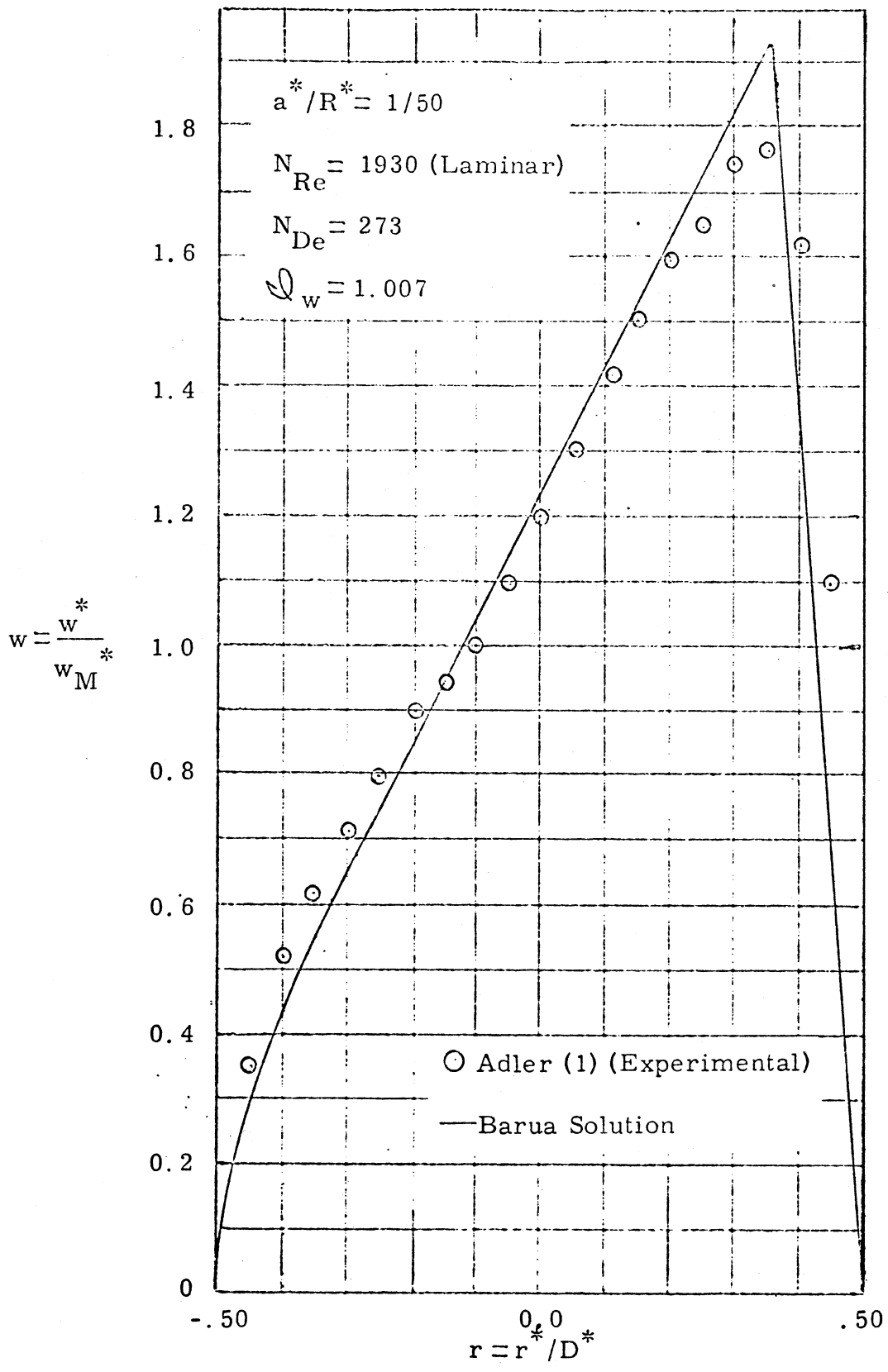


Figure 20. Axial Velocity Profile in the Plane of Symmetry,  $N_{De} = 273$

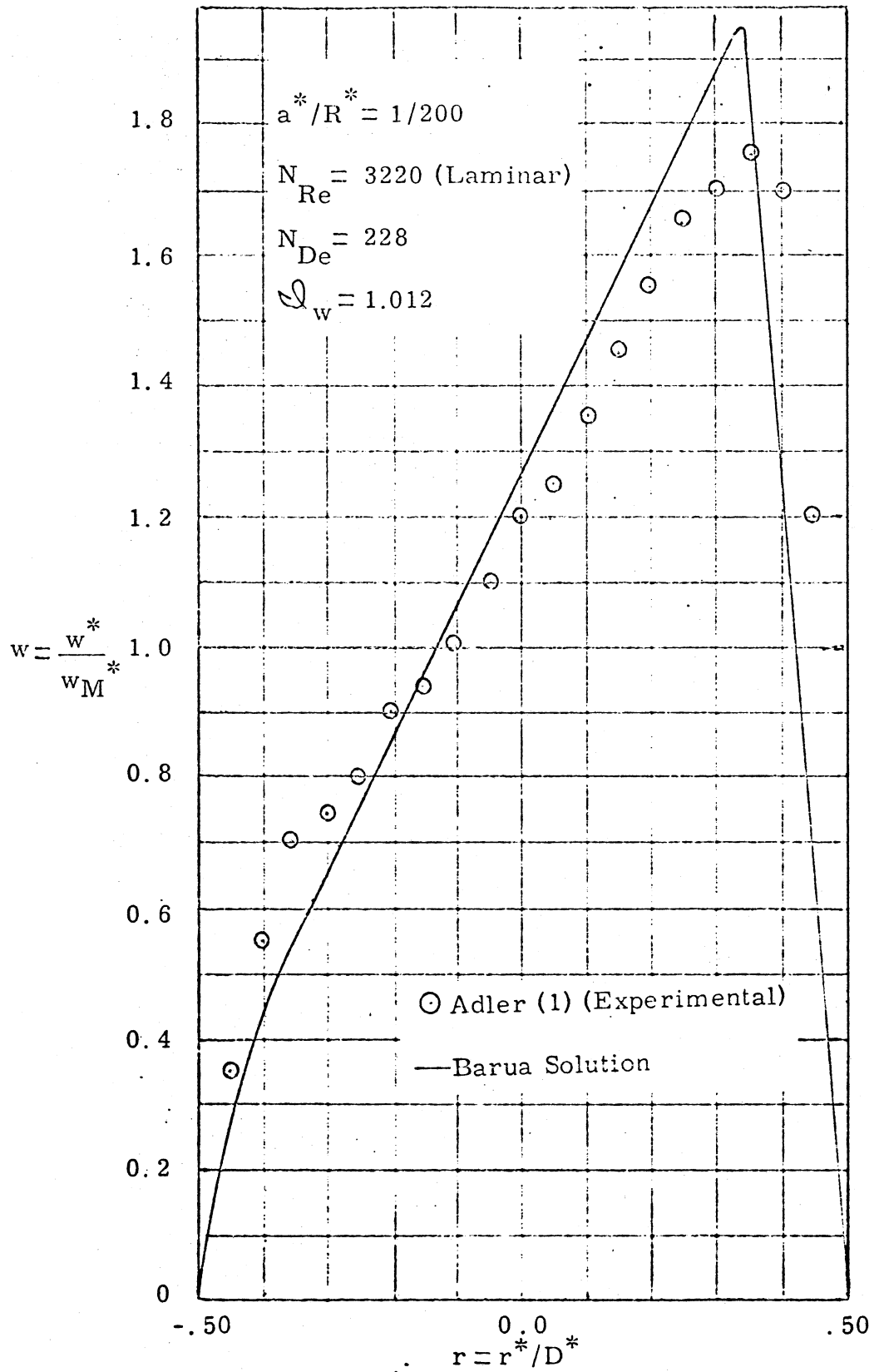


Figure 21. Axial Velocity Profile in the Plane of Symmetry,  $N_{De} = 228$

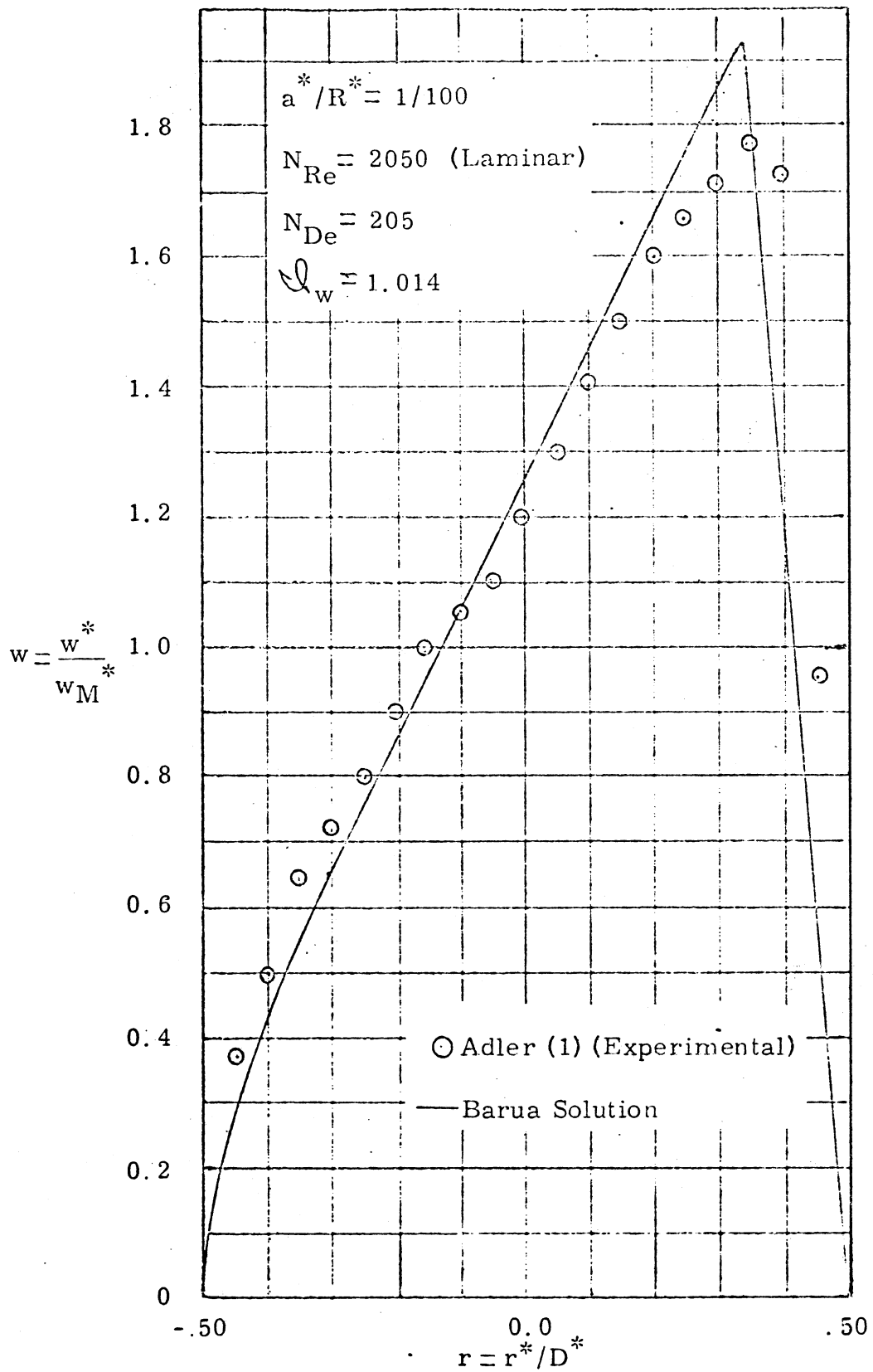


Figure 22. Axial Velocity Profile in the Plane of Symmetry,  $N_{De} = 205$

- (1) The equation preceding equation (7) should include a negative sign on the left hand side.
- (2) Equation (16) should have a negative sign on the right hand side.
- (3) The constant preceding the second term on the left hand side of equation (20) should be  $+ .4667/4$ .
- (4) In equation (25), a negative sign should precede the  $h^2 \cos \Psi$  coefficient and the numerator of the last term inside the brackets on the right hand side should be  $D \sin \Psi$ .
- (5) The sentence following equation (27) should read, "In order to determine the unknown constant h, we rewrite (20) as . . . ."
- (6) In equation (28) and the equation previous to it, the  $\frac{\partial g}{\partial \Psi}$  term should be followed by an plus sign.
- (7) Table 1 is constructed from equations (22) and (25) by neglecting the  $\sin \Psi$  terms with respect to terms containing  $R/a$ .
- (8) The last part of the equation following equation (32) should read ". . . .  $d\Psi dr$ ."
- (9) The equation preceding equation (36) should include an  $A^{1/2}$  in the denominator of both the first and second bracketed terms on the left hand side.
- (10) An  $A^{1/2}$  should be included in the denominator of the left hand side of equation (36).

The dimensionless analogs of the equations given by Barua are

presented below. The following equations are numbered in such a way that the second number corresponds to the analogous Barua equation.

Denoting the constants in Barua's work as  $A^*$ ,  $B^*$ , and  $C^*$ , one can write,

$$A = \frac{A^*}{\left[\frac{N_{Re}}{2}\right]^{2/3}} \psi^*, \quad B = \frac{B^*}{w_M^{*2}}, \quad C = \frac{C^*}{4a^{*2}}$$

Thus,

$$u_P = \frac{A}{R + r \sin \psi} \left[ \frac{1}{4N_{Re}} \right]^{1/3} \quad (\text{outside the boundary layer})$$

(33-1)

$$w = \frac{B}{2A} \left[ 4N_{Re} \right]^{1/3} \left[ R + r \sin \psi + \frac{C}{R + r \sin \psi} \right] \quad (\text{outside the boundary layer})$$

(34-2)

Equations analogous to Barua's equations (3) - (8) are presented in Appendix A.

$$\int_{1/2-\epsilon}^{1/2} \left[ u \frac{\partial v}{\partial r} + 2v \frac{\partial v}{\partial \psi} \right] dr + \int_{1/2-\epsilon}^{1/2} \frac{(w_0^2 - w^2) \cos \psi}{R + 1/2 \sin \psi} dr$$

$$= \frac{1}{N_{\text{Re}}} \int_{1/2-\delta}^{1/2} \frac{\partial^2 v}{\partial r^2} dr = \frac{1}{N_{\text{Re}}} \left[ \frac{\partial v}{\partial r} \right]_{r=1/2} \quad (35-9)$$

$$\begin{aligned} & \int_{1/2-\delta}^{1/2} \left[ u \frac{\partial w}{\partial r} + 2v \frac{\partial w}{\partial \Psi} \right] dr + \int_{1/2-\delta}^{1/2} \frac{vw \cos \Psi}{R + 1/2 \sin \Psi} dr \\ &= \frac{1}{N_{\text{Re}}} \left[ \frac{\partial w}{\partial r} \right]_{r=1/2} \end{aligned} \quad (36-10)$$

$$u \Big|_{1/2-\delta} = \int_{1/2-\delta}^{1/2} 2 \frac{\partial v}{\partial \Psi} dr + \int_{1/2-\delta}^{1/2} \frac{v \cos \Psi}{R + 1/2 \sin \Psi} dr \quad (37-11)$$

$$2 \int_{1/2-\delta}^{1/2} \frac{\partial (v^2)}{\partial \Psi} dr + \frac{\cos \Psi}{R + 1/2 \sin \Psi} \int_{1/2-\delta}^{1/2} v^2 dr + \frac{\cos \Psi}{R + 1/2 \sin \Psi}$$

$$\int_{1/2-\delta}^{1/2} (w_0^2 - w^2) dr = \frac{1}{N_{\text{Re}}} \left[ \frac{\partial v}{\partial r} \right]_{r=1/2} \quad (38-12)$$

$$\begin{aligned} & 2 \int_{1/2-\delta}^{1/2} \frac{\partial (vw)}{\partial \Psi} dr + \frac{2 \cos \Psi}{R + 1/2 \sin \Psi} \int_{1/2-\delta}^{1/2} v w dr - w_0 \left[ 2 \int_{1/2-\delta}^{1/2} \frac{\partial v}{\partial \Psi} dr \right. \\ & \left. + \frac{\cos \Psi}{R + 1/2 \sin \Psi} \int_{1/2-\delta}^{1/2} v dr \right] = \frac{1}{N_{\text{Re}}} \left[ \frac{\partial w}{\partial r} \right]_{r=1/2} \end{aligned} \quad (39-13)$$



$$v = v_0 (\eta - 2\eta^2 + \eta^3) = v_0 f(\eta) \quad (\text{inside boundary layer})$$

$$\text{where, } \eta = \frac{1/2 - r}{\delta}, \quad v_0 = \frac{v_0^*}{w_{M^*}} \quad (40-14)$$

$$w = w_0 (2\eta - \eta^2) = w_0 \phi(\eta) \quad (\text{inside boundary layer}) \quad (41-15)$$

$$\left[ 2 \frac{\partial(v_0^2 \delta)}{\partial \Psi} + \frac{v_0^2 \delta \cos \Psi}{R + 1/2 \sin \Psi} \right] \int_0^1 f^2 d\eta + \frac{w_0^2 \delta \cos \Psi}{R + 1/2 \sin \Psi}$$

$$\left[ 1 - \int_0^1 \phi^2 d\eta \right] = - \frac{v_0}{N_{Re} \delta} \left[ \frac{\partial f}{\partial \eta} \right]_{\eta=0} \quad (42-16)$$

$$\left[ 2 \frac{\partial(v_0 w_0 \delta)}{\partial \Psi} + \frac{2(v_0 w_0) \delta \cos \Psi}{R + 1/2 \sin \Psi} \right] \int_0^1 (f\phi) d\eta$$

$$- w_0 \left[ 2 \frac{\partial(v_0 \delta)}{\partial \Psi} + \frac{v_0 \delta \cos \Psi}{R + 1/2 \sin \Psi} \right] \int_0^1 f d\eta = - \frac{w_0}{N_{Re} \delta} \left[ \frac{\partial \phi}{\partial \eta} \right]_{\eta=0}$$

$$(43-17)$$

$$\int_0^1 f d\eta = .08333, \quad \int_0^1 f\phi d\eta = 0.05$$

$$\int_0^1 f^2 d\eta = .009524, \quad \int_0^1 \phi^2 d\eta = .5333 \quad (44-18)$$

$$\left[ \frac{\partial f}{\partial \eta} \right]_{\eta=0} = 1.0, \quad \left[ \frac{\partial \phi}{\partial \eta} \right]_{\eta=0} = 2.0$$

$$\delta = \frac{\delta_1}{2} \left[ \frac{A}{B} \right]^{1/2} \left[ \frac{2}{N_{Re}} \right]^{2/3}$$

$$v_0 = g (B/A) \left[ \frac{N_{Re}}{2} \right]^{1/3} \quad (45-19)$$

$$C = D/4$$

$$\text{where, } \delta = \frac{\delta^*}{2a^*}$$

$$(0.009524) \left[ \frac{\partial}{\partial \Psi} (g^2 \delta_1) + \frac{(g^2 \delta_1)}{2} \frac{\cos \Psi}{R + 1/2 \sin \Psi} \right] + \left[ \frac{0.4667}{2} \right] \\ \left[ \frac{\delta_1 \cos \Psi (R + 1/2 \sin \Psi + C/R + 1/2 \sin \Psi)^2}{R + 1/2 \sin \Psi} \right] + \frac{g}{\delta_1} = 0 \quad (46-20)$$

$$-0.0333 \frac{\partial}{\partial \Psi} (g \delta_1) + \frac{g \delta_1}{2} \frac{\cos \Psi}{R + 1/2 \sin \Psi} \left[ (.05) \right. \\ \left. \left[ \frac{(R + 1/2 \sin \Psi)^2 - C}{(R + 1/2 \sin \Psi)^2 + C} \right] + 0.01667 \right] + \frac{2}{\delta_1} = 0 \quad (47-21)$$

$$g \delta_1 = \frac{-h \cos \Psi}{(2R + \sin \Psi)} \quad (48-22)$$

$$h = \frac{A}{(.08333) (B/A)^{1/2}} \quad (49-23)$$

$$2g = 0.0333 (g \delta_1) \frac{\partial}{\partial \Psi} (g \delta_1) - \frac{(g \delta_1)^2}{2} \frac{\cos \Psi}{R + 1/2 \sin \Psi}$$

$$\left[ (.05) \left[ \frac{(R + 1/2 \sin \Psi)^2 - C}{(R + 1/2 \sin \Psi)^2 + C} \right] + .01667 \right] \quad (50-24)$$

$$60g = \frac{-h^2 \cos \Psi}{(2R + \sin \Psi)^2 + D} \left[ \sin \Psi + \frac{3 \cos^2 \Psi}{(2R + \sin \Psi)} + \frac{D \sin \Psi}{(2R + \sin \Psi)^2} \right] \quad (51-25)$$

$$[4R^2 + D]^2 - 3[4R^2 + D] - 24R^2 = 0 \quad (52-26)$$

$$D = -4R^2 + 2\sqrt{6} R \quad (53-27)$$

$$\begin{aligned} & \frac{\partial g}{\partial \Psi} + \frac{g \cos \Psi}{(2R + \sin \Psi)} \left[ 1 + \frac{1}{(0.0333)} \left( (.05) \left[ \frac{(2R + \sin \Psi)^2 - D}{(2R + \sin \Psi)^2 + D} \right] \right. \right. \\ & \left. \left. + 0.01667 \right) \right] + \frac{.4667}{(4)(.009524)} \left[ \frac{1}{g} \right] \frac{\cos \Psi}{(2R + \sin \Psi)} \left[ (2R + \sin \Psi) \right. \\ & \left. + \frac{D}{(2R + \sin \Psi)} \right]^2 + \frac{g^2}{(g \delta_1)^2} \left[ \frac{2}{0.0333} + \frac{1}{0.009524} \right] = 0 \quad (54-28) \end{aligned}$$

$$\begin{aligned} & \left[ \frac{(g)_{\Psi=0}}{2R} \left[ 1 + \frac{1}{.0333} \left( (.05) \left[ \frac{4R^2 - D}{4R^2 + D} \right] + .01667 \right) \right] \right] \quad (55-29) \\ & + \left[ \frac{12.2}{(g)_{\Psi=0}} \right] \frac{1}{2R} \left[ 2R + \frac{D}{2R} \right]^2 + \left[ \frac{g^2}{(g \delta_1)^2} \right]_{\Psi=0} (165) = 0 \end{aligned}$$

$$(g \delta_1)_{\Psi=0} = \frac{-h}{2R} \quad (56-30)$$

$$h = 28.4 (R)^{3/4} \quad (57-31)$$

$$\frac{B}{A} \left[ \frac{N_{Re}}{2} \right]^{1/3} \left[ \frac{1}{\sqrt{6}} \right] \left[ 3 - 4 \delta_M \right] = 1 \quad (58-33)$$

$$\text{where, } \delta_M = \frac{\delta_{M^*}}{2a^*}$$

$$\delta_M = \frac{30}{16.93} \left[ \frac{A}{B} \right]^{1/2} \left[ \frac{2}{N_{Re}} \right]^{2/3} (2R)^{1/4} \quad (59-34)$$

$$N_{De} = N_{Re} \left[ \frac{a^*}{R^*} \right]^{1/2} = N_{Re} \left[ \frac{1}{2R} \right]^{1/2} \quad (60-35)$$

$$\left[ \frac{B}{A} \right]^{1/2} N_{Re}^{2/3} \left[ \frac{1}{2R} \right]^{1/4} = 1.871 + \left[ (1.871)^2 + 1.03 N_{De} \right]^{1/2} \quad (61-36)$$

$$A^{1/2} = (1.335) (B)^{1/6} (R)^{1/4} \quad (62-37)$$

$$B = \frac{3.96 R^{3/2}}{N_{Re}^2} \left[ (1.871) + \left( (1.871)^2 + 1.03 N_{De} \right)^{1/2} \right]^3 \quad (63-38)$$

A vector diagram similar to that of figure 19 gives the  $u$  and  $v$  velocity components outside the boundary layer.

$$\begin{aligned}
 u &= u_p \sin \Psi \\
 v &= u_p \cos \Psi
 \end{aligned}
 \tag{64}$$

The  $u$  component of velocity in the boundary layer is calculated by putting the boundary layer equation of continuity in finite difference form and integrating numerically. Thus,

$$u_{m,\lambda} = u_{m+1,\lambda} + \frac{\Delta r}{r_m} \left[ \frac{\partial v}{\partial \Psi} \right]_{m,\lambda} + \frac{(\Delta r) v_{m,\lambda} \cos \Psi_\lambda}{(R + r_m \sin \Psi_\lambda)}
 \tag{65}$$

## APPENDIX C

### DEVELOPMENT OF CALCULATION SCHEME

#### Development of Finite Difference Approximations

Consider the function  $f(r, \Psi, \theta)$  defined on the semi-infinite volume of the  $(r, \Psi, \theta)$  coordinate system bounded by

$$0 \leq r \leq 1/2,$$

$$-\pi/2 \leq \Psi \leq \pi/2,$$

and  $0 \leq \theta < \infty$

Let a series of semi-circular grids of mesh spacing  $(\Delta r, \Delta \Psi)$  be superimposed on this domain a distance of  $\Delta Z$  apart, where  $\Delta Z = R\Delta\theta$ .

Define

$$r_m = (m-1) \Delta r, \quad 1 \leq m \leq N+1 \quad (66)$$

$$\Psi_\ell = \pi/2 - (\ell-1)\Delta\Psi, \quad 1 \leq \ell \leq 2J+1 \quad (67)$$

$$\theta_z = (z-1)\Delta\theta, \quad 1 \leq z < \infty \quad (68)$$

$$Z_z = R\theta_z = (z-1)R\Delta\theta \quad (69)$$

and

$$f_{m, \ell, z} = f \left[ (m-1) \Delta r, \quad \pi/2 - (\ell-1)\Delta\Psi, \quad (z-1)\Delta\theta \right] \quad (70)$$

By a Taylor's series expansion about some point, a,

$$\begin{aligned}
f(r, \Psi, \theta) &= f(a, \Psi, \theta) + (r-a) \left[ \frac{\partial f}{\partial r} \right]_{a, \Psi, \theta} \\
&+ \frac{(r-a)^2}{2!} \left[ \frac{\partial^2 f}{\partial r^2} \right]_{a, \Psi, \theta} + \dots \\
&+ \frac{(r-a)^{i-1}}{(i-1)!} \left[ \frac{\partial^{i-1} f}{\partial r^{i-1}} \right]_{a, \Psi, \theta} + R_i
\end{aligned} \tag{71}$$

where  $R_i = \frac{(r-a)^i}{i!} \left[ \frac{\partial^i f}{\partial r^i} \right]_{\xi, \Psi, \theta}$

and  $\left| \xi - \frac{r+a}{2} \right| < \left| \frac{r-a}{2} \right|$

Applying this expansion to the finite difference grid

$$f_{m+1, \ell, z} = f_{m, \ell, z} + \Delta r \left[ \frac{\partial f}{\partial r} \right]_{m, \ell, z} + 0(\Delta r^2) \tag{72}$$

$$f_{m-1, \ell, z} = f_{m, \ell, z} - \Delta r \left[ \frac{\partial f}{\partial r} \right]_{m, \ell, z} + 0(\Delta r^2) \tag{73}$$

Combining the above equations gives

$$\left[ \frac{\partial f}{\partial r} \right]_{m, \ell, z} = \frac{f_{m+1, \ell, z} - f_{m-1, \ell, z}}{2\Delta r} + 0(\Delta r^2) \tag{74}$$

The functional symbol  $O(\quad)$  indicates a truncation error which is proportional to the value of the argument of the function.

By a similar manipulation of Taylor series expansions, the following finite difference approximations may be derived with the order of their associated truncation error.

$$\left[ \frac{\partial f}{\partial r} \right]_{m, \ell, z} = \frac{3f_{m, \ell, z} - 4f_{m-1, \ell, z} + f_{m-2, \ell, z}}{2 \Delta r} + O(\Delta r^2) \quad (75)$$

$$\left[ \frac{\partial f}{\partial r} \right]_{m, \ell, z} = \frac{f_{m+1, \ell, z} - f_{m, \ell, z}}{\Delta r} + O(\Delta r) \quad (76)$$

$$\left[ \frac{\partial^2 f}{\partial r^2} \right]_{m, \ell, z} = \frac{f_{m+1, \ell, z} - 2f_{m, \ell, z} + f_{m-1, \ell, z}}{\Delta r^2} + O(\Delta r^2) \quad (77)$$

A simple interchange results in approximations for derivatives with respect to  $\Psi$  and  $\theta$ .

For example,

$$\left[ \frac{\partial f}{\partial \Psi} \right]_{m, \ell, z} = \frac{f_{m, \ell+1, z} - f_{m, \ell, z}}{\Delta \Psi} + O(\Delta \Psi) \quad (78)$$

and 
$$\left[ \frac{\partial f}{\partial \theta} \right]_{m, \ell, z} = \frac{f_{m, \ell, z+1} - f_{m, \ell, z}}{\Delta \theta} + O(\Delta \theta) \quad (79)$$



### Calculation Scheme for Velocity Components

Neglecting the  $u$  and  $v$  components of velocity and considering the finite difference grid shown in figure 4, axial velocities were calculated as point functions using the Barua (3) method outlined in Appendix B. At each grid point, a check was made to determine if the point was inside or outside the boundary layer. The results of this test determined the expression used to calculate the axial velocity at that point.

### Numerical Integration for Mean Velocity

The average or mean axial velocity,  $w_M^*$ , is determined by summing all axial velocities over the cross section and dividing by the cross-sectional area (4). Thus, one writes

$$w_M^* = \frac{2}{\pi a^{*2}} \int_{r^*=0}^{r^*=a^*} \int_{\Psi=\pi/2}^{\Psi=-\pi/2} w^* r^* dr^* d\Psi \quad (80)$$

In dimensionless form, this becomes

$$w_M = 1 = \frac{8}{\pi} \int_{r=0}^{r=1/2} \int_{\Psi=\pi/2}^{\Psi=-\pi/2} w r dr d\Psi = \mathcal{I}_w \quad (81)$$

Since this expression is identically equal to unity, the integration

provides an indication as to the accuracy of the axial velocities generated using Barua's (3) technique.

The integration can be accomplished numerically using Simpson's rule twice. Since the expression is exact in the mathematical sense, one can write,

$$\mathcal{Q}_w = 8/\pi \int_{\Psi = -\pi/2}^{\Psi = \pi/2} \left\{ \int_{r=0}^{r=1/2} wr dr \right\} d\Psi \quad (82)$$

Considering the first integration to be that with respect to  $r$ , the numerical approximation is,

$$\left\{ \int_{r=0}^{r=1/2} wr dr \right\}_\lambda = \sum \frac{\Delta r}{3} \left[ wr \Big|_{m-1} + 4wr \Big|_m + wr \Big|_{m+1} \right] = F_\lambda(\Psi) \quad (83)$$

for  $m = 2, 4, \dots, N$  and  $1 \leq \lambda \leq 2J + 1$ .

With the values of  $F_1(\Psi)$ ,  $F_2(\Psi)$ ,  $\dots$ ,  $F_{2J+1}(\Psi)$  known, the numerical integration for  $\mathcal{Q}_w$  is completed by writing,

$$\mathcal{Q}_w = 8/\pi \sum \frac{\Delta \Psi}{3} \left[ F_{\lambda-1}(\Psi) + 4F_\lambda(\Psi) + F_{\lambda+1}(\Psi) \right] = 8/\pi \int_{-\pi/2}^{\pi/2} F(\Psi) d\Psi \quad (84)$$

for  $\lambda = 2, 4, \dots, 2J$ .

Finite Difference Representation of the Equation of Energy  
and Calculation Scheme for Temperature Fields

Neglecting the u and v components of velocity, the equation of energy can be written as

$$\begin{aligned} \frac{w}{R+r \sin \Psi} \frac{\partial T}{\partial \theta} = & \left[ \frac{1}{N_{Pe}} \left( \frac{\sin \Psi}{R+r \sin \Psi} + \frac{1}{r} \right) \right] \frac{\partial T}{\partial r} \\ + & \left[ \frac{\cos \Psi}{N_{Pe} r (R+r \sin \Psi)} \right] \frac{\partial T}{\partial \Psi} + \frac{1}{N_{Pe}} \frac{\partial^2 T}{\partial r^2} \end{aligned} \quad (85)$$

At  $\Psi = \pi/2$  (in the plane of symmetry), the equation of energy reduces to

$$\frac{w}{R+r} \frac{\partial T}{\partial \theta} = \left[ \frac{1}{N_{Pe}} \left( \frac{1}{R+r} + \frac{1}{r} \right) \right] \frac{\partial T}{\partial r} + \frac{1}{N_{Pe}} \frac{\partial^2 T}{\partial r^2} \quad (86)$$

Adopting the notation that

$$\begin{aligned} w_{m, \ell} &= w \left[ (m-1) \Delta r, \pi/2 - (\ell-1) \Delta \Psi \right] \\ T_{m, \ell, z} &= T \left[ (m-1) \Delta r, \pi/2 - (\ell-1) \Delta \Psi, (z-1) \Delta \theta \right] \end{aligned}$$

and writing equation (86) in finite difference form, one obtains

$$\frac{w_{m,1}}{R+r_m} \left[ \frac{T_{m,1,z+1} - T_{m,1,z}}{\Delta\theta} \right] = \left[ \frac{1}{N_{Pe}} \left( \frac{1}{R+r_m} + \frac{1}{r_m} \right) \right]$$

$$\left[ \frac{T_{m+1,1,z+1} - T_{m-1,1,z+1}}{2\Delta r} \right] + \frac{1}{N_{Pe}} \left[ \frac{T_{m+1,1,z+1} - 2T_{m,1,z+1} + T_{m-1,1,z+1}}{\Delta r^2} \right] \quad (87)$$

Rearranging, one obtains,

$$\frac{1}{N_{Pe}} \left[ \frac{1}{2\Delta r} \left( \frac{1}{R+r_m} + \frac{1}{r_m} \right) - \frac{1}{(\Delta r)^2} \right] T_{m-1,1,z+1}$$

$$+ \left[ \frac{1}{\Delta\theta} \left( \frac{w_{m,1}}{R+r_m} \right) + \frac{2}{N_{Pe}(\Delta r)^2} \right] T_{m,1,z+1}$$

$$+ \frac{1}{N_{Pe}} \left[ -\frac{1}{2\Delta r} \left( \frac{1}{R+r_m} + \frac{1}{r_m} \right) - \frac{1}{(\Delta r)^2} \right] T_{m+1,1,z+1}$$

$$= \frac{1}{\Delta\theta} \left[ \frac{w_{m,1}}{R+r_m} \right] T_{m,1,z}, \quad \text{for } 2 \leq m \leq N. \quad (88)$$

Special attention must be given to equation (86) at  $r=0$ , as

$$\frac{1}{N_{Pe}} \left( \frac{1}{r} \frac{\partial T}{\partial r} \right) \text{ is undefined.}$$

Using L'Hospital's rule,

$$\lim_{r \rightarrow 0} \left[ \frac{1}{N_{Pe}} \left( \frac{1}{r} \frac{\partial T}{\partial r} \right) \right] = \frac{1}{N_{Pe}} \frac{\partial^2 T}{\partial r^2}$$

Thus, at  $r=0$ , equation (86) becomes,

$$\frac{w}{R} \frac{\partial T}{\partial \theta} \Big|_{r=0} = \frac{1}{N_{Pe} R} \frac{\partial T}{\partial r} \Big|_{r=0} + \frac{2}{N_{Pe}} \frac{\partial^2 T}{\partial r^2} \Big|_{r=0} \quad (89)$$

In finite difference notation, equation (89) appears as

$$\begin{aligned} \frac{w_{1,1}}{R} \left[ \frac{T_{1,1,z+1} - T_{1,1,z}}{\Delta \theta} \right] &= \frac{1}{N_{Pe} R} \left[ \frac{T_{2,1,z+1} - T_{0,1,z+1}}{2 \Delta r} \right] \\ &+ \frac{2}{N_{Pe}} \left[ \frac{T_{2,1,z+1} - 2T_{1,1,z+1} + T_{0,1,z+1}}{\Delta r^2} \right] \end{aligned} \quad (90)$$

It is obvious that  $T_{0,1,z+1} = T_{2,2J+1,z+1}$ . If  $T_{2,2J+1,z+1}$  is approximated by  $T_{2,2J+1,z}$  the error will be of the order of  $\Delta \theta$ .

Rearranging equation (90) and incorporating the above approximation, one obtains

$$\begin{aligned} \left[ \frac{w_{1,1}}{R \Delta \theta} + \frac{4}{N_{Pe} (\Delta r)^2} \right] T_{1,1,z+1} &+ \frac{1}{N_{Pe}} \left[ -\frac{1}{2 \Delta r} \frac{1}{R} - \frac{2}{\Delta r^2} \right] T_{2,1,z+1} \\ &= \left[ \frac{w_{1,1}}{R \Delta \theta} \right] T_{1,1,z} + \frac{1}{N_{Pe}} \left[ \frac{2}{\Delta r^2} - \frac{1}{2 \Delta r} \frac{1}{R} \right] T_{2,2J+1,z} \end{aligned} \quad (91)$$

Equations (88) and (91) represent the system of linear algebraic equations approximating the equation of energy at  $\psi = \pi/2$ . In matrix-vector notation, this system can be represented as

$$\underline{A}_1 \vec{t}_1 = \vec{b}_1 \quad (92)$$

The coefficient matrix  $\underline{A}_1$  is a tridiagonal matrix given by,

$$\underline{A}_1 = \begin{bmatrix} B_1 & C_1 & & & \\ A_2 & B_2 & C_2 & & \\ & \ddots & \ddots & \ddots & \\ & & & C_{N-1} & \\ & & & A_N & B_N \end{bmatrix} \quad (93)$$

$$\text{where, } B_1 = \frac{w_{1,1}}{R\Delta\theta} + \frac{4}{N_{Pe}\Delta r^2} \quad (94)$$

$$C_1 = \frac{1}{N_{Pe}} \left[ -\frac{1}{2\Delta r(R)} - \frac{2}{\Delta r^2} \right] \quad (95)$$

and for  $2 \leq m \leq N$ ,

$$A_m = \frac{1}{N_{Pe}} \left[ \frac{1}{2\Delta r} \left( \frac{1}{R+r_m} + \frac{1}{r_m} \right) - \frac{1}{\Delta r^2} \right] \quad (96)$$

$$B_m = \frac{1}{\Delta\theta} \left[ \frac{w_{m,1}}{R+r_m} \right] + \frac{2}{N_{Pe}\Delta r^2} \quad (97)$$

$$C_m = \frac{1}{N_{Pe}} \left[ -\frac{1}{2\Delta r} \left( \frac{1}{R+r_m} + \frac{1}{r_m} \right) - \frac{1}{\Delta r^2} \right] \quad (98)$$

The solution vector  $\vec{t}_1$  is given by

$$\vec{t}_1 = \begin{bmatrix} T_{1,1,z+1} \\ T_{2,1,z+1} \\ \vdots \\ T_{N,1,z+1} \end{bmatrix} \quad (99)$$

and the constant vector  $\vec{b}_1$  is given as,

$$\vec{b}_1 = \begin{bmatrix} b_1 \\ b_2 \\ \vdots \\ b_N \end{bmatrix} \quad (100)$$

$$\text{where, } b_1 = \left[ \frac{w_{1,1}}{R\Delta\theta} \right] T_{1,1,z} + \frac{1}{N_{Pe}} \left[ \frac{2}{\Delta r^2} - \frac{1}{2\Delta r} \frac{1}{R} \right] T_{2,2J+1,z} \quad (101)$$

for  $2 \leq m \leq N-1$ ,

$$b_m = \frac{1}{\Delta\theta} \left[ \frac{w_{m,1}}{R+r_m} \right] T_{m,1,z} \quad (102)$$

$$b_N = \frac{1}{\Delta\theta} \left[ \frac{w_{N,1}}{R+r_N} \right] T_{N,1,z} + \frac{1}{N_{Pe}} \left[ \frac{1}{2\Delta r} \left( \frac{1}{R+r_N} + \frac{1}{r_N} \right) + \frac{1}{\Delta r^2} \right] \quad (103)$$

As the values of  $T$  at  $\Psi = \pi/2$ , ( $\ell = 1$ ), have been calculated, one can now proceed to calculate values of  $T$  at  $\ell = \ell + 1$ .

(Note: As the center line temperature has been calculated, one needs only consider values of  $m$  for  $2 \leq m \leq N$ , for  $1 < \ell \leq 2J + 1$ .)

In finite difference form, equation (85) becomes,

$$\begin{aligned} \frac{w_{m,\ell}}{R + r_m \sin \Psi_\ell} \left[ \frac{T_{m,\ell,z+1} - T_{m,\ell,z}}{\Delta \theta} \right] &= \left[ \frac{1}{N_{Pe}} \left( \frac{\sin \Psi_\ell}{R + r_m \sin \Psi_\ell} + \frac{1}{r_m} \right) \right. \\ &\left. \left[ \frac{T_{m+1,\ell,z+1} - T_{m-1,\ell,z+1}}{2 \Delta r} \right] + \left[ \frac{\cos \Psi_\ell}{N_{Pe} (r_m) (R + r_m \sin \Psi_\ell)} \right] \left[ \frac{T_{m,\ell-1,z+1} - T_{m,\ell,z}}{\Delta \Psi} \right] \right. \\ &\left. + \frac{1}{N_{Pe}} \left[ \frac{T_{m+1,\ell,z+1} - 2T_{m,\ell,z+1} + T_{m-1,\ell,z+1}}{\Delta r^2} \right] \right] \quad (104) \end{aligned}$$

Rearranging, one obtains,

$$\begin{aligned} \frac{1}{N_{Pe}} \left[ \frac{1}{2 \Delta r} \left( \frac{\sin \Psi_\ell}{R + r_m \sin \Psi_\ell} + \frac{1}{r_m} \right) - \frac{1}{\Delta r^2} \right] T_{m-1,\ell,z+1} &+ \left[ \frac{1}{\Delta \theta} \right. \\ &\left. \left( \frac{w_{m,\ell}}{R + r_m \sin \Psi_\ell} \right) + \frac{1}{\Delta \Psi} \left( \frac{\cos \Psi_\ell}{N_{Pe} r_m (R + r_m \sin \Psi_\ell)} + \frac{2}{N_{Pe} \Delta r^2} \right) \right] T_{m,\ell,z+1} \\ &+ \frac{1}{N_{Pe}} \left[ -\frac{1}{2 \Delta r} \left( \frac{\sin \Psi_\ell}{R + r_m \sin \Psi_\ell} + \frac{1}{r_m} \right) - \frac{1}{\Delta r^2} \right] T_{m+1,\ell,z+1} = \frac{1}{\Delta \theta} \\ &\left( \frac{w_{m,\ell}}{R + r_m \sin \Psi_\ell} \right) T_{m,\ell,z} + \frac{1}{\Delta \Psi} \left[ \frac{\cos \Psi_\ell}{N_{Pe} r_m (R + r_m \sin \Psi_\ell)} \right] T_{m,\ell-1,z+1} \quad (105) \end{aligned}$$



The system of equations described above can be written in vector-matrix notation as

$$\underline{A}_\lambda \vec{t}_\lambda = \vec{b}_\lambda, \quad \lambda = 2, 3, \dots, 2J+1 \quad (106)$$

The coefficient matrix,  $\underline{A}_\lambda$ , is tridiagonal and is given as

$$\underline{A}_\lambda = \begin{bmatrix} B_2 & C_2 & & & \\ A_3 & B_3 & C_3 & & \\ & \ddots & \ddots & \ddots & \\ & & & C_{N-1} & \\ & & & A_N & B_N \end{bmatrix} \quad (107)$$

where, for  $2 \leq m \leq N$ ,

$$A_m = \frac{1}{N_{Pe}} \left[ \frac{1}{2 \Delta r} \left( \frac{\sin \Psi_\lambda}{R + r_m \sin \Psi_\lambda} + \frac{1}{r_m} \right) - \frac{1}{\Delta r^2} \right] \quad (108)$$

$$B_m = \frac{1}{\Delta \theta} \left[ \frac{w_{m,\lambda}}{R + r_m \sin \Psi_\lambda} \right] + \frac{1}{\Delta \Psi} \left[ \frac{\cos \Psi_\lambda}{N_{Pe} r_m (R + r_m \sin \Psi_\lambda)} \right] + \frac{2}{N_{Pe} \Delta r^2} \quad (109)$$

$$C_m = \frac{1}{N_{Pe}} \left[ -\frac{1}{2 \Delta r} \left( \frac{\sin \Psi_\lambda}{R + r_m \sin \Psi_\lambda} + \frac{1}{r_m} \right) - \frac{1}{\Delta r^2} \right] \quad (110)$$

The solution vector  $\vec{t}_\lambda$  is given by

$$\vec{t}_\lambda = \begin{bmatrix} T_{2, \lambda, z+1} \\ T_{3, \lambda, z+1} \\ \vdots \\ T_{N, \lambda, z+1} \end{bmatrix} \quad (111)$$

The constant vector,  $\vec{b}_\lambda$ , is given by

$$\vec{b}_\lambda = \begin{bmatrix} b_2 \\ b_3 \\ \vdots \\ b_N \end{bmatrix} \quad (112)$$

where,

$$\begin{aligned} b_2 = & \frac{1}{\Delta\theta} \left[ \frac{w_{2,\lambda}}{R + r_2 \sin\psi_\lambda} \right] T_{2, \lambda, z} \\ & + \frac{1}{\Delta\psi} \left[ \frac{\cos\psi_\lambda}{N_{Pe} r_2 (R + r_2 \sin\psi_\lambda)} \right] T_{2, \lambda-1, z+1} \\ & - \frac{T_{1,1,z+1}}{N_{Pe}} \left[ \frac{1}{2 \Delta r} \left( \frac{\sin\psi_\lambda}{R + r_2 \sin\psi_\lambda} + \frac{1}{r_2} \right) - \frac{1}{\Delta r^2} \right] \end{aligned} \quad (113)$$

$$\begin{aligned}
b_m = & \frac{1}{\Delta\theta} \left[ \frac{w_{m,\ell}}{R + r_m \sin\psi_\ell} \right] T_{m,\ell,z} \\
& + \frac{1}{\Delta\psi} \left[ \frac{\cos\psi_\ell}{N_{Pe} r_m (R + r_m \sin\psi_\ell)} \right] T_{m,\ell-1,z+1} \quad (114)
\end{aligned}$$

for  $3 \leq m \leq N-1$ , and

$$\begin{aligned}
b_N = & \frac{1}{\Delta\theta} \left[ \frac{w_{N,\ell}}{R + r_N \sin\psi_\ell} \right] T_{N,\ell,z} \\
& + \frac{1}{\Delta\psi} \left[ \frac{\cos\psi_\ell}{N_{Pe} r_N (R + r_N \sin\psi_\ell)} \right] T_{N,\ell-1,z+1} \\
& + \frac{1}{N_{Pe}} \left[ \frac{1}{2 \Delta r} \left( \frac{\sin\psi_\ell}{R + r_N \sin\psi_\ell} + \frac{1}{r_N} \right) + \frac{1}{\Delta r^2} \right] \quad (115)
\end{aligned}$$

The marching pattern in the angular direction is continued for  $1 < \ell \leq 2J + 1$ . When all the temperatures have been calculated at a given cross section, a step of length  $\Delta Z$  is taken in the axial direction, and the entire procedure started anew.

### Solution of Systems of Equations

The finite difference approximations for the equation of energy result in systems of linear algebraic equations, which when represented in matrix-vector notation have a coefficient matrix which is tridiagonal in form. For systems of this variety, a computational algorithm based

on the Gaussian elimination technique is available (13). This scheme is highly accurate and quite economical with respect to computer time.

This technique can best be illustrated by considering a system of equations represented by

$$\begin{bmatrix} A_1 & B_1 & & & & \\ C_2 & A_2 & B_2 & & & \\ & \ddots & \ddots & \ddots & & \\ & & & & B_{N-1} & \\ & & & C_N & A_N & \end{bmatrix} \begin{bmatrix} X_1 \\ X_2 \\ \vdots \\ X_{N-1} \\ X_N \end{bmatrix} = \begin{bmatrix} D_1 \\ D_2 \\ \vdots \\ D_{N-1} \\ D_N \end{bmatrix} \quad (116)$$

The computational algorithm is

$$W_1 = A_1$$

$$W_m = A_m - C_m Q_{m-1} \quad (m = 2, 3, 4, \dots, N)$$

$$Q_{m-1} = \frac{B_{m-1}}{W_{m-1}}$$

$$G_1 = \frac{D_1}{W_1} \quad (117)$$

$$G_m = \frac{D_m - C_m G_{m-1}}{W_m} \quad (m = 2, 3, 4, \dots, N)$$

$$X_N = G_N$$

$$X_m = G_m - Q_m X_{m+1} \quad (m = N-1, N-2, \dots, 1)$$

Notice that at the most, three multiplications, three divisions, and three additions are required per grid point, and the amount of computational time is directly proportional to the number of grid points.

### Mean Temperature

The "mixing-cup" or mean temperature (4) is defined as

$$T_M^* = \frac{\frac{2}{\pi a^{*2}} \int_{\Psi=-\pi/2}^{\Psi=\pi/2} \int_{r^*=0}^{r^*=a^*} T^* w^* r^* d r^* d \Psi}{\frac{2}{\pi a^{*2}} \int_{\Psi=-\pi/2}^{\Psi=\pi/2} \int_{r^*=0}^{r^*=a^*} w^* r^* d r^* d \Psi} \quad (118)$$

In dimensionless form, equation (118) becomes,

$$T_M = \frac{8/\pi \int_{\Psi=-\pi/2}^{\Psi=\pi/2} \int_{r=0}^{r=1/2} T w r d r d \Psi}{8/\pi \int_{\Psi=-\pi/2}^{\Psi=\pi/2} \int_{r=0}^{r=1/2} w r d r d \Psi} = \frac{\mathcal{Q}_T}{\mathcal{Q}_w} \quad (119)$$

The numerical integration yielding  $\mathcal{Q}_T$  can be performed in a manner similar to that used to determine  $\mathcal{Q}_w$ , i. e., using Simpson's rule twice.

Writing  $\mathcal{Q}_T$  as,

$$\mathcal{Q}_T = 8/\pi \int_{\Psi = -\pi/2}^{\Psi = \pi/2} \left\{ \int_{r=0}^{r=1/2} T w r dr \right\} d\Psi \quad (120)$$

and taking the first integration to be that with respect to  $r$ , the numerical formulation is

$$\left\{ \int_{r=0}^{r=1/2} T w r dr \right\}_{\lambda} = \sum \frac{\Delta r}{3} \left[ T w r \Big|_{m-1} + 4 T w r \Big|_m + T w r \Big|_{m+1} \right] = G_{\lambda}(\Psi) \quad (121)$$

for  $m = 2, 4, \dots, N$  and  $1 \leq \lambda \leq 2J + 1$ .

With the values of  $G_1(\Psi), G_2(\Psi), \dots, G_{2J+1}(\Psi)$  known, the numerical integration for  $\mathcal{Q}_T$  is completed by writing

$$\begin{aligned} \mathcal{Q}_T &= 8/\pi \int_{\Psi = -\pi/2}^{\Psi = \pi/2} \left( \int_{r=0}^{r=1/2} T w r dr \right) d\Psi = 8/\pi \int_{-\pi/2}^{\pi/2} G(\Psi) d\Psi \\ &= 8/\pi \sum \frac{\Delta \Psi}{3} \left[ G_{\lambda-1}(\Psi) + 4G_{\lambda}(\Psi) + G_{\lambda+1}(\Psi) \right] \quad (122) \end{aligned}$$

for  $\lambda = 2, 4, \dots, 2J$ .

### Nusselt Numbers

The local Nusselt number is defined by

$$N_{Nu} = \frac{h^* D^*}{k_M^*} = \frac{D^* k_w^*}{k_M^*} \frac{\left. \frac{\partial T^*}{\partial r^*} \right|_{r^* = a^*}}{(T_w^* - T_M^*)} \quad (123)$$

Putting this in dimensionless form

$$N_{Nu} = \frac{k_w}{k_M} \frac{\left. \frac{\partial T}{\partial r} \right|_{r=1/2}}{(1 - T_M)} \quad (124)$$

As the fluid properties are assumed constant,  $k_w = k_M = 1$ . Thus,

$$N_{Nu} = \frac{\left. \frac{\partial T}{\partial r} \right|_{r=1/2}}{(1 - T_M)} \quad (125)$$

A finite difference approximation of this equation is

$$N_{Nu} = \frac{[3T_{N+1, \ell, z+1} - 4T_{N, \ell, z+1} + T_{N-1, \ell, z+1}]}{2 \Delta r (1 - T_M)} \quad (126)$$

The local Nusselt numbers of interest are at the inner and outer walls of the pipe in the plane of symmetry, i. e., at  $\ell = 1$ ,  $\ell = 2J + 1$ .

The first law of thermodynamics written for an element of volume fixed in space is

$$Q^* = \iiint_{\text{vol}} \left( H^* + \frac{\vec{V}^* \cdot \vec{V}^*}{2} + g_L L^* \right) \rho^* \vec{V}^* \cdot dA \quad (127)$$

Neglecting potential and kinetic energy terms in comparison with the enthalpy term, this equation is reduced to

$$Q^* = \Delta \left\{ \int_{r^*=0}^{r^*=a^*} 2 \int_{\Psi=-\pi/2}^{\Psi=\pi/2} \rho^* w^* H^* r^* dr^* d\Psi \right\} = \Delta \left\{ W_f^* \int_{T_0^*}^{T_M^*} C_p^* dT^* \right\} \quad (128)$$

Defining the arithmetic mean-heat transfer coefficient,  $h^*_{\text{a.m.}}$ , by

$$Q^* = h^*_{\text{a.m.}} (\pi D^* L^*) \left[ \frac{(T_w^* - T_0^*) + (T_w^* - T_M^*)}{2} \right] \quad (129)$$

one can combine equations (128) and (129) to obtain

$$h^*_{\text{a.m.}} = \frac{2 \int_{r^*=0}^{r^*=a^*} \int_{\Psi=-\pi/2}^{\Psi=\pi/2} \rho^* w^* H^* r^* dr^* d\Psi}{(\pi D^* L^*) \left[ \frac{(T_w^* - T_0^*) + (T_w^* - T_M^*)}{2} \right]} \quad (130)$$

When various dimensionless quantities are substituted into the right hand side of equation (130), the expression can be written as,



$$h_{a.m.}^* = \frac{16 k_0^*}{\pi^2 D^*} \frac{N_{Gz}}{(2 - T_M)} \int_{r=0}^{r=1/2} \int_{\Psi=\pi/2}^{\Psi=-\pi/2} \rho H w r dr d\Psi \quad (131)$$

Defining the arithmetic-mean Nusselt number to be

$$N_{Nu_{a.m.}} = \frac{h_{a.m.}^* D^*}{k_{a.m.}^*} \quad (132)$$

substitution of equation (131) into equation (132) yields

$$N_{Nu_{a.m.}} = \frac{16 N_{Gz}}{\pi^2} \frac{\int_{r=0}^{r=1/2} \int_{\Psi=\pi/2}^{\Psi=-\pi/2} \rho H w r dr d\Psi}{k_{a.m.}^* (2 - T_M)} \quad (133)$$

As the fluid's properties are considered to be constant,  $\rho = 1$ ,

$k_{a.m.}^* = 1$ , and

$$H = \frac{H^*}{C_{p0}^* (T_w^* - T_0^*)} = \frac{C_{p0}^* (T^* - T_0^*)}{C_{p0}^* (T_w^* - T_0^*)} = T \quad (134)$$

Therefore,

$$N_{Nu_{a.m.}} = \frac{16 N_{Gz}}{\pi^2} \frac{\int_{r=0}^{r=1/2} \int_{\Psi=\pi/2}^{\Psi=-\pi/2} T w r dr d\Psi}{(2 - T_M)} \quad (135)$$

## APPENDIX D

### COMPUTER APPLICATION OF CALCULATION SCHEME

#### Computer and Computer Language

The calculations were made on an IBM 360 digital computer operated by the Engineering Computer Center at the University of Missouri's Columbia campus. The programming language utilized was FORTRAN-IV, described in reference (17).

#### Outline of Computer Program

The overall program is composed of a main program and two SUBROUTINE sections.

SUBROUTINE VELCOM calculates the velocity components  $u$ ,  $v$ , and  $w$  as point functions both inside and outside the boundary layer.

SUBROUTINE TRIDAG employs the computational algorithm described in Appendix C to solve a system of linear algebraic equations, the coefficient matrix of which is tridiagonal in form.

The main program calculates the various elements of the matrices and vectors describing the finite difference approximations of the equations of energy. The temperature field and resulting arithmetic mean and local Nusselt numbers are also calculated as a function of the Graetz number.

Input data includes the dimensionless quantities  $(R^*/a^*)$ ,  $N_{Pr}$ ,  $N_{Re}$ ,

and parameters specifying the finite difference grid size,  $N$ ,  $J$ , and  $\Delta\theta$ .

It should be noted that the program was constructed with the hope that all three velocity components,  $u$ ,  $v$ , and  $w$ , could be used to obtain a numerical solution. As stability problems were encountered when the radial and angular velocities were non-zero, a DO LOOP is employed at the end of SUBROUTINE VELCOM to set  $u=v=0$  everywhere in the cross section.

To aid the reader, COMMENT statements are used liberally throughout the program.

### Computer Program Nomenclature

AOVR - $(a^*/R^*)$	ETA - $\eta$
B ( ) - elements of vector $\vec{b}_r$	FPSI(L) - $F_r(\Psi)$
DD ( ) - elements of vector $\vec{b}_1$	G - $g$
DEAN - $N_{De}$	GPSI(L) - $G_r(\Psi)$
DELPDE - $\Delta\Psi$ (degrees)	GR - $N_{Gz}$
DELPSI - $\Delta\Psi$ (radians)	PARDL - $\frac{\partial \delta}{\partial \Psi}$
DELTA - $\delta$	PARDL1 - $\frac{\partial \delta_1}{\partial \Psi}$
DELTA1 - $\delta_1$	PARF - $\frac{\partial f}{\partial \eta}$
DELTAM - $\delta_M$	PARG - $\frac{\partial g}{\partial \Psi}$
DELTAR - $\Delta r$	
DELTHA - $\Delta\theta$ (radians)	
DLTHAD - $\Delta\theta$ (degrees)	

$$\text{PARV} - \frac{\partial v}{\partial \Psi}$$

$$\text{PARV0} - \frac{\partial v_0}{\partial \Psi}$$

$$\text{PE} - N_{\text{Pe}}$$

$$\text{PR} - N_{\text{Pr}}$$

$$\text{PSI(L)} - \Psi_{\ell} \text{ (radians)}$$

$$\text{PSIDEG(L)} - \Psi_{\ell} \text{ (degrees)}$$

$$\text{R(M)} - r_m$$

$$\text{RC} - R$$

$$\text{RE} - N_{\text{Re}}$$

$$\text{ROVA} - (R^*/a^*)$$

$$\text{T(M, L, Z)} - T_{m, \ell, z}$$

$$\text{THETA} - \theta \text{ (radians)}$$

$$\text{THETAD} - \theta \text{ (degrees)}$$

$$\text{TINTGL} - \mathcal{Q}_T$$

$$\text{TM} - T_M$$

$$\text{U(M, L)} - u_{m, \ell}$$

$$\text{V(M, L)} - v_{m, \ell}$$

$$\text{V0} - v_0$$

$$\text{W(M, L)} - w_{m, \ell}$$

$$\text{W0} - w_0$$

$$\text{WINTGL} - \mathcal{Q}_w$$

$$\text{XLOVD} - Z$$

$$\text{XNU} - N_{\text{Nu}} \text{ a. m.}$$

$$\text{XNUI} - N_{\text{Nu}} \Big|_{\Psi = -\pi/2}$$

$$\text{XNUO} - N_{\text{Nu}} \Big|_{\Psi = \pi/2}$$

$$\left. \begin{array}{l} \text{X( )} \\ \text{Y( )} \\ \text{Z( )} \end{array} \right\} - \text{elements of the matrix } \underline{A_{\ell}}$$

$$\left. \begin{array}{l} \text{XX( )} \\ \text{YY( )} \\ \text{ZZ( )} \end{array} \right\} - \text{elements of the matrix } \underline{A_1}$$

Computer Program

The program used to implement the numerical solution is listed below. (Double spacing denotes a new card.)

```
DIMENSION U(60, 60), V(60, 60), W(60, 60), R(105), PSI(105),
PSIDEG(105),
```

```
1GPSI(100)
```

```
DOUBLE PRECISION T(60, 60, 2), RC, PE, RPR, RPS, DELPSI,
DELTAR, DELTHA,
```

```
1SI(60), E1, E2, E3, E4, XX(60), YY(60), ZZ(60), DD(60), F1, F2,
F3, F4, F5,
```

```
2G1, G2, G3, G4, H1, H2, H3, H4, H5, H6, H7, X(60), Y(60), Z(60), B(60
```

```
1 READ(5, 5)N, J, RE, ROVA, PR, DELTHA
```

```
5 FORMAT(2I5, 4F10.0)
```

```
PI=3.1415926535
```

C

C THE ABOVE READS IN THE REYNOLDS NUMBER, THE R OVER A  
CURVATURE RATIO,

C THE PRANDTL NUMBER AND THE GRID PARAMETERS N AND J.  
THE SPACING

C BETWEEN GRIDS, DELTA THETA, IS ALSO READ IN

C

```
XN=N
```

```
XJ=J
```

```
DELTAR=1.0/(2.0*XN)
```

DELPSI=PI/(2.0\*XJ)

DELPDE=DELPSI\*180.0/PI

DLTHAD=DELTHA\*180.0/PI

NP1=N+1

JJ=(2\*J)+1

DO 10 M=1, NP1

XM=M

10 R(M)=(XM-1.0)\*DELTAR

DO 15 L=1, JJ

XL=L

PSI(L)=(PI/2.0)-(XL-1.0)\*DELPSI

15 PSIDEGL(L)=PSI(L)\*(180.0)/PI

C

C THE ABOVE PORTION OF THE PROGRAM CALCULATES THE  
VALUES OF DELTA R,

C DELTA PSI, AND DETERMINES THE VALUES OF R AND PSI AS  
A FUNCTION OF

C GRID LOCATION

C

PE=RE\*PR

RC=(1.0/2.0)\*ROVA

DEAN=RE\*((1.0/(2.0\*RC))\*\*0.5)

AOVR=1.0/ROVA

C

C THE ABOVE STATEMENTS DETERMINE THE PECLET NUMBER,  
THE DIMENSIONLESS

C RADIUS OF CURVATURE, THE DEAN NUMBER, AND THE A OVER  
R CURVATURE

C RATIO

C

WRITE(6, 20)

20 FORMAT(1H1, 99HTHE RESULTS OBTAINED BY APPLYING  
THE FINITE DIFFEREN

1CE METHOD OF SOLUTION TO THE EQUATION OF ENERGY/  
1H0, 57HDESCRIBING

2HEAT TRANSFER IN A CURVED TUBE ARE SHOWN BELOW/.

WRITE(6, 25)DELTAR, DELPSI, DELPDE, DELTHA, PE, DEAN,  
RE, PR, ROVA, AOV,

1N, J

25 FORMAT(1H , 8HDELTA R=, F20. 8/1H0, 10HDELTA PSI=,  
F20. 8/1H0, 21HDELTA P

1SI IN DEGREES=, F20. 8/1H0, 12HDELTA THETA=, F20. 8/1H0,  
14HPECLET NUMBE

2R=, F20. 8/1H0, 12HDEAN NUMBER=, F20. 8/1H0, 16HREYNOLI  
NUMBER=, F20. 8/1

3H0, 15HPRANDTL NUMBER=, F20. 8/1H0, 29HTHE R OVER A  
CURVATURE RATIO=, F

420. 8/1H0, 29HTHE A OVER R CURVATURE RATIO=, F20. 8/  
1H0, 2HN=, I5/1H0, 2H

5J=; I5///)

```
DO 30 L=1, JJ
```

```
DO 30 M=1, NP1
```

```
30 T(M, L, 1)=0.0
```

C

C THE STATEMENTS ABOVE SET THE DIMENSIONLESS TEMPERATURE  
EQUAL TO

C ZERO EVERYWHERE IN THE CROSS SECTION AT THE BEGINNING  
OF THE HEAT

C TRANSFER SECTION

C

```
NZ=1
```

```
THETA=0.0
```

```
CALL VELCOM(U, V, W, R, PSI, N, J, RE, ROVA, WINTGL)
```

```
WRITE(6, 27)WINTGL
```

```
27 FORMAT(1H , 31HTHE VALUE OF THE INTEGRAL OF W=,  
F20.8///)
```

```
WRITE(6, 35)
```

```
35 FORMAT(1H , 10X, 1HR, 12X, 13HPSI (DEGREES), 14X, 1HU,  
19X, 1HV, 19X, 1HW//)
```

```
DO 36 L=1, JJ
```

```
DO 36 M=1, NP1
```

```
36 WRITE(6, 37)R(M), PSIDEG(L), U(M, L), V(M, L), W(M, L)
```

```
37 FORMAT(1H , 5F20.10)
```

```
WRITE(6, 26)
```



```
26  FORMAT(1H , 10X, 1HR, 12X, 15HTHETA (DEGREES), 5X,
      13HPSI (DEGREES), 14X,
```

```
      11HT///)
```

```
39  DO 40 L=1, JJ
```

```
40  T(NP1, L, 2)=1.0
```

C

C THE ABOVE SETS THE BOUNDARY CONDITION THAT THE  
DIMENSIONLESS

C TEMPERATURE IS EQUAL TO A VALUE OF ONE AT THE WALL

C

```
E1=W(1, 1)/(RC*DELTHA)
```

```
E2=4.0/(PE*(DELTAR**2))
```

```
E3=(1.0/(PE*RC))-U(1, 1)
```

```
E4=2.0/(PE*(DELTAR**2))
```

```
YY(1)=E1+E2
```

```
ZZ(1)=(-1.0/(2.0*DELTAR))*E3-E4
```

```
DO 45 M=2, N
```

```
RPR =RC+R(M)
```

```
F1=1.0/(PE*RPR)
```

```
F2=1.0/(PE*R(M))
```

```
F3=1.0/(PE*(DELTAR**2))
```

```
F4=W(M, 1)/RPR
```

```
F5=2.0/(PE*(DELTAR**2))
```

```
XX(M)=(1.0/(2.0*DELTAR))*(F1+F2-U(M,1))-F3
YY(M)=(1.0/DELTHA)*F4+F5
45 ZZ(M)=(-1.0/(2.0*DELTAR))*(F1+F2-U(M,1))-F3
G1=W(1,1)/(RC*DELTHA)
G2=2.0/(PE*(DELTAR**2))
G3=(1.0/(PE*RC))-U(1,1)
DD(1)=G1*T(1,1,1)+T(2,JJ,1)*(G2-(1.0/(2.0*DELTAR))*G3)
DO 50 M=2, N
RPR=RC+R(M)
G4=W(M,1)/RPR
50 DD(M)=(1.0/DELTHA)*G4*T(M,1,1)
DD(N)=DD(N)-ZZ(N)
CALL TRIDAG(N,YY,ZZ,XX,DD,S1)
DO 55 M=1, N
55 T(M,1,2)=S1(M)
DO 56 L=2, JJ
56 T(1,L,2)=T(1,1,2)
XZ=NZ
THETAD=XZ*DLTHAD
DO 60 M=1, NP1
60 WRITE(6,65)R(M), THETAD, PSIDEG(1), T(M,1,2)
65 FORMAT(1H , 3F20.10, F20.14)
```

```

L=2
66 DO 70 M=2, N
    S=SIN(PSI(L))
    C1=COS(PSI(L))
    RPS=RC+R(M)*S
    H1=S/(PE*RPS)
    H2=1.0/(PE*R(M))
    H3=1.0/(PE*(DELTAR**2))
    H4=W(M, L)/RPS
    H5=C1/(PE*R(M)*RPS)
    H6=V(M, L)/R(M)
    H7=2.0/(PE*(DELTAR**2))
    X(M-1)=(1.0/(2.0*DELTAR))*(H1+H2-U(M, L))-H3
    Y(M-1)=(1.0/DELTHA)*H4+(1.0/DELPSI)*(H5-H6)+H7
    Z(M-1)=(-1.0/(2.0*DELTAR))*(H1+H2-U(M, L))-H3
70 B(M-1)=(1.0/DELTHA)*H4*T(M, L, 1)+(1.0/DELPSI)*(H5-H6)
    *T(M, L-1, 2)
    B(1)=B(1)-T(1, 1, 2)*X(1)
    B(N-1)=B(N-1)-Z(N-1)
    NM1=N-1
    CALL TRIDAG(NM1, Y, Z, X, B, S1)
    DO 75 M=1, NM1
75 T(M+1, L, 2)=S1(M)

```

```

DO 80 M=1, NP1

80 WRITE(6, 85)R(M), THETA, PSIDEG(L), T(M, L, 2)

85 FORMAT(1H , 3F20.10, F20.14)

L=L+1

IF(L-JJ)66, 66, 90

90 THETA=THETA+DELTA

XLOVD=RC*THETA

GR=PI*PE/(4.0*RC*THETA)

J2=2*J

DO 92 L=1, JJ

SUM6=0.0

DO 91 M=2, N, 2

91 SUM6=SUM6+T(M-1, L, 2)*W(M-1, L)*R(M-1)+4.0*T(M, L, 2)
  *W(M, L)*R(M)+

  1T(M+1, L, 2)*W(M+1, L)*R(M+1)

92 GPSI(L)=DELTAR*SUM6/3.0

SUM66=0.0

DO 93 L=2, J2, 2

93 SUM66=SUM66+GPSI(L-1)+4.0*GPSI(L)+GPSI(L+1)

TINTGL=(8.0/PI)*DELPSI*SUM66/3.0

TM=TINTGL/WINTGL

XNU=((16.0/(PI**2))*GR*DELPSI*(SUM66/3.0))/(2.0-TM)

```

$XNUO = (3.0 * T(N+1, 1, 2) - 4.0 * T(N, 1, 2) + T(N-1, 1, 2)) / (2.0 * DELTA * (1.0 - TM))$

1)

$XNUI = (3.0 * T(N+1, JJ, 2) - 4.0 * T(N, JJ, 2) + T(N-1, JJ, 2)) / (2.0 * DELTA * (1.0 -$

$1TM))$

WRITE(6, 94)GR, XNU, XNUO, XNUI, XLOVD, TINTGL, TM

94 FORMAT(1H , 14HGRAETZ NUMBER=, F20.8/1H0, 31HARITHMETIC MEAN NUSSELT

1NUMBER=, F20.8/1H0, 35HLOCAL NUSSELT NUMBER AT OUT WALL=, F20.8/1H0

2, 35HLOCAL NUSSELT NUMBER AT INNER WALL=, F20.8/1H0, 29HDISTANCE DOWN

3 THE PIPE (L/D)=, F20.8/1H0, 14HINTEGRAL OF T=, F20.8/1H0, 17HMEAN TEM

4PERATURE=, F20.8///)

NZ=NZ+1

IF(NZ-100)210, 201, 202

201 DELTHA=3.0\*DELTHA

202 IF(NZ-200)210, 203, 210

203 DELTHA=(10.0/3.0)\*DELTHA

210 IF(NZ-300)95, 95, 200

95 DO 100 L=1, JJ

DO 100 M=1, NP1

100 T(M, L, 1)=T(M, L, 2)

GO TO 39

200 GO TO 1

STOP

END

SUBROUTINE VELCOM(U, V, W, R, PSI, N, J, RE, ROVA, WINTGL

C

C THE PURPOSE OF THIS SUBROUTINE IS TO CALCULATE THE  
VELOCITY COMPONENTS

C U, V, AND W THROUGH USE OF THE DIMENSIONLESS BARUA METH

C

DIMENSION U(60, 60), V(60, 60), W(60, 60), R(105), PSI(105),  
PSIDEG(105),

1FPSI(100)

PI=3.1415926535

NP1=N+1

JJ=(2\*J)+1

RC=(1.0/2.0)\*ROVA

DEAN=RE\*((1.0/(2.0\*RC))\*\*0.5)

AOVR=1.0/ROVA

C

C THE ABOVE STATEMENTS CALCULATE THE DIMENSIONLESS  
RADIUS OF CURVATURE

C , THE DEAN NUMBER, AND THE RECIPROCAL CURVATURE RATI

C

B1=(((1.871\*\*2)+1.03\*DEAN)\*\*0.5)

B2=(1.871+B1)\*\*3

B3=3.96\*(RC\*\*1.5)/(RE\*\*2)

B=B3\*B2

$$A=(1.335**2)*(B**0.333)*(RC**0.5)$$

$$D=-4.0*(RC**2)+2.0*SQRT(6.0)*RC$$

$$C=D/4.0$$

$$H=28.4*(RC**0.75)$$

$$XN=N$$

$$XJ=J$$

$$DELTAR=1.0/(2.0*XN)$$

$$DELPSI=PI/(2.0*XJ)$$

$$DELPDE=DELPSI*180.0/PI$$

C

C THE ABOVE PORTION OF THE PROGRAM CALCULATES VALUES FOR THE BOUNDARY

C LAYER CONSTANTS B, A, D, C, AND H. ALSO, THE VALUES OF DELTA R, DELTA PSI,

C AND DELTA PSI EXPRESSED IN DEGREES ARE FOUND

C

$$L=1$$

$$M=NP1$$

$$45 \quad RPS=2.0*RC+SIN(PSI(L))$$

$$S=SIN(PSI(L))$$

$$C1=COS(PSI(L))$$

$$Z1=-(1.0/60.0)*(H**2)$$

$$Z2=C1/((RPS**2)+D)$$



$$Z3 = 3.0 * (C1^{**2}) / RPS$$

$$Z4 = D * S / (RPS^{**2})$$

$$G = Z1 * Z2 * (S + Z3 + Z4)$$

$$DELTA1 = -(H/G) * C1 / RPS$$

$$DELTA = (DELTA1 / 2.0) * ((A/B)^{**0.5}) * ((2.0 / RE)^{**0.667})$$

$$DELTAN = (30.0 / 16.93) * ((A/B)^{**0.5}) * ((2.0 / RE)^{**0.667}) * ((2.0 * RC)^{**0.25})$$

1)

$$BOUNDE = 0.5 - DELTAM$$

$$IF(R(M) - BOUNDE) 60, 50, 50$$

$$50 \quad VO = G * (B/A) * ((RE/2.0)^{**0.333})$$

$$WO = (B / (2.0 * A)) * ((4.0 * RE)^{**0.333}) * (RC + (0.5 - DELTAM) * S + (C / (RC + (0.5 -$$

$$1DELTA) * S)))$$

$$ETA = (0.5 - R(M)) / DELTAM$$

$$F = (ETA - 2.0 * (ETA^{**2}) + (ETA^{**3}))$$

$$PARF = (1.0 - 4.0 * ETA + 3.0 * (ETA^{**2}))$$

$$X1 = -S / ((RPS^{**2}) + D)$$

$$X2 = 3.0 * (C1^{**2}) / RPS$$

$$X3 = D * S / (RPS^{**2})$$

$$X4 = -(C1^{**2}) * 2.0 * RPS / (((RPS^{**2}) + D)^{**2})$$

$$X5 = C1 / ((RPS^{**2}) + D)$$

$$X6 = 6.0 * C1 * S / RPS$$

$$X7=3.0*(C1**3)/(RPS**2)$$

$$X8=D*C1/(RPS**2)$$

$$X9=2.0*D*S*C1/(RPS**3)$$

$$PARG=-((H**2)/60.0)*(X1*(S+X2+X3)+X4*(S+X2+X3)+X5*(C1-X6-X7+X8-X9)$$

1)

$$PARVO=(B/A)*((RE/2.0)**0.333)*PARG$$

$$Y1=H*S/(G*RPS)$$

$$Y2=H*(C1**2)/(G*(RPS**2))$$

$$Y3=H*C1/((G**2)*RPS)$$

$$PARDL1=Y1+Y2+Y3*PARG$$

$$PARDL=0.5*((A/B)**0.5)*((2.0/RE)**0.667)*PARDL1$$

$$PARV=F*PARVO-(VO*ETA/DELTA)*PARF*PARDL$$

C

C THE ABOVE PORTION OF THE PROGRAM CALCULATES VALUES  
NEEDED TO DETERMINE

C VELOCITY COMPONENTS IN THE BOUNDARY LAYER

C

$$V(M, L)=VO*(ETA-2.0*(ETA**2)+(ETA**3))$$

$$W(M, L)=WO*(2.0*ETA-(ETA**2))$$

IF(M-NP1)55, 65, 65

55  $U(M, L)=U(M+1, L)+(DELTAR/R(M))*PARV+(DELTAR*V(M, L)*C1)/(RC+R(M)*S)$

GO TO 70

C

C THE ABOVE STATEMENTS CALCULATE THE VELOCITY COMPONENTS U, V, AND W IN

C THE BOUNDARY LAYER

C

60 S=SIN(PSI(L))

C1=COS(PSI(L))

W(M, L)=(B/(2.0\*A))\*((4.0\*RE)\*\*0.333)\*(RC-R(M)\*S+(C/(RC+R(M)\*S)))

UP=(A/(RC+R(M)\*S))+((1.0/(4.0\*RE))\*\*0.333)

U(M, L)=UP\*S

V(M, L)=UP\*C1

GO TO 70

C

C THE STATEMENTS ABOVE CALCULATE THE VELOCITY COMPONENTS U, V, AND W

C OUTSIDE THE BOUNDARY LAYER

C

65 U(NP1, L)=0.0

C

C THE ABOVE SETS THE U-COMPONENT OF VELOCITY AT THE WALL EQUAL TO ZERO

C

70 M=M-1

IF(M-1)80, 45, 45

```
L=L+1
IF(L-JJ)85, 85, 100
85 M=NP1
GO TO 45
100 DO 101 L=1, JJ
    U(1, L)=U(1, 1)
101 V(1, L)=V(1, 1)
    J2=2*J
    DO 106 L=1, JJ
        SUM1=0.0
        DO 105 M=2, N, 2
105 SUM1=SUM1+W(M-1, L)*R(M-1)+4.0*W(M, L)*R(M)+W(M+1, L)
        *R(M+1)
106 FPSI(L)=DELTAR*SUM1/3.0
        SUM11=0.0
        DO 107 L=2, J2, 2
107 SUM11=SUM11+FPSI(L-1)+4.0*FPSI(L)+FPSI(L+1)
        WINTGL=(8.0/PI)*SUM11*DELPSI/3.0
        DO 108 L=1, JJ
            DO 108 M=1, NP1
                U(M, L)=0.0
108 V(M, L)=0.0
```

RETURN

END

SUBROUTINE TRIDAG(N, A, BB, C, D, S1)

C

C THE PURPOSE OF THIS SUBROUTINE IS TO SOLVE A SYSTEM  
OF LINEAR

C EQUATIONS, THE COEFFICIENT MATRIX OF WHICH IS TRI-  
DIAGONAL

C

DOUBLE PRECISION W(100), A(100), BB(100), C(100), D(100),  
G(100),

1S(100)

W(1)=A(1)

DO 10 I=2, N

10 W(I)=A(I)-C(I)\*(BB(I-1)/W(I-1))

G(1)=D(1)/W(1)

DO 15 I=2, N

15 G(I)=(D(I) - C(I)\*G(I-1))/W(I)

S1(N)=G(N)

20 I=N-1

21 S1(I)=G(I)-(BB(I)\*S1(I+1))/W(I)

I=I-1

IF (I-1)25, 21, 21

25 RETURN

END

## VITA

William Terry Sappenfield was born in Kansas City, Missouri, on October 28, 1945. He attended public school in Lee's Summit, Missouri, graduating from Lee's Summit High in 1963. In September, 1963, the author entered William Jewell College in Liberty, Missouri, where he continued his studies for one year. In the fall of 1964, he entered the University of Missouri at Columbia, graduating with the degree Bachelor of Science in Chemical Engineering in August, 1967.

During the fall of 1967, the author entered graduate school at the University of Missouri, supported by a National Defense Education Act Title IV Fellowship.

The author is a member of Tau Beta Pi, Pi Mu Epsilon, and Alpha Chi Sigma honorary societies and the Kappa Alpha Order social fraternity.

He is married to the former Nancy Jean Powell of Lee's Summit, Missouri.

University Libraries  
University of Missouri

Digitization Information Page

Local identifier            Sappenfield1969

Source information

Format	Book
Content type	Text
Source ID	Gift copy from department; not added to MU collection.
Notes	Copy in MU Libraries' repository shows "1969" as publishing date while the gift copy has 1968

Capture information

Date captured	July 2023
Scanner manufacturer	Fujitsu
Scanner model	fi-7460
Scanning system software	ScandAll Pro v. 2.1.5 Premium
Optical resolution	600 dpi
Color settings	8 bit grayscale
File types	tiff
Notes	

Derivatives - Access copy

Compression	Tiff: LZW compression
Editing software	Adobe Photoshop
Resolution	600 dpi
Color	grayscale
File types	pdf created from tiffs
Notes	Images cropped, straightened, brightened